POLITECNICO DI MILANO

Department of Energy Engineering for Environmentally Sustainable World [EE-ESW]

A COMPARATIVE STUDY OF SOLAR-HYBRID COMBINED CYCLE SYSTEMS

Supervisor:
Dr. Paolo Silva

Simone Perini

Student number: 800603

Academic Year: 2013 - 2014

ABSTRACT

The development of concentrating solar power technologies (CSP) represents an opportunity to reduce fuel dependency and greenhouse emissions. The possibility of hybridization with fossil-fuel based systems can enhance the attractiveness of CSP systems. The integration with combined cycle can provide the following benefits: high conversion efficiency, higher solar share and increased power dispatchabity.

In the present work, two different integration schemes are investigated: parabolic trough collectors are used to supply additional heat to the Rankine cycle power block in the integrated solar combined cycle scheme (ISCC). In the solar hybrid combined cycle system (SHCC), the solar energy is used to pre-heat the combustion air in the gas turbine power block. A pressurized volumetric receiver and a solar tower system are used to collect the solar radiation.

The energy, exergy and economic analysis have been performed considering a period of one year. A solar share of 35% can be achieved with the SHCC system. This value is limited to 9% in the ISCC arrangement. The net incremental solar efficiency for the SHCC plant is 20% and it is higher respect to the other system (15%) because the solar share is increased. From the exergetic point of view, the integrated solar combined cycle system seems to have higher performances than the SHCC plant: the average exergy efficiencies of the overall plant are 44.83% and 43.4% respectively. However, the variation of the exergy efficiency per unit of solar power input is higher in the case of ISCC scheme. This means that the specific exergy destruction of the solar thermal power is higher in the system using the parabolic trough collectors. Finally, the levelized electricity cost (LEC) is evaluated. The minimum electricity selling price for the SHCC and the ISCC plant are 0.05 $/kWh and 0.04 $/kWh respectively. The solar LEC for the SHCC plant is 0.08 $/kWh, lower than the 0.13 $/kWh calculated for the ISCC scheme.

In conclusion, the yearly average energy and exergy efficiency are higher for the integrated solar combined cycle and the LEC results to be lower. However,. the SHCC seems to be a promising option to integrate concentrating solar technologies and combined cycle power plant, because higher solar share and lower solar LEC can be achieved. More attention should be focused in future to develop efficient systems for the integration of the solar energy at higher temperature.

Keywords:

Concentrating solar power, gas turbines, hybridization systems, pressurized volumetric receiver, parabolic trough collector

ACKNOWLEDGEMENTS

I would like to acknowledge my supervisor Dr. Paolo Silva from Politecnico di Milano for his time and support during the preparation of this work. I thank Dr. Ossama Badr from Cranfield University for the assistance during this project. I would like to show my gratitude to Dr. Peter Turner for the help and for his competence.

I would have not been able to complete this thesis project without the presence in my life of special people and I would like to use this page to thank them all.

I would like to thank my fellow students at Cranfield University: Lorenzo, Francesca, Diego, Paolo, Alessio and Luc and my flatmates Daniele and Mauro. Living together one year, we became a family. We had great time in the middle of nowhere and I wish to all of you to reach your personal goals in the future.

I have applied from the Erasmus program because of my successful Politong experience. For this reason, I would like to thank Marco, Luca, Matteo, Stefano, Andrea, Nikolas, Dario and Lorenzo for sharing hundred of moments with me in Shanghai.

I bless my friends from Cremona: Michela, Enrica, Giula(s), Lorenzo, Luca, Massimo, Riccardo and all the others. We live separated, but you proved me that friendship can overcome any distance. I have really appreciated your constant support and I am glad that people like you are part of my life.

Finally I would like to thank my family. I am indebted to our common friends whose warm affect was unwavering. I thank my aunt Ivana and cousins Michele and Nicole for their support. I am grateful to my grandparent because they have always been a constant reference point in my life.

I would like to give a special thank my parent because they have always believed in me and they gave me the strength to go forward. I thank my mum for her unconditional love.

I dedicate this work to my dad Enzo. He comforted and supported me even when I was supposed to help him. He showed me how to find hope even in the darkest moments. You were really interested in reading the first version, now this thesis is for you. Vola alto!

TABLE OF CONTENTS

LIST OF FIGURE

LIST OF TABLE

LIST OF ABBREVIATION

ANU	Australian National University
CC	Combined cycle
CSP	Concentrating solar power
DIAPR	Direct Irradiation Air Pressurized Receiver
DISS	Direct Solar Steam
DLR	Deutsches Zentrum fur Luft und Raumfahrt (Germa Aerospace Center)
DSG	Direct steam generation
EUD	Energy utilization diagram
HCE	Heat collection element
HFLCAL	Heliostat Field Layout Calculator
HRSG	Heat recovery steam generator
HT	High Temperature
IEA	International Energy Agency
IRR	Internal rate of return
ISCC	Integrated solar combined cycle
ISO	International organization for Standard
LEC	Levelized electricity cost
LFR	Linear Fresnel reflector
LT	Low Temperature
MT	Medium Temperature
NPV	Net present value
NREL	National Renewable Laboratory
ORC	Organic Rankine cycle
PCM	Phase change materials
PDC	Parabolic dish collector
ppi	Pores per inch
PTC	Parabolic trough collector
S&L	Sargent and Lundy Consulting Group
SCOT	Solar Concentration Off Tower
SEGS	Solar Energy Generation Station
SES	Sterling energy system
SHCC	Solar hybrid combined cycle
STP	Solar tower power
TIT	Turbine Inlet Temperature

NOMENCLATURE

A	Area	m^2
a	Annuity	$

$c_{O\&M}$	Specific cost for plant maintenance	\$/kWh
CF	Cash Flow	\$
c_p	Specific heat capacity at constant pressure	J/kg K
$\bar{c}_p$	Molar specific heat capacity at constant pressure	J/kmol K
c_v	Specific heat capacity at constant volume	J/kg K
d	distance of the first row of heliostats from the solar tower	m
D	Diameter	m
DNI	Direct normal irradiation	W/m^2
Δh_f	Enthalpy of formation	J/kmol
$\dot{E}$	Electrical power	W
eff	Effectiveness	-
f	Receiver convective heat loss factor	-
f_{CO_2}	carbon dioxide emissions per fuel heating rate	$kgCO_2/MJ$
f_P	Pressure coefficient	-
f_T	Temperature coefficient	-
F_{view}	Radiation view factor	-
h	Enthalpy	J/kg
H	Convective heat transfer coefficient	W/m^2 K
$\bar{h}$	Enthalpy	J/kmol
I	Incident Flux	kW/m^2
k	Polytrophic index	-
K	Solar angle modifier	-
L	Heliostat field length	m
LHV	Lower heating value	J/kg
$\dot{m}$	Mass flow rate	kg/s
m	Interest rate	-
MM	Molar mass	kg/ kmol
n	Years	-
$\dot{n}$	Molar flow rate	kmol/s
P	Pressure	bar
R	Gas constant	J/kmol K

$\dot{S}_{gen}$	Entropy generation rate	W
s	Entropy	J/kg K
T	Temperature	K
t	Solar tower height	m
$\dot{W}$	Mechanical power	W
X	Solar share	-
x	Molar fraction	-
$\dot{x}$	Physical exergy rate	W
ΔT	Temperature variation	K
ΔP	Pressure variation	bar
P	Heliostat field density	-
$\dot{\Psi}$	Exergy destruction rate	W
α	Absorbitivity	-
β	Pressure ratio	-
ε	emissivity	-
γ	Solar incident angle	rad
η_I	Energy efficiency	-
η_{II}	Exergy efficiency	-
$\eta_{net\_incr\_sol}$	Net incremental solar efficiency	-
κ	Waste boiler economic analysis coefficient	W/ K
λ	Air/fuel ratio	-
ϑ	Carnot coefficient	-
ρ	Density	kg/m^3
σ	Stefan-Boltzmann constant	W/m^2 K
ξ	Waste boiler heat loss coefficient	-
ψ	Specific chemical exergy	J/kg

Subscripts

AC	Air compressor
cond	Condenser
cool	Coolant fluid

fg	Flue/ exhaust gases
field	Solar field
GT	Power gas turbine
HTF	Heat transfer fluid
HTX	Heat exchanger
is	Isentropic process
rec	Receiver
ref	Reference plant
ST	Steam turbine

1 INTRODUCTION

Solar energy offers a clean, accessible and inexhaustible energy resource. The highest solar potential is found in the so called Solar Belt, the ground surface comprised between 15° and 35° latitude. According to the IEA (2011), in a future carbon-constrained scenario, solar thermal energy together with solar photovoltaic energy could provide up to 25% of global electricity by 2050.Therefore, sun-derived power generation is an excellent way to reduce fossil fuel dependency representing at the same time the opportunity to achieve the international commitment of CO_2 reduction (Barigozzi et al., 2012). Among the different options for harnessing Sun's power, Concentrating solar power (CSP) technologies present specific benefits such as the centralized large scale electricity production, the economy of scale and the possibility of thermal storage integration (Paolo Silva, 2013).

The Technology Road Map of the International Energy Agency (IEA, 2010) predicted that CSP plants would provide 148 GW in 2020. However, the same institution (IEA, 2012) forecasted that the global installed capacity of solar thermal power-generation will reach only 11 GW by the end of 2017, a much lower value than the Agency and the industry have anticipated earlier. The increased competition from solar photovoltaic systems and the inability to reduce electricity generation cost through economies of scale were the factors affecting the CSP development. However, the possibilities of employing thermal storage and the hybridization with fossil fuel-fired plants could enhance projects attractiveness.

1.1 FUNDAMENTALS OF CONCENTRATING SOLAR POWER

Concentrating solar power plants consist of four different sub-systems: solar collectors, receiver and absorber, transport and storage equipment and power conversion block.

1.1.1 Solar Collectors

The collector captures and concentrates direct normal incident solar radiation (DNI) onto the receiver. In general, collectors are reflective surfaces (for a heliostat field of a central receiver system) or parabolic mirrors in case of parabolic though and parabolic dish systems. These mirrors follows the apparent sun path using a single or two axes tracking devices and they focus the beams onto the absorber (Barlev et al., 2011).

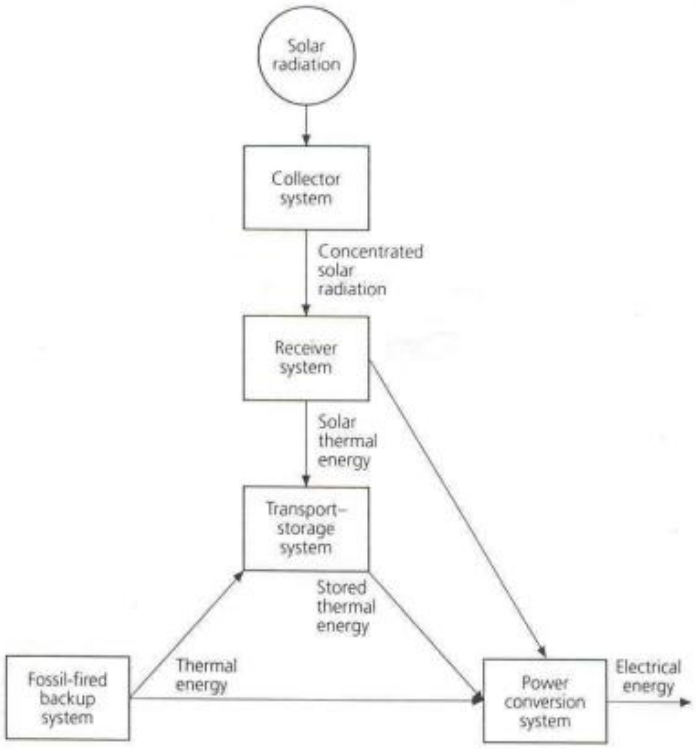

Figure 1-1 Schematic of a solar-thermal electric-power plant (Badr, 2013).

1.1.2 Receiver And Absorber

The receiver is a heat exchanger that absorbs the concentrated radiation and transfer the thermal power to a working fluid.

Distributed receivers are irradiated by dedicated concentrators and heat locally a heat transport fluid. A large number of collectors are needed. In point focus systems the receivers are located at the central point of the parabolic dish collectors, while the absorbers are placed along the focal line of parabolic collectors in a line focus plant.

In central receivers systems, the heliostat field concentrates the radiation onto a single absorber at the top of a tower. The main advantages of this technology are:

- single receiver;
- higher concentration ratio;
- possible exploitation of economy of scale.

Different kinds of central receivers have been developed: cavity receivers operate with tubes lining the walls of a cavity on top of the tower, whereas in external receivers tubes are placed on the outside surface. Section 1.2 explains the specific receiver installed in the different CSP schemes.

1.1.3 Transport And Storage Equipment

The energy exchange from the working fluid to the power conversion unit is regulated by the transport-storage system. Fans or pumps are needed to circulate the working fluid in the system. In some solar-thermal plants, a portion of the thermal energy is stored for later use. Due to the cyclic and random nature of the solar radiation, three kind of thermal storage are necessary for maintaining a constant supply of solar thermal power:

- Very short-term storage: small storage system to avoid transient period when sun is temporarily covered by clouds. Usually the storage capability is 30 minutes;
- Short-term storage: the excess energy harvested during the day is saved to allow the plant operations during the night;
- Long-term storage: part of the higher energy flux collected in spring and summer is stored to support the limited radiation during cold seasons. Long term storage systems have not been proved yet at large scale.

Thermal energy storage can be implemented according to the following strategies (Barlev et al., 2011):

- Sensible heat storage: a solid or a liquid material or the working fluid itself is heated and it is insulated from the environment. Reinforced concrete, solid sodium chloride and silica fire bricks can be used as indirect solid storage medium. Usually the heat transfer fluid is in liquid phase and can be directly stored. Mineral oil, synthetic oil, silicone oil, molten nitrate, molten nitrite and carbonate salts are sensible heat storage liquids.
- Latent heat storage: solid liquid phase change can be used to reserve energy. Phase change stores a great amount of thermal energy, and can be utilized for night time energy storage. A large number of Phase change materials (PCM) have been investigated as storage systems due to the potential high efficiency. However, the pressure drop required affects the performances of the power system. Organic and inorganic compounds have being studied because PCM have typically low thermal conductivity and slow heat exchange rate (Barlev et al., 2011).
- Chemical storage: solar thermal energy can be used in reversible synthesis/de-synthesis endothermic/ exothermic reactions. Reformation of methane and CO_2, metal oxide/metal conversions and ammonia synthesis/dissociation are heat-assisted chemical reactions that can be exploited. Chemical storage is the most suitable energy saving system for long-term or seasonal storage (Barlev et al., 2011).

1.1.4 Power Conversion Block

The power-conversion system consists of a heat engine, coupled to an electricity generator. A secondary conventional fossil-fuel-driven heat source

can be installed as back-up system to supply the power unit when radiation is unavailable or limited.

Different thermodynamic cycles can be integrated with solar thermal power plants:

- Rankine-cycle systems, using steam or other suitable working fluids;
- Brayton-cycle systems using Helium, CO_2 or air as the working fluid;
- Combined-cycle systems;
- Stirling engines.

It is noteworthy to highlight that CSP systems might not be exclusively used to generate power, but they can be applied to industrial heat processes, chemical production, water desalination, heating and cooling devices.

1.2 CONCENTRATING SOLAR POWER TECHNOLOGIES AND APPLICATIONS

Nowadays four CSP technologies have been developed: Parabolic dish systems, Parabolic trough collectors, linear Fresnel reflectors, and Solar power towers (Zhang et al., 2013).

1.2.1 Parabolic Dish

The sunrays are concentrated at the focal point supported above the center of the dish in parabolic dish collector (PDC).Usually in point focus collectors, an open cavity receiver is placed at the focal point of a parabolic mirror, but external receiver could be used due to the high concentration factor (100 -1000 suns). Parabolic dish plants show the highest solar to electricity efficiency among the CSP technologies, but they are not compatible with thermal storage and hybridization. The simplicity of the system seems feasible for mass production, but the low power capacity limits the development of this technology. Dish systems are commonly coupled with sterling engines for power generation.

The first pilot plant was the Solar Total Energy Project built in 1982 in Georgia (USA). The world's largest solar concentrating parabolic dish is the SG3 Big Dish, a prototype plant installed in 1994 at the Australian National University (ANU), in Canberra. With a 400 m^2 hexagonal aperture area, the plant was able to provide some 60 MWh of electricity to the local grid over the period 1996-2000 (Figure 1.2). The company Sterling Energy Systems (SES) developed the SunCatcher , a commercial dish-Stirling engine system for the deployment in large utility-size grid connected fields (Greenpeace International, 2009). Based on this technology, SES planned to build two different parabolic dish plants in California (NREL, 2013):

- The Calico-Solar One was designed to generate a total power of 850 MW exploiting 34000 SunCatcher dish system. The installation of the first 575 MW should be completed by 2014.
- The Imperial Valley-Solar Two, a 30000-SunCatcher dish system with a total power output of 750 MW.

- 

Figure 1-2 Prototypes of SG3 Big Dish at ANU Campus (Badr, 2013)

1.2.2 Parabolic Trough Collectors

In Parabolic trough collector a group of curved reflectors focus the sunrays onto the absorber. The mirrors are composed of sheet of reflective material (low iron glass) bent into a parabolic shape. The receiver is a metal tube with evacuated glass covering, mounted along the focal line of the linear array. A coated glass pipe encloses a black metal pipe to limit heat loss by convection and to allow the transmissivity. The metal tube is covered with selective coating to increase solar absorbance and reduce the emittance. Thermal oil is commonly used as heat transfer medium, but water is employed in direct steam generators. This system can operate at relatively low maximum temperatures usually 400°C for oil or up to 550°C for direct steam generators. The latter system presents technical challenges due to the high pressure involved in boiling and the annual average solar-to-electricity conversion efficiency is about 15% for current designs (IEA, 2011). Parabolic though collectors can be also employed to provide thermal power to industrial processes.

Solar Energy Generating Stations (SEGS) were the first commercial plants. They were built in California between 1981 and 1991providing 12TWh of electricity up to 2004.

The Direct Solar Steam (DISS) facility was installed in 1998 to test the direct generation of high-temperature and high-pressure steam in the absorber tubes. The eleven, 550m long modified Luz parabolic trough collectors (LS-3) proved the feasibility of the direct steam generation under real solar conditions in more than 4000 hours of operation. The largest plant using parabolic trough collectors is NOOR I located in Morocco. The beginning of operations is planned to be in 2015, when the system will be able to generate 160 MW of power. Parabolic-trough systems represented about 95% of all facilities in operation globally at the end of 2011 and 75% of plants under construction by mid-2012 (NREL, 2013).

Figure 1-3 Installation of parabolic trough collector at the SEGS V, California (Badr, 2013).

Figure 1-4 The collector field of the German/Spanish Direct Solar Steam (DISS) project (Badr, 2013).

1.2.3 Linear Fresnel Reflectors

Linear Fresnel reflectors (LFR) approximate the parabolic shape of the trough systems by using long rows of flat or slightly curved mirrors to reflect the radiation onto a downward facing linear receiver. Linear Fresnel systems are less capital intensive than parabolic though and they are usually employed as steam generators, since the receiver is fixed and a higher pressure is allowed. However this technology has a lower efficiency and it is difficult to install a thermal storage.

The first LFR prototype was installed in Liege in 2009. Solar Heat and Power Pty Ltd, the University of Sydney and the University of New South Wales developed the first commercial concentrating linear Fresnel array for supplying about 10 MW of thermal energy to feed-water heaters of the steam cycle of the 2 GW Liddell coal-fired power station in New South Wales, Australia. The 1.4 MW Fresnel solar power demonstration plant Puerto Errado 1 (PE 1) was installed at Calasparra (Spain) in March 2009 by the German company Novatec Solar. The plant is capable of producing 2 GWh of electricity annually. In 2010 the same company built the utility-scale 30 MW linear Fresnel plant Puerto Errado 2 (PE 2 , see Figure 1.5). The plant went into operation in August 2012 and produce 49 GWh of electricity in one year. The most recent installation is the 100MW Dhursar plant in India (expected to start operation in May 2013). Kogan Creek Solar Boost Project, currently under construction in Australia is expected to be the largest solar integration with a coal-fired power station in the world when it will be completed in 2014 (NREL, 2013).

Figure 1-5 The 30 MW PE 2 solar plant at Calasparra, Murcia, southern Spain (Badr, 2013).

1.2.4 Solar Towers

Solar power towers (SPT) are central receiver systems that use a heliostat field collector. Heliostats are usually flat or slightly concave mirrors that follow the sun by two axis tracking. In the central receiver on the top of the tower, concentrated solar radiation is absorbed by a heat transfer fluid (water, molten-salt, thermal fluid or air). However, The Weizmann institute developed the Solar Concentration Off-Tower (SCOT), also named Beam-down system. A tower-mounted secondary hyperboloid mirror redirects the concentrated solar beams downwards towards a lower focal region near ground level. A SCOT solar concentrator was recently built in Masdar, Abu Dhabi in 2013 (Mokri et al., 2013).

There are different kinds of central receiver: external tubular, cavity tubular and volumetric. Tubular systems are more appropriate for boiling processes, while volumetric receivers have been tested for high temperature applications. Porous structure increase the transfer surface and gas fluid such air with low heat transfer coefficient can be used.

Central receiver can be classified according to the working fluid used or absorber coolant: this could be liquid, gaseous or solid (Ho and Iverson, 2014).

Figure 1-6 The Beam-down solar concentrator in Masdar City, Abu Dhabi, UAE (Badr, 2013).

Liquid receiver can be organized in two classes:

- Liquid tubular receivers are composed of an array of thin-walled tubes (stainless steel or alloyed) that force the working fluid (water/steam or molten salt) in multiple passes through incident concentrated sunlight.
- Gravity force drives the fluid in *falling-film receivers*. The coolant flows along an inclined wall while it is irradiated, reducing the pumping work.

Water/steam receivers were first investigated since1981 (Aringhoff, 2005). Sodium and Nitrate salt were analyzed as working fluid, but more recently prototypes of air receivers have been developed.

Receiver that employ a gaseous coolant are subdivided in:

- volumetric air receivers: A porous structures, usually honeycombs or porous ceramics is used as absorber and the air that flows through the material is heated up to 1500°C when Silica carbide is used.
- submicron carbon particles are suspended in pressurized air and heated by concentrated sunlight in particle air receiver design.
- tubular receivers have been designed and tested by DLR for application in the order of 100 kW-1MW. The multi-layer pipes consist of Inconel material with copper sandwiched in between. The hydro-forming process enhances the heat transfer and distribution. Tubular receivers that

employ supercritical CO_2 as heat transfer have been studied because of the growing interest in supercritical-CO_2 Brayton cycle.

TSA-PHOEBUS project was the first one employing a volumetric receiver in 1993. In 1998 the Weizmann Institute introduced the first pressurized volumetric receiver. The Direct Irradiated Air Pressurized Receiver (DIAPR) consists of a high-pressure fused silica window and a compact ceramic volumetric absorber, capable of heating compressed air at 20 bar to about 1200°C (Kribus et al., 1998). In 2008, the Julich Institute and the German Aerospace Centre (DLR) tested a receiver cooled by ambient air that supply a 11.5 MW water-steam power cycle (DLR, (2009)). Finally, solid particle receivers were investigated to increase the receiver outlet temperature to over 1000°C exploiting the storage capability of the solid particles. In this kind of receiver, sand-like ceramic particles are heated by direct radiation falling through a cavity. Thermal stresses due to high temperature and high pressure fluid can be avoided (Ávila-Marín, 2011).

The first solar tower commercial plant was the Planta Solar (PS10) in Spain (Figure 1.7). It began operation in 2007, designed to produce 24 GWh. Ivanpah Solar Power Generating Station is most recent solar tower installed and it started operation at the beginning of 2014. This plant consists of three units for a total installed capacity of 392 MW and it is expected to produce 1.08 TWh of energy every year (NREL, 2013).

The integration of CSP systems into high efficiency thermodynamic cycle has been studied in the literature. Dunham et al.(2014) discussed the application of a Solar Power Tower to different power generation system (He-Brayton, regenerated CO_2-Brayton, CO_2-recompression Brayton, steam Rankine, and CO_2–ORC combined cycle) and showed that the steam Rankine cycles achieve the best thermal efficiency. Previous investigators focused their studies on thermodynamic or exergonomic optimization of central receiver applied to combined cycle. In particular, thermo-economic optimization has been done about green-field totally solar driven heliostat solar towers (Spelling et al., 2009 & 2012)

Figure 1-7 The 24 GW Planta Solar (PS10) in Spain (Badr, 2013).

1.3 CONCENTRATING SOLAR POWER TECHNOLOGIES COMPARISON

Advantages and disadvantages of the different CSP technologies must be evaluated according to the size, the location, the purpose and the budget of the specific project (Barlev et al., 2011).

Parabolic trough collectors are the most mature technology within the commercial CSP plants. PTCs are well-tested systems and they can be coupled to fossil fuel or geothermal energy sources. Synthetic oils are the most used option as heat transfer fluid, but they are expensive to manufacture and they cannot be used in high temperature systems such as solar towers. Steam can be used as working fluid but Fresnel collectors are preferable in this case. Furthermore, the operating temperature in PTC is usually around 400°C, making this technology more suitable for industrial process integration rather than for power generation. The low temperature achieved by the working fluid is partly related to the limited concentrating ratio of PTC (up to 80 suns). Increasing the solar radiation concentration, higher working temperatures and better thermodynamic efficiencies can be achieved. In solar tower power plants, very high temperatures (up to 2000°C) are reached since the amount of irradiation focused on a single receiver is larger (200–1000 kW/m2). Thus the system can operate very efficiently using complex energy conversion cycles, such as the combined cycle (Zhang et al., 2013). The reduction of heat losses and the simplification of heat transport can reduce costs (Zhang et al., 2013). In addition, the solar tower scheme can be coupled to all three thermal storage methods discussed, increasing the attraction of investors in comparison with other CSP systems. Nevertheless, the cost for the heliostat field and the receiver are still too expensive to be competitive in the market (Barlev et al., 2011).

1.4 CONCENTRATING SOLAR POWER HYBRIDIZATION

Fossil fuel back-up systems are usually installed in parallel with CSP technologies in order to supply thermal power when the sun is not available or the collected power is not sufficient due to lower irradiation. However, the utilization of such plants is limited and in order to improve utilization factor hybrid systems or thermal storage can be exploited. Hybridization of solar plants allows the use of both solar energy and fossil fuels concurrently. Issues and advantages of the hybridization of solar thermal power in electricity generation was reviewed, described, and analyzed by Williams et al.(1994). Four options for hybridization have been compared:

- Redundant system hybridization: two independent power plants are constructed, one fossil-fired and one solar-heated. The main disadvantage is the cost related to electricity redundancy, but the different heat engines can be optimized in the proper temperature range and a greater flexibility is ensured;
- Parallel fossil/heater hybridization: a fossil energy source is used in parallel with solar heater to supply a common input to the power block. The sources are at different temperatures and the working fluid is mixed prior to enter the heat engine, increasing the exergy destruction. In this case, the overall conversion efficiency of the Rankine cycle changes as the relative make-up of the solar and natural gas generated steam change. SEGS VIII and IX plants with parabolic trough collectors exploit this strategy;
- Augmented hybridization: Solar thermal power can be used as an augmentation of the fossil fuel source. In this case, the solar heat is input through only a portion of the thermodynamic cycle. The most significant benefit of this approach is that the temperature of the solar heater and the fossil -fuel burner no longer need to match. Integrated solar combined-cycle systems use this approach;
- Solar preheat hybridization: the fossil-generated heat provides temperature topping. In this approach, energy from fossil fuel combustion is used to raise the temperature of the working fluid that has previously been heated using a CSP technology, to match the thermal level required by the heat engine. The lower the temperatures difference between the sources, the higher the efficiency. Due to the high temperature involved, solar towers are preferred as CSP technology in this case.

Furthermore, Jamel et al. (2013) proved that the advantages of hybrid plant over solar only installations include:

- the opportunity for higher energy conversion efficiency;
- lower capital investment in new technology;
- higher valued energy due to dispatchability;
- lower energy cost.

Finally, it is noteworthy to highlight that retrofitting CSP technologies to existing plant is not feasible. Carbon emission cannot be significantly reduced and the

fluctuating price of the fossil fuels affects the economic return of the solar investment. For this reason, only green field systems are considered.

In order to increase the power production and dispatchability and at the same time reducing the energy costs, the hybridization with high efficient cycles and the integration with thermal storage must be considered for solar tower.

1.4.1 Concentrating Solar Power Technologies And Combined Cycle

The potential of the integration of CSP systems and combined cycle is the possibility to:

- achieve the highest possible conversion efficiency;
- supply solar heat at the highest temperature and to reach the largest possible solar share (at design conditions);
- hybrid operations, to provide dispatchable full capacity at all times.

Two options have been studied to exploit solar radiation in combined cycle:

- The thermal power harvested from the concentrated solar radiation is supplied to the compressed air in the Joule-Brayton cycle. The proposed layout of the plant is illustrated in Figure 1.8 Option II.
- The steam in the bottoming cycle is generated using the solar radiation captured by the collector system (see Figure 1.8 Option I).

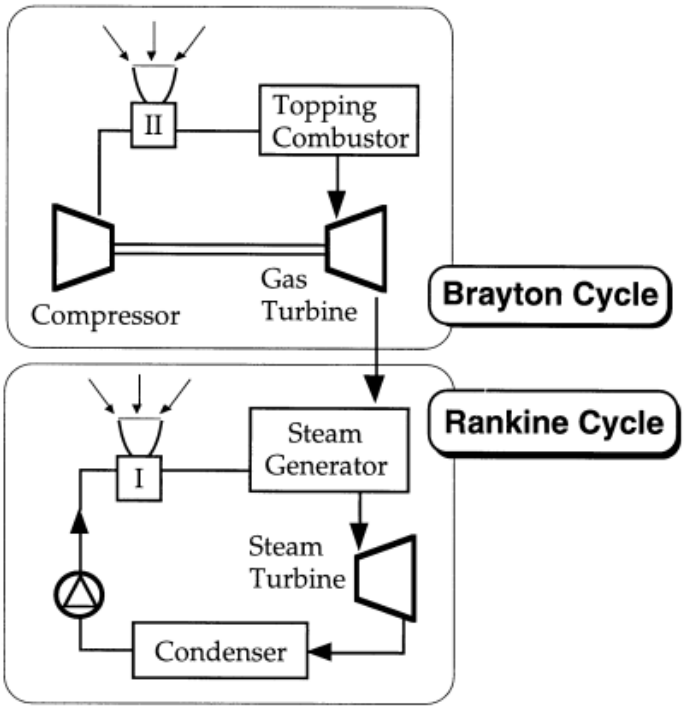

Figure 1-8 Solar hybrid combined cycle integration options (Kribus et al., 1998).

1.4.1.1 Integrated solar combined cycle

Solar energy from a parabolic-trough field can be integrated with a combined-cycle power plant to increase its efficiency. The concept of the integrated solar -hybrid CC power plants started in the early 1990s, initially proposed by Luz Solar International as a means of integrating PTCs with modern combined cycle power plants.

In an Integrated Solar Combined Cycle (ISCC), the solar heaters supply energy to the bottoming Rankine cycle of a combined cycle. Generally, there are two kinds of ISCC schemes: thermal oil systems and steam systems.

In one of the schemes, thermal oil is used as heat transfer fluid in the parabolic trough solar field. The solar thermal power is used to evaporate part of the high pressure steam. The flue gases are used to pre-heat the feed- water and to superheat the steam. HRSG are generally designed with one or two pressure levels. Steam turbine, pre-heater, super-heater and condenser of an ISCC have to be larger than the corresponding parts of a CC plant using the same gas turbine type because of the increased steam mass flow for the integrated plant. Allani et al. (1997) evaluated the feasibility of the implementation of a pilot plant in Tunisia, using the thermo-economic optimization approach. They found that the ISCC system showed several advantages compared with a purely solar steam cycle or any of the various other hybrid solar concepts existing at that time. Dersch et al. (2004) proved that ISCC plants show lower specific CO_2 emissions than optimized CC plants if properly designed and operated and they perform better than pure solar parabolic though collectors (as SEGS plants) considering 24-hours operation a day and no thermal storage. Horn et al. (2004) analyzed the technical and economic aspects of an ISCC plant to be implemented in Egypt. In this case, they compared two types of solar system for the integration: PTC field and volumetric air receiver tower. They demonstrated that both parabolic trough collectors and volumetric receiver had a positive impact on the ISCC system.

Direct Steam Generation (DSG) parabolic trough solar collector can be coupled with the bottoming steam cycle and the feed-water is directly evaporated in the solar field. Employing DGS trough, low irreversibility at the heat recovery steam generator and high system thermal efficiency were obtained. Recently Li et al. (2014) demonstrated that a two pressure stages ISCC with direct stream generation can achieve a fossil fuel saving ratio of 23.6% with solar share of 27.8%. Franchini et al. (2013) proved that the solar power production and the solar-to-electric efficiency are higher in ISCC coupled with a solar tower field because the combined effect of the higher solar tower collection efficiency and the higher CC conversion efficiency.

The first ISCC was installed in Italy in 2010. The plant employ molten salt (sodium and potassium nitrate) as the heat transfer fluid in the solar field and as heat storage medium.

More recently, Abengoa Solar developed the project of the ISCC Agua Prieta II, 470 MW power plant at Agua Prieta, Mexico, due to be commissioned in 2014

(NREL, 2013). Most of the CSP projects in the Middle East and North Africa are integrated solar-combined cycle power plants (NREL, 2013).

1.4.1.2 Solar hybrid combined cycle

Solar energy input at high temperature could be an efficient heat source for driving a combine cycle power plant. The development of collector with elevated concentration ratio and high temperature receiver allows the solar radiation to preheat the working fluid in the gas turbine. Experimental studies and analytical simulations have proved that the increase in efficiency offsets the high initial investment required for this solar application, resulting in a more effective solar electricity generation system (Schwarzbözl et al., 2006). The major advantages of solar gas turbine systems compared to other solar-fossil hybrid power plants are the high solar shares with high conversion efficiencies. Solar shares of 40%up to 90% can be realized in the design case and annual solar shares up to 30% can be achieved in base load. The conversion efficiencies of the solar heat can vary from around 40% up to more than 50%, using modern gas turbine systems (with recuperator or combined cycle mode) (Schwarzbözl et al., 2006). Kribus et al. (1998) analyzed the performances of a SCOT/CC hybrid plant. Employing the beam down collector that focused the solar radiation on a multistage DIAPR receiver, they demonstrated that this technology offers the potential for high performance and low installed cost and levelized electricity cost.

Solar preheating at the topping Brayton cycle was proposed by Bohn et al. (1995). They showed that this scheme offers high conversion efficiency but limited solar contribution to the plant's overall electricity production. Price et al. (1996) proposed a hybrid solar tower system using high concentration optics and high temperature air receivers to drive the CC power plant. They analysed the solar energy use at a high exergy level as a heating source for the topping GT cycle. Kolb (1998) examined the economic potential of using different configurations of hybrid and solar-only tower power plants. Results showed the hybrid plants are more economical compared with solar only power plants for solar tower integrated to combined cycle and coal-fired power plants. More recently, Heide et al. (2010) proposed a new configuration of CC with solar tower. The solar heat directly feed the gas turbine between the compressor outlet and the combustor inlet, increasing the solar share. They named this alternative configuration Solar Hybrid Combined Cycle (SHCC).

Solar-hybrid gas turbines with combined cycle systems shows interestingly low expense for moderate power level in centralized electricity generation. Cost comparable with ISCC plants can be achieve with a smaller system (16 MW instead of 310 MW) and with a significantly higher solar share (28% instead of 9%). Small-scale plants (<5–10 MW) should be applied in distributed markets using cogeneration to be economically feasible (Schwarzbözl et al., 2006).

Solar hybrid gas turbines have a high potential since they present high efficiency power conversion systems and the advantages of hybrid power

plants: variable solar share, fully dispatchable power, 24 hours operation without storage. This could be an important step towards cost reduction of solar thermal power.

1.5 AIMS AND OBJECTIVES OF THE CURRENT STUDY

In the present work the integration of concentrating solar energy technologies with combined cycles is assessed. The aim of this thesis is to analyze and compare the performances of two different integration schemes: the solar hybrid combined cycle system, described in Chapter 2 and the integrated solar combined cycle plant (Chapter 4). Parabolic trough collectors are used to supply additional heat to the Rankine cycle power block in the ISCC scheme. In the SHCC arrangement, the solar energy is used to pre-heat the combustion air in the gas turbine power block. A pressurized volumetric receiver and a solar tower system are used to collect the solar radiation.

The energy and exergy efficiencies and the levelized electricity cost of the two systems are compared in order to evaluate the advantages and disadvantages of the different arrangements (Chapter 6). The comparison is aimed to identify critical issues related to solar energy integration with combined cycle power plants and to specify the most significant points to be developed in future works.

The following steps will be covered to reach the final objective:

- Implement a mathematical model for the SHCC and perform the energy and exergy analysis of the system.
- Define the total costs and the levelized electricity cost of the plant.
- Develop the mathematical model for the ISCC system to evaluate the energy and exergy efficiency;
- Determine the total cost and the levelized electricity cost for the considered ISCC power plant;
- Compare the performances of the SHCC plant with the ones of the ISCC systems to define the future development needed to achieve the best integration of combine cycle with concentrating solar power technologies.

2 MODELLING THE SOLAR HYBRID COMBINED CYCLE SYSTEM

2.1 MODEL DESCRIPTION

A diagram of the solar hybrid combined cycle considered in this study is represented in Figure 2.1. The plant consists of a heliostat field, a solar tower equipped with a pressurized volumetric receiver, a gas turbine and a heat recovery steam generator which supplies thermal energy to a steam Rankine-cycle power system.

The heliostats concentrate the solar radiation onto the aperture area of the volumetric receiver where pressurized air is pre-heated. A detailed description of the pressurized volumetric receiver is given in Section 2.1.1. The pre-heated air enters the combustion chamber of the gas turbine, where fossil fuel burns to provide the energy necessary to reach the rated turbine inlet temperature. The gas turbine generates the power from the expansion of high pressure and temperature gases and the thermal energy available in the exhaust gases is recovered in the waste heat boiler or Heat Recovery Steam Generator (HRSG). Refer to Chapter 2.1.2 for specific information related to the gas turbine system. Finally, the steam generated in the HRSG runs the bottoming Rankine cycle. The assumptions and the parameters selected for the design of this part of the system are reported in Section 2.1.3.

2.1.1 Pressurized Volumetric Receiver

The German Aerospace Center (DLR) and its partners have developed a prototype of pressurized volumetric receiver to demonstrate the feasibility of introducing solar energy into the gas turbine of combined cycle power generation systems (Buck et al, 2002). They first developed the Refros volumetric receiver: it consists of a secondary concentrator mirror coupled with a pressure vessel where the absorber material is located. A domed quartz window was selected to separate the ambient from the pressurized chamber. Figure 2.2 represents a schematic diagram of the Refros receiver. The secondary concentrators were introduced to increase the radiation flux incident on the absorber. Increasing intensity of the incident solar energy allows the air to reach a higher temperature. In the first prototype the absorber was made of several layers of heat-resistant wire screens (Inconel 600).

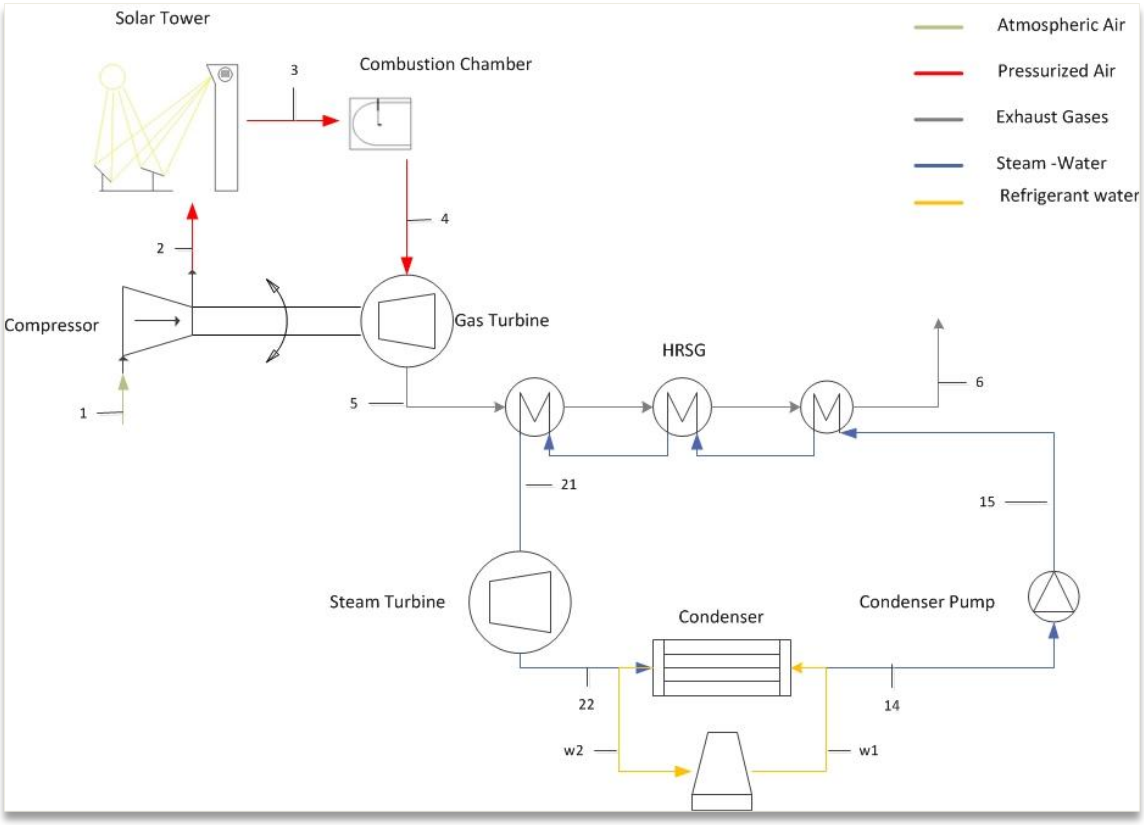

Figure 2-1 Solar hybrid combined cycle diagram

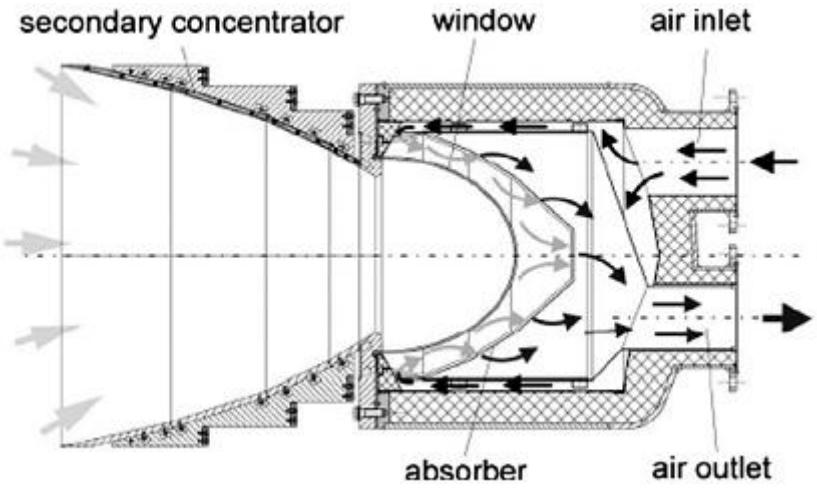

Figure 2-2 Refros receiver module (Buck et al., 2002)

Starting from 1996, theoretical analysis and experiments have been carried out to evaluate the performance of the secondary concentrator and to demonstrate the thermal efficiency and the reliability of the system. The tests proved that by modifying the shape of the secondary concentrator, the optical efficiency of these elements can be improved to 86% (Buck et al, 2002). During the experiments in 2002 in the CESA-1 tower facility in Plataforma Solar de Almeria (Spain), for the first time a pressurized volumetric receiver withstood an input thermal capacity up to 400kWth at 15bar without damage. One important advantage of this system was the low pressure drop achieved (18 mbar only) (Heller 2006; Ho and Iverson 2014). Problems related to the degradation of the window surface arose even though these tests were short compared to lifetime requirements.

Many studies have focused on the possibility to integrate CSP technologies to industrial gas turbines systems. Among these, the European Commission funded the Solgate project started in 1998 with the main goal of developing a solar receiver cluster able to provide pressurized air at 1000°C to feed a conventional gas turbine. The pressurized solar receiver system consisted of three 400 kW_{th} Refros modules. Each element was equipped with a secondary concentrator. The modules had a hexagonal aperture and were connected in series (Figure. 2.3(a)). The low temperature receiver (top module in Figure 2.3(b)) was developed in order to decrease the overall cost of the receiver employing cheaper material for the first heating stage. In this case a multi-tube coil was employed in combinations with the secondary concentrator (Figure 2.4). The optimized layout consists of 16 tubes connected in parallel, each with a length of 2.3 meters and a diameter of 28 millimeters. This concept was selected to reduce mechanical stresses and increase the heat transfer coefficient ensuring higher performances. The medium temperature receiver and the high temperature modules (in the middle and at the bottom of Figure 2.3(b) respectively) have the structure of the Refros pressurized volumetric receivers. In the high temperature receiver the metal-wire absorber was replaced with a ceramic one in order to meet the target temperature (1000°C). The ceramic absorber was made of silicon carbide (SiC) with 20 ppi porosity coated with a silica layer and tempered to increase absorbitivity to 96%. The geometry was defined using ray tracing calculation (Avilà-Marin, 2011).

The metal casing of the typical Refros system was replaced by a fiber-reinforced alumina-based supporting structure. In order to limit the material amount and the cost, 12 rib segments held together by two clamping rings were selected as final layout (European Commission, 2005).

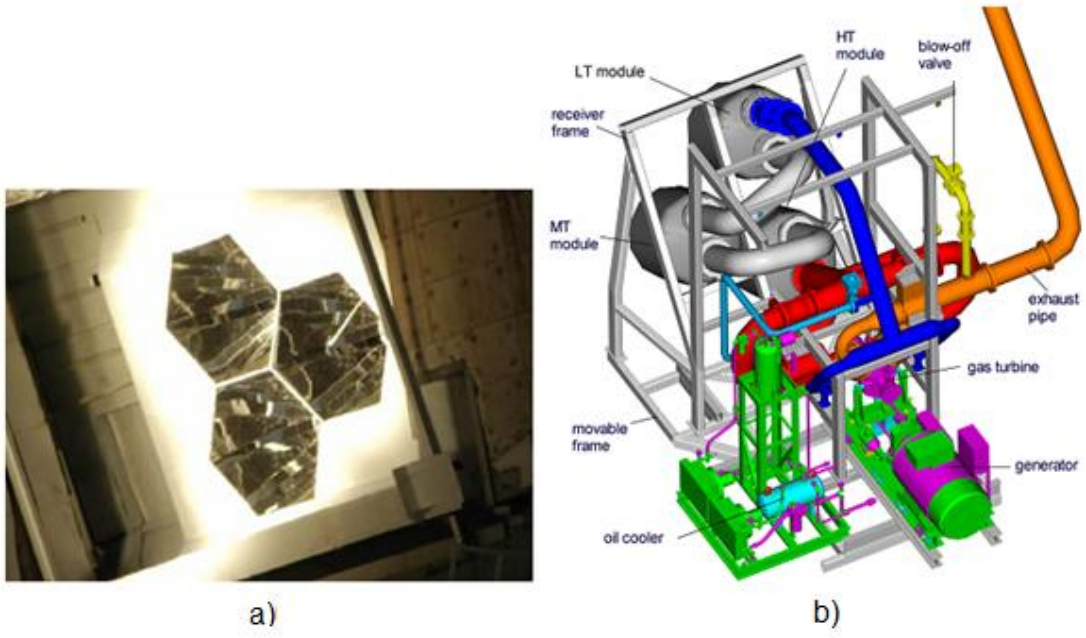

Figure 2-3 Solgate receiver cluster. a) receiver aperture area b) solar cluster final layout (European Commission 2005).

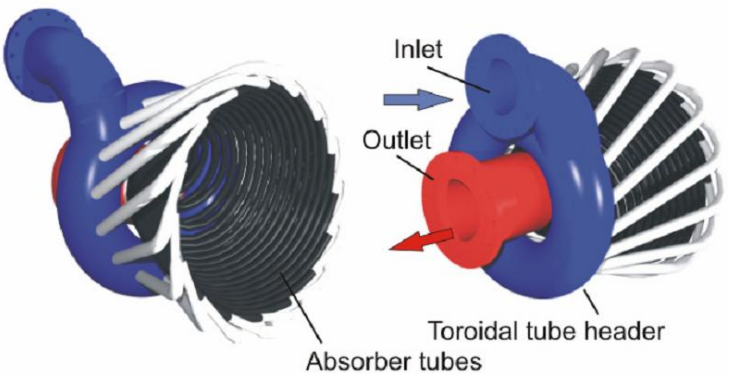

Figure 2-4 Schematic view of the low temperature module (European Commission, 2005).

The high temperature module window is cooled by an active outer cooling system, as particularly at high temperatures, re-crystallization of the quartz

glass could occur. Air jet blowers are installed to cool the windows. Simulations demonstrated that a system with 18 nozzles is the best configuration. The computed parasitic consumption for the cooling system is estimated as the 0.2% of the produced power, for the tested small scale gas turbine (European Commission, 2005).

The testing campaign for the receiver cluster was divided into two parts. In the first stage, the ability of the receiver to provide enough power to supply a modified helicopter engine gas turbine was proved. The average air temperature outside the receiver reached the design operating conditions of 800°C. In the second stage, the target receiver outlet air temperature was increased to 1000°C using the innovative high temperature Refros element equipped with the ceramic absorber. In this occasion, the receiver outlet temperature arose to 960°C when the direct normal irradiation was about 770W/m^2 and the receiver efficiency was 70%. The pressure drops across the medium and high temperature modules were 20 mbar, while the pressure decreased by 150 mbar in the low temperature section (European Commission, 2005; Heller 2006; Heide, 2010). The target temperature was not achieved due to a lack in the control system of the turbine. However, the experiments showed that temperatures close to common gas turbine working temperatures can be reached using solar power and the flow pressure can be controlled. The system performance appeared promising for future solar power generation systems and for this reason it was decided to apply this technology to the current study.

Several analyses have been done on the receiver optics in solar tower power plants. Two main solutions have been developed: Tower-Top central receiver and Tower Reflector central receiver (Segal and Epstein, 1999). In Tower-Top systems, the receiver is mounted at the top of the tower. The power block can be installed at the same level of the receiver or at the ground. In Tower Reflector systems a hyperbolic mirror redirects the concentrated solar beams toward the aperture area of the receiver which lies at the bottom of the tower. This solar tower layout is also known as Solar Concentration Off Tower (SCOT) system or Beam-Down receiver. Although this kind of arrangement is becoming popular in the Middle East, Segal and Epstein (1999) have demonstrated that none of the described optical technologies have a significant optical advantage. An economical optimization should be carried out to determine the best option. A Tower-Top central receiver is considered in the current study, with the power block installed at ground level. Table 2.1 report the specifications related to the pressurized volumetric receiver and heliostat field that are assumed to model the solar field (Section2.2).

Table 2-1 Pressurized receiver cluster specification

Max air Outlet Temperature	960	°C
Pressure	15	bar
Total Pressure drop	200	mbar
Low Temperature Module Pressure Drop	150	mbar
Medium Temperature Module Pressure Drop	20	mbar
High Temperature Module Pressure Drop	20	mbar

2.1.2 Gas Turbine Power Block

Recent studies in the literature focused their effort in accessing the performances of innovative hybrid systems such as SHCC plants and in simulating up-scaled plants with power between 5-30 MW (European Commission, 2005; Heller, 2006; Heide, 2010; Ho and Iverson 2014).

Since gas turbines have not been designed for application in solar hybrid power plants up to now, theoretical studies have been carried out considering several power block arrangements. In the Solgate project, a small scale Heron H1 recuperated gas turbine (1.2 MW), a 4 MW Solar Mercury 50 and the Nuova Pignone PTG 10 gas turbine coupled with a Rankine bottoming cycle (total electrical power 16 MW) were considered as the power generation unit to be coupled with the volumetric receiver cluster. The combined cycle configuration with an annual solar share of 16% working for 24 hour was the arrangement that gave the lowest levelized electricity cost (0.06 €/kWh). The LEC increased for the case when the plant runs during solar hours only (European Commission, 2005). More recently, Heide et al. (2010) analyzed the performance of a MAN TURBO 1304 solar-hybrid gas turbine in a solar-hybrid combined cycle. They modelled the performances of direct and indirect systems. In the direct arrangement, two solar-hybrid gas turbines feed a steam generator. In the indirect system, a closed CO_2 cycle exchanging heat with the air and the feed water was simulated. They concluded that any preference to the one or other system designs depends on the proportion between fossil fuel costs and solar installation costs, but an economic analysis was not carried out. This publication demonstrated that the most important design feature of gas turbines suitable for the integration of solar heat is the possibility to split the flow pass in between the compressor exit and the combustor inlet in order to integrate the solar receiver (Heide, 2010). The maximum firing temperature

also is a fundamental factor influencing the combined cycle integration with CSP technology. Nowadays receiver outlet temperatures in the range 850 - 950°C are practicable. The gas turbine should reach full load at a turbine inlet temperature close to these values in order to limit the fuel consumption in hybrid systems.

Taking into account these key points, the gas turbine considered in this study will have the characteristic described in Table 2.2. The rated power at ISO conditions is 10660 kW, with a thermal efficiency of 32.5%. The cooling mass flow rate is assumed to be zero for this gas turbine. Considering part of the compressed air to be used to cool the blades of the turbine, the process temperature and the specific fuel consumption increase. This means that if some compressor air is bled off, then this would result in the process temperature and the specific fuel consumption increasing (Heide, 2010). A more detailed analysis should consider this factor in the future.

Table 2-2 Gas turbine parameters.

Shaft output (ISO condition)	10660	kW
Efficiency (ISO condition)	32.5	%
Combustion Air Flow	42.3	kg/s
Compressor Pressure Ratio	15:1	[-]
Turbine Inlet Temperature	1100	°C
Compressor isentropic efficiency	84	%
Turbine isentropic efficiency	91	%

2.1.3 Rankine Cycle Power Block

The bottoming cycle system considered in the current study comprehends (see Figure 2.5):

- Single Pressure Level HRSG: a typical waste heat boiler is considered in this study. The feed-water is pre-heated in two economizers. A deaerator is installed the removal of oxygen and other dissolved gases from the water stream. The steam is generated and then superheated by the hot exhaust gas in the evaporator and super-heater sections;
- Steam turbine: the water vapor is expanded is a single stage steam turbine

- Condenser: steam is reduced to saturated liquid in a shell and tube heat exchanger with evaporative tower;
- Condensate pump: pump is needed to recycle the saturated water;

Previous publications have demonstrated that a two pressure level HRSG should be chosen in order to increase the cycle efficiency (Spelling et al., 2009 & 2012), but for the sake of simplicity only one pressure level steam generator is analysed in this study.

No supplementary firing is considered and re-heating sections are not included in the Waste Heat Boiler. Dry cooling is recommended for application with CSP technologies since they are usually installed in desert area and the water consumption should be limited (Heide, 2010). In the current analysis the condenser is assumed to be a shell and tube heat exchanger using water as the coolant. The cooling water is chilled in an evaporative tower. The values of the inlet and outlet temperature are assumed to be constant throughout the day and are determined considering typical combine cycle plant technologies examples (Lozza, 2007). Table 2.3 reports the values of the main parameters assumed to model the system for the current study. They are taken from the current literature (European Commission, 2005 ; Heide, 2010). The ΔT pinch point in the condenser is the temperature difference between the condensing steam and the coolant at the outlet section. Further studies should investigate the effect of dry-cooling on the performance of the plant.

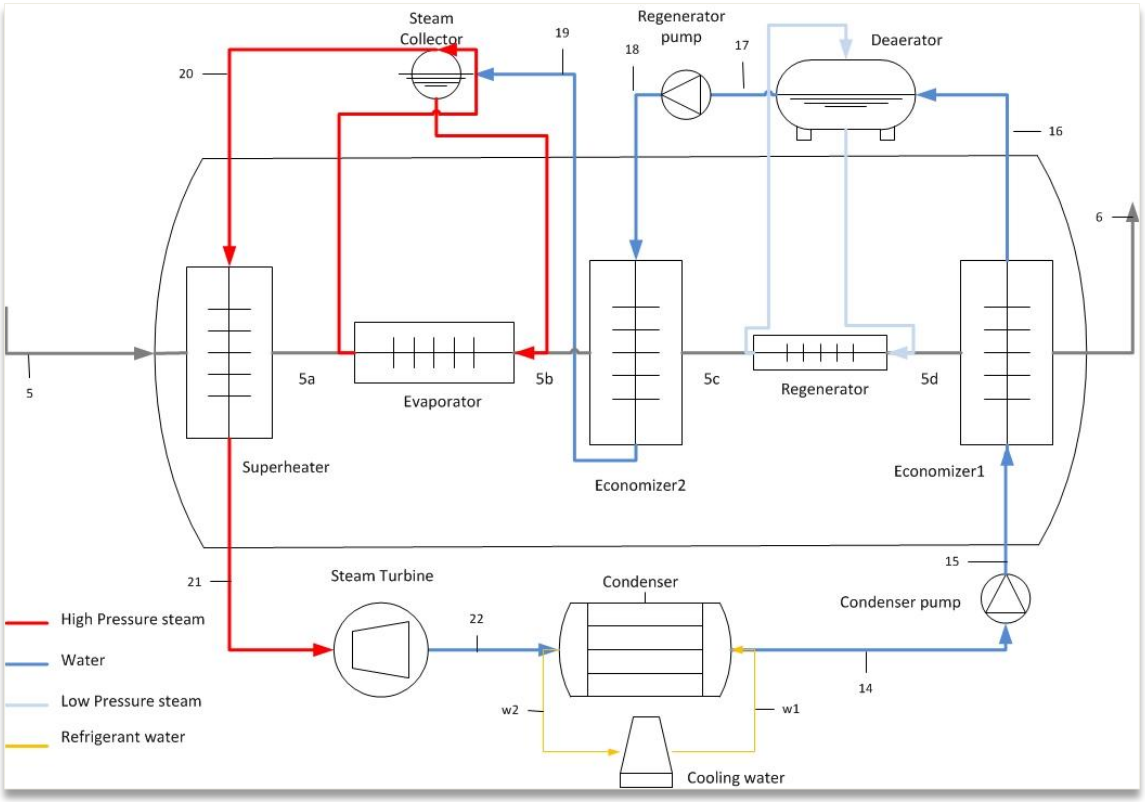

Figure 2-5 SHCC bottoming Rankine cycle power block diagram

Table 2-3 Rankine Cycle Parameters

Steam Turbine isentropic efficiency	91	%
Condensation Pressure	0.05	bar
ΔT pinch point	10	K
ΔT approach	15	K
ΔT sub-cooling	2	K
ΔT water in tower	10	K
ΔT pinch condenser	3	K

2.2 ENERGY ANALYSIS

The thermodynamic model of the SHCC system is described in this section. The model of the plant has been developed based on the energy balance of each component.

The following general assumptions have been taken into consideration and are valid for all the systems:

- All gases are treated as ideal gases,
- All chemical reactions are in equilibrium;
- Internal distribution of temperature, pressure, and gas compositions in each component are uniform;
- All kinetic and potential effects are negligible;
- Constant pressure loss ratios are considered in the system components;
- All system components are adiabatic.

2.2.1 Modelling The Solar Field

Specific software can be used to design and optimize the heliostats arrangement and the receiver area in order to minimize the number of concentrators, the occupied land and thus the investment cost. Since these programs are licensed, the optimization is not considered in the current work. These programs can be based on two different calculation methods (Augsburger and Favrat, 2013):

- In convolution-based codes the solar radiation is estimated using a statistical distribution of the sun disc intensity. The distribution of the power intercepted by the receiver is obtained by the convolution of the defined sun shape reflected by each heliostat taking into account heliostat slope and tracking errors. HFLCAL by DLR have been developed considering a normal distribution of the sun power since this simplifies the mathematics without significant errors;
- The ray-tracing codes simulate a large amount of rays from virtual sources. These rays are blocked or reflected by the virtual objects placed within the environment. In this way the amount of ray incident on one of these objects can be measured. SolTrace by NREL use a Monte Carlo ray-tracing code.

It is noteworthy to highlight that the installation of the secondary concentrator on the pressurized receiver influences the layout of the heliostat field. The reduced acceptance angle of the receiver cause the heliostat field to be to longer and more stretched than usual, with mirrors more distant from the

receiver supporting structure. The tower has to be built higher than usual. Future analysis should consider these aspects to correctly set the optimization tools.

In this study, the main characteristic of the solar field to be modeled are: the collected power at the receiver surface, the heliostat reflective area, the receiver thermal efficiency, the heliostat optical efficiency. A simple code implemented in Matlab is used to estimate these parameters. The assumptions and equations used to develop the design tool are explained in the following paragraphs. The code executes the following instructions:

- compute the receiver efficiency (η_{rec}) given the radiation flux density (I);
- calculate the power intercepted by the heliostat field knowing the design power at the receiver;
- interpolate the efficiency of the heliostat field;
- compute the heliostat field area, given the power and the efficiency;
- Calculate the maximum distance of the last mirror (the length of the field);
- Determine the diameter of the sun images considering optical errors. This value represents the receiver area (A_{rec});
- compute the radiation flux incident on the receiver;

This procedure is iterated until the value of the power collected by the mirrors converges (the difference between the consecutive value is lower than a defined tolerance error assumed to be 1.0 W).

The following assumptions have been made to build the model of the solar system:

- The thermodynamic properties of the fluids are computed using Refprop library;
- The reference point conditions are defined at 298 K and 1 bar;
- The receiver cluster is modelled as a single unit. Furthers analysis should consider the temperature difference within the high, medium and low temperature modules;

The thermal power absorbed by the receiver is limited by maximum temperature that the materials can withstand. For this reason the design thermal power delivered to the pressurized air can be calculated as:

$$\dot{Q}_{rec,design} = \dot{m}_{air} \cdot (h_{rec,\max} - h_{rec,in}) \tag{2.1}$$

where $\dot{m}_{air}$ is the pressurized air mass flow rate (see Table. 2.2), $h_{rec,in}$ is the enthalpy of the air at the outlet section of the compressor and $h_{rec,\max}$ is the enthalpy of the air at the maximum receiver temperature.

The thermal efficiency of the receiver (η_{rec}) is defined as the ratio between the heat delivered to the working fluid and the intercepted power at the receiver aperture area. Assuming that the absorbed radiations energy is totally transferred to the air, the main losses involved in the receiver are due to thermal radiation emission and convection. Ho and Iverson (2014) introduced the following equation to express the receiver thermal efficiency:

$$\eta_{rec} = \frac{\alpha \cdot \dot{Q}_{in} - \dot{Q}_{loss}}{\dot{Q}_{in}} = \alpha - \frac{F_{view} \cdot \varepsilon \cdot \sigma \cdot T_{rec}^{\ 4}}{I} - \frac{f_{conv} \cdot H \cdot \left(T_{rec} - T_{amb}\right)}{I} \tag{2.2}$$

where α and ε are the total absorbitivity and emissivity of the absorber material respectively. In the current study the receiver is modeled as a grey body with an absorbitivity of 0.96 and an emissivity of 0.85 (European Commission, 2005; Ho and Iverson 2014). For the sake of simplicity, in this work the receiver cluster is model as a single element and the detailed analysis of the different modules interaction will be carried out in the future. T_{rec} is the design receiver outlet temperature for the working fluid. As it has been explained in Section2.1.1 the highest temperature that can be achieved in modern pressurized receiver is assumed to be 960°C. F_{view} is the view factor used to calculated the actual radiations emitted by the absorber in the receiver cluster. A simple enclosure can be defined to model the thermal radiation heat exchange inside the receiver:

- Surface 1: The absorber is assumed to be a perfect hemisphere emitting to the surrounding as a grey body;
- Surface 2: The surrounding ambient can be modeled as a plane grey surface that corresponds to the end section of the secondary receiver. Refer to Figure 2.6.

It can be easily demonstrated that the view factor of the hemispheric surface to the plane corresponding to the sky is 0.5.

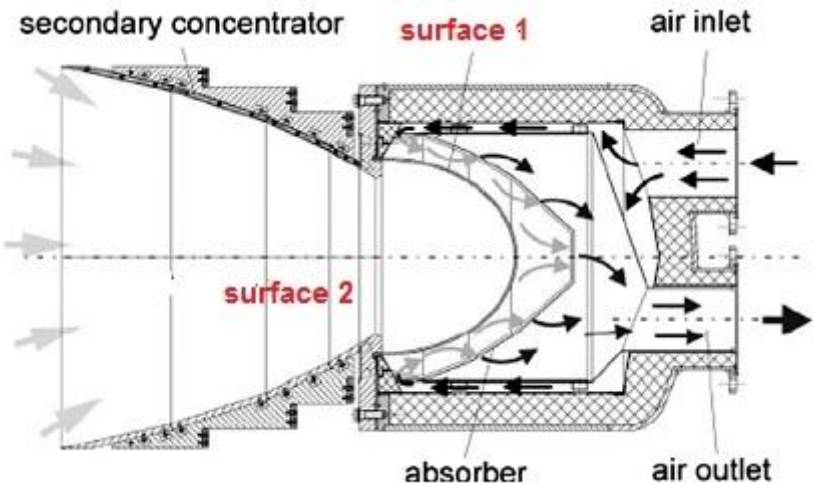

Figure 2-6 Receiver enclosure

In order to estimate the convection losses from the hot surface of the absorber to the ambient air, the convective heat transfer coefficient H should be computed. The parameter f represents the weight factor for the convection losses. The value of H and f can be calculated using specific correlation related to the shape of the receiver that can be found in the literature (Epstein, 1999). For pressurized volumetric receivers, the convective heat transfer coefficient can be assumed to be zero because the thermal exchange with the external air through convection are negligible compared to radiation losses (European Commission, 2005). Equation (2.3) was developed for any receiver and it does not consider the effect of the secondary concentrator. These mirrors introduce optical losses and the average value of the secondary concentrator efficiency is assumed to be 90.2% (European Commission, 2005). The receiver thermal efficiency depends on the incident radiation flux on the aperture area, namely I . This variable can be expressed as the ratio between the power concentrated onto receiver and the receiver area. The receiver thermal efficiency is higher when the incident flux increases. For this reason the secondary collectors have been introduced.

Given the design power to be transferred to the fluid and the receiver thermal efficiency, it is possible to evaluate the thermal energy which the heliostat field must be able to concentrate on the receiver aperture area:

$$\dot{Q}_{helio} = \frac{\dot{Q}_{rec,design}}{\eta_{rec}} \tag{2.3}$$

The thermal power at the receiver aperture area must be the same reflected by the heliostat field. For this reason, it is possible to use the Equation (2.4) to estimate the solar field surface:

$$\dot{Q}_{helio} = \frac{DNI}{1000} \cdot A_{field} \cdot \eta_{field} \tag{2.4}$$

The term η_{field} is the heliostat field efficiency. Several variables influence this parameter. Part of the incident solar radiation can be shadowed or the reflected beams can be blocked by other mirrors. The losses caused by adding distance between a heliostat and the receiver are called Atmospheric losses: refraction and reflection due to particles can reduced the concentrated power and this phenomenon increases when more air is interposed between the heliostat and the receiver. Optical and tracking errors (also called astigmatism) deviate part of the radiation from the target: this is known as the spillage effect. The most significant inefficiency of the heliostat field is due to the fact that the collectors cannot always face the sun at 90°. The effective area is therefore reduced by a factor equal to the cosine of the angle at which the mirror is tilted respect to the normal radiation plane. This is called cosine effect (Epstein, 1999).

In the current study, the field efficiency has been estimated using empirical correlation, interpolated from real HFLCAL data (Turner, 2014). The efficiency has been expressed as a function of the thermal power at the receiver.

For the sake of simplicity, the field is assumed to be rectangular. The length is assumed to be two times longer than the width of the field. The first line of collector is usually installed at a minimum distance from the tower ($d_{\min}$) to guarantee that most of the radiation reach the receiver; in the current study the gap between the first heliostats and the tower is equal to one half of the tower height. It can be easily demonstrate that the distance of the last row of collectors is given by Equation 2.5:

$$L_{field} = \sqrt{\frac{2 \cdot A_{field}}{\mathrm{P}_{field}}} + d_{\min} \tag{2.5}$$

where P_{field} is defined as the heliostat field density. This variable represents the ratio between the total reflective surface of the collectors and the land area occupied by the systems. For the purposes of this analysis, the field density is assumed to be 0.2: this value is typical for small solar power tower plant (Collado, 2007). Note that the field density should be one of the parameters to be optimized using specific design software and this variable affects the efficiency of the field.

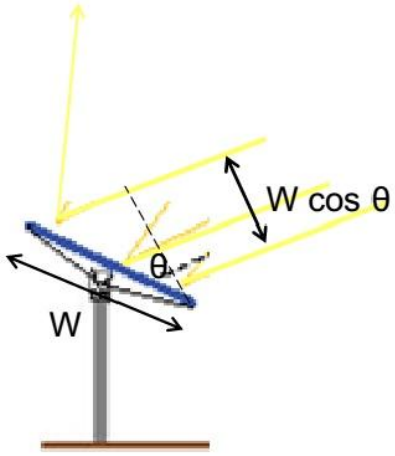

Figure 2-7 Cosine effect (Turner, 2014)

The image of the sun reflected on the aperture area of the receiver depends on the focal distance of each mirror: the closer the collector, the smaller the sun spot. For this reason the size of the sun image, also called the minimum beam diameter is determined by the distance of the last row of heliostats (Figure 2.8).

Moreover, the dimension of the spot is affected by the slope error. It is defined as the standard deviation of a normal probability distribution describing the deviation of the normal vector of the heliostat reflecting surface with regard to the one of an ideal reference surface, this means, free of optical errors. Due to the slope error, the surface needed to intercept the radiation flux increases. In this study a slope error of 1.5 mrad is assumed.

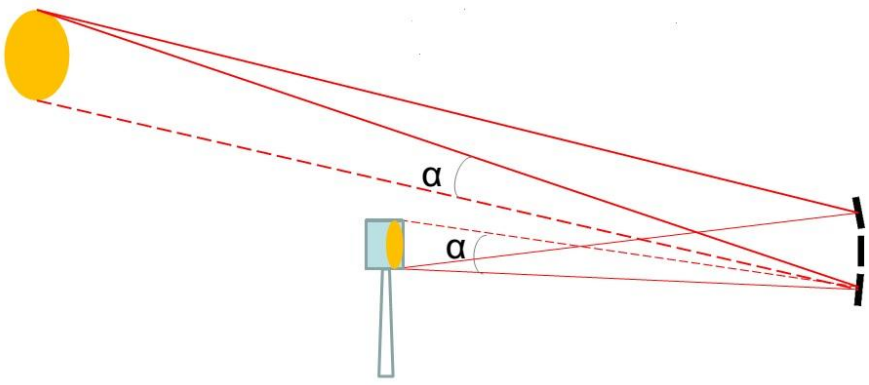

Figure 2-8 Sun image and minimum beam diameter (Turner, 2014)

Furthermore, the tracking error refers to the error in the mechanism for tracking the sun and getting the image to be aligned with the intended target. This will cause a loss if the sun's image is large or if the image is targeted close to the edges of the receiver. In the current study, the tracking error is assumed to be 0.3 mrad.

Finally the size of the sun image can be computed considering the collector optics just described. The following mathematical correlation defines the beam diameter as a function of the distance of the collector from the receiver (Turner, 2014):

$$D_{rec} = 0.0129 * \mathrm{L}_{field} + 0.0214 \tag{2.6}$$

We assumed that the aperture area of the secondary receiver (or the receiver aperture area) should be able to intercept all the concentrated power and it has to contain the sun image. For this reason we defined the receiver aperture area as:

$$A_{rec} = \pi \frac{\mathrm{D}^2_{rec}}{4} \tag{2.7}$$

The average incident flux radiation can be calculated as:

$$I = \frac{\dot{Q}_{helio}}{A_{rec}} \tag{2.8}$$

The simple model explained in this Section has been validated considering the experimental result from the Solgate project (European Commission, 2005). The chosen location is Dagget (California, USA), with a given annual direct normal radiation of 2791 kWh/m^2 and a designed solar share of 58%. Refer to Appendix A for the calculations.

2.2.2 Modeling Of The Power Block

The power block model is based on energy balances. The equations used to develop the models of the several parts of the plant are reported. The following assumptions should be considered for the power block system analysis:

- Steady state and steady flow working conditions;
- Methane is used as fossil fuel.

The program Refprop is used to determine the thermodynamic properties of the different working fluids. The Refprop subroutine software implemented in Matlab computes the required thermodynamic variables for pure substance (like water),

predefined mixtures (air), or user defined mixtures (such as flue gases) using the following syntax:

```
result=refpropm(prop_req,  spec1,  value1,  spec2,  value2,
substance1)
```
(2.9)

```
result=refpropm(prop_req,  spec1,  value1,  spec2,  value2,
mixture1)
```
(2.10)

```
result=refpropm(prop_req,spec1,value1,spec2,          value2,
sub1,sub2,.., x)
```
(2.11)

where the term x represents a vector containing the mass fractions for each substance in the mixture. The properties are computed according to the International System of Units. The reference state conditions are 0 K and 1.013 bar.

Refprop does not calculate the mixing entropy of a mixture. For these reason this value has been computed considering the partial pressure of each component.

2.2.2.1 Compressor

The thermodynamic performances of the gas turbine unit are evaluated computing the compressor and turbine performances.

The real mechanical power required by the compressor can be computed as:

$$\dot{W}_{AC} = \dot{m}_{air} \cdot (h_2 - h_1) \tag{2.12}$$

where h_1 is the enthalpy at the compressor inlet section and it is computed using Eq. 2.10. The value of the air enthalpy at the compressor outlet section (h_2) can be determined applying the definition of the isentropic efficiency:

$$\eta_{is,AC} = \frac{h_{2,is} - h_1}{h_2 - h_1} \tag{2.13}$$

where h_{2is} is the air enthalpy after an isentropic compression and it can be easily computed with Equation (2.10) knowing the value of the entropy at inlet section and the compressor pressure ratio.

2.2.2.2 Combustion Chamber

The model adopted to simulate the combustion chamber is the one presented by Shirazi et al. (2012) and it is based on the following energy balance:

$$0 = -\dot{Q}_{losses} + \sum_{R} \dot{n}_i \cdot \bar{h}_i - \sum_{P} \dot{n}_j \cdot \bar{h}_j \tag{2.14}$$

where $\dot{Q}_{losses}$ represents the thermal losses in the burner and it is considered to be constant and equal to zero. The parameter $\dot{n}$ defines the molar flow rate while the enthalpies of the products and the reactants are computed considering the enthalpy of formation of each chemical species defined respect to the reference point condition:

$$\bar{h} = \bar{h}_0 + \int_{T_0}^{\bar{T}} \bar{c}_p(\mathrm{T}) dT + \Delta h_f^0 \tag{2.15}$$

The values for the enthalpy of formation and for the specific heat capacity are taken for the literature (Perry, 2008). The combustion is assumed to be ideal: this means that all the fuel is burned and no by-products such as CO and NO_x are generated. The flue gases are composed by carbon dioxide (CO_2), water vapor (H_2O), excess oxygen (O_2) and nitrogen (N_2).

Given the inlet air mass flow rate and temperature, the combustion chamber model computes the fuel consumption necessary to be burned in order to reach the desired turbine inlet temperature. The flue gases composition (molar and mass fractions) and mass flow rate are also calculated.

2.2.2.3 Gas Turbine

The real mechanical work generated by the expansion of the flue gases is computed as:

$$\dot{W}_{GT} = \dot{m}_{fg} \cdot (h_4 - h_5) \tag{2.16}$$

The gas flow rate is determined by the combustor model. The enthalpy of the flue gases at the gas turbine inlet section is calculated using Equation (2.11).

Similarly to the compressor model, the enthalpy of the exhausts can be computed using the definition of the isentropic efficiency:

$$\eta_{is,GT} = \frac{h_4 - h_5}{h_4 - h_{5,is}} \tag{2.17}$$

The enthalpy of the exhaust gas after the isentropic expansion ($h_{5,is}$) can be found with Equation 2.11 ones the temperature at this point have been determined. Assuming a polytrophic transformation, the isentropic temperature at point 5 can be computed as:

$$T_{5,is} = T_4 \cdot \beta_{GT}^{\frac{k-1}{k}} \tag{2.18}$$

where β_{GT} is the gas turbine pressure ratio and it can be expressed as:

$$\beta_{GT} = \frac{P_4}{P_5} \tag{2.19}$$

k is the polytrophic index and for an adiabatic transformation is defined using the Mayer equation:

$$k = \frac{c_p}{c_v} \tag{2.20}$$

The numerical value of the polytrophic index is determined at the turbine inlet temperature using Equation (2.11).

2.2.2.4 Heat recovery steam generator and rankine cycle

The live stream pressure is determined considering the optimal evaporation temperature for the specific heat-recovery cycle. For a single pressure ideal heat-recovery cycle, the evaporation temperature which maximizes the recovery efficiency can be defined as (Lozza, 2007):

$$T_{evap} = \sqrt{T_{fg} \cdot T_0} \tag{2.21}$$

where T_{ex} is the average exhaust gas temperature at the outlet section of the gas turbine, while T_0 is the reference temperature set to 298 K.

Considering the energy balance at the different elements inside the waste heat boiler it is possible to determine the thermodynamic properties of the water-steam and the exhaust gases. Taking into account the assumptions made in Section 2.1.3, the energy balance between the super-heater and the evaporator states that:

$$\dot{m}_{steam} \cdot (h_{21} - h_{19}) = \dot{m}_{fg} \cdot \int_{T_{5b}}^{T_5} cp(T)dT \cdot (1-\xi) \tag{2.22}$$

The enthalpies of the water at the inner section of the evaporation (h_{19}) and at the outlet section of the super-heater (h_{21}) can be computed using Equation (2.9). The evaporation temperature has been already determined using Equation (2.21), while the temperature of the super-heated steam is defined as:

$$T_{21} = T_5 - \Delta T_{approach} \tag{2.23}$$

where the value of $\Delta T_{approach}$ has been assumed is Section 2.1.3. The parameter ξ represents the loss coefficient in the analyzed heat exchanger and it is assumed to be 0.05. No further thermal energy losses are considered in the other sections. However the exhaust gas pressure drop in each section is computed as:

$$\Delta P = \frac{P_5 - P_6}{5} \tag{2.24}$$

The thermodynamics properties of the steam-water and the exhaust gas in the rest of the HRSG can be determined following the same procedure.

The mechanical work converted by the steam turbine is calculated using the following equation:

$$\dot{W}_{ST} = \dot{m}_{steam} \cdot (h_{21} - h_{22}) \tag{2.25}$$

where h_{22} is enthalpy at the steam turbine outlet section and it is determined considering the definition of the isentropic efficiency:

$$\eta_{is,ST} = \frac{h_{21} - h_{22}}{h_{21} - h_{22,is}} \tag{2.26}$$

The value of the steam enthalpy outside of the expander after the isentropic expansion ($h_{22,is}$) is calculated using Equation (2.9). The specification variable to be used are the entropy of the steam at the super-heater outlet section (s_{21}) and the turbine outlet pressure, which corresponds to the condensation pressure.

The power wasted at the condenser is defined as:

$$\dot{Q}_{cond} = \dot{m}_{steam} \cdot (h_{22} - h_{14}) \tag{2.27}$$

where h_{14} is computed using Equation (2.9) knowing the flow is composed by saturated liquid at the condensation pressure. The regenerator and condenser pumps power consumption is calculated using the same procedure.

The condenser refrigerant mass flow rate can be calculated as follow:

$$\dot{Q}_{cond} = \dot{m}_{cool} \cdot (h_{w2} - h_{w1}) \tag{2.28}$$

The enthalpies of the water at the inlet and outlet section are determined using Equation (2.9) knowing the refrigerant inlet and outlet temperature. The pressure drops in the condenser is assumed to be null and the circulating pumping work is neglected.

2.3 EXERGY ANALYSIS

Exergy is the maximum obtainable work that a system can generate considering its evolution from a given state to the surrounding conditions. The exergy analysis of a thermodynamic system allows the cause and amplitude of the losses to be determined. The steady state exergy balance equation for an open system can be derived applying the first and second laws of thermodynamics. Assuming that T_0 and P_0 are the temperature and pressure of the surrounding and $\dot{Q}_j$ are the thermal powers exchanged by the system with other thermal systems, the maximum power that can be extracted from the system can be expressed as follows (Galliani, 2006):

$$\dot{W} = \sum_{in} \dot{x}_i - \sum_{out} \dot{x}_o + \dot{Q}_j \cdot \vartheta_j - \mathrm{T}_0 \cdot \dot{S}_{gen} \tag{2.29}$$

where the term $T_0 \cdot \dot{S}_{gen}$ is also referred as Exergy Destructed Rate ($\dot{\Psi}_D$) and ϑ_j is known as the Carnot coefficient and it is defined as:

$$\vartheta_j = 1 - \frac{T_j}{T_0} \tag{2.30}$$

Neglecting electromagnetic, electric, nuclear, and surface tension forces, the physical exergy rate of a stream can be calculated using the following expression:

$$\dot{x} = \dot{m} \cdot ((h - h_0) - \mathrm{T}_0 \cdot (s - s_0)) \tag{2.31}$$

Assuming an ideal reversible process, the entropy generation is zero, and it is possible to derive the definition of the reversible work from Equation (2.29):

$$\dot{W}_{rev} = \sum_{in} \dot{x}_i - \sum_{out} \dot{x}_o + \dot{Q}_j \cdot \vartheta_j \tag{2.32}$$

Considering Equations (2.29) and (2.32), the exergy balance for a real process can be written as:

$$\dot{W} = \dot{W}_{rev} - \dot{\Psi}_D \tag{2.33}$$

where $\dot{\Psi}_D$ is the exergy destruction rate. Equation (2.31) is known as Gouy-Stodola equation and it introduces the concept of the exergy destruction. In any thermodynamic process the irreversibility decreases the useful work that the system could have generated. Through the second principle analysis it is possible to estimate the exergy destruction and to determine the component where more entropy is generated.

Exergy analysis and performance assessment for solar thermal power plan are limited in the literature. Tyagi et al (2007) performed a parametric study of a concentrating type solar collectors (parabolic trough) using the Hottel–Whillier model. Xu et al (2011) have studied energy and exergy balances in a central receiver solar tower power plant with molten salt as heat transfer fluid. Spelling (2009) assessed the energetic and exergetic performances of a fully solar combined cycle. Referring to solar hybrid systems, the first study considering the exergy analysis was carried out in 1988 (Oda et al, 1998). In this paper a comparison between three different integration methods of solar energy with combined cycle were considered: pre-heating of the combustion air, supplementary heat to the Rankine cycle and the combination of these two. More recently the exergonomic analysis have been presented for a ISCC system in Iran (Baghernejad et al , 2010). Peng et al (2014) performed the exergy evaluation of a solar-hybrid coal-fired power in China adopting the graphical exergy analysis or EUD methodology. Mitsos et al (2012) presented a review of the available hybrid solar–fossil fuel power generation systems and they studied the different evaluation matrices that could be adopted to assess the cycle performances. In this paper the author states that the exergy analysis is a better measure of hybrid cycle efficiency because it takes into account the weighted contributions of the input of the two different sources. On the other hand, the second law efficiency results similar to the first law efficiency for any hybrid system since the value of the fuel exergy is close to the low heating value and the solar exergy can vary from 93% to 95% of the solar energy according to the assumptions made. This short literature review indicates that a small number of studies considering the exergetic analysis of solar hybrid power plants are available. Furthermore, different methodologies have been used to assess the exergy efficiency of solar thermal systems. In this regard, the purpose of these paragraphs is to indicate the theoretical framework for the exergy analysis of a solar hybrid combined cycle that has been adopted to evaluate the losses due to irreversibility in the overall power plant and in each component.

Referring to Equation (2.29) and to Figure 2.1, the global exergy balance for the solar hybrid combined cycle power plant states that:

$$\dot{W}_{GT,net} + \dot{W}_{ST,net} = \dot{x}_1 - \dot{x}_6 + \dot{x}_{w1} - \dot{x}_{w2} + \dot{Q}_{sol} \cdot \vartheta_{sol} + \dot{\Psi}_{fuel}^{CH} - \dot{\Psi}_{D,tot} \tag{2.34}$$

where $\dot{W}_{GT,net}$ and $\dot{W}_{ST,net}$ are the net power output of the Joule-Brayton cycle and the steam Rankine cycle respectively. $\dot{\Psi}_{fuel}^{CH}$ is the chemical exergy power generated by the fuel combustion.

The total exergy efficiency can be computed as the ratio between the total useful work extracted from the system and the exergy input:

$$\eta_{II,cycle} = \frac{\dot{W}_{tot}}{\dot{\Psi}_{in}} \tag{2.35}$$

where the exergetic input of the system is defined as

$$\dot{\Psi}_{in} = \dot{Q}_{sol} \cdot \vartheta_{sol} + \dot{\Psi}_{fuel}^{CH} \tag{2.36}$$

Point-wise analysis has been carried out to evaluate the physical exergy in each part of the system. Moreover the exergy destruction rate has been evaluated for each component.

2.3.1 Solar System Exergy Analysis

The exergy balance of the solar system is useful to understand how the concentrated solar power is partially wasted in the receiver and in the heliostat field. The main loss mechanism in central receiver technologies is the cosine effect of the heliostat (Section 2.2.1). Radiation spillage, blocking and shadowing of the collectors, atmospheric attenuation determine other irreversibility. Heat loss mechanisms due to radiation and convection are involved in the receiver section, but the latter is less significant.

The definition of the solar exergy has been previously discussed in the literature (Mitsos, 2012). There are different ways to compute the solar exergy. The first method is to approximate the sun as a constant temperature black body in equilibrium with the surrounding. The useful work that can be extracted from this system until it reaches the dead state is the solar exergy. Within this group, several approaches have been proposed assuming different models of the radiation system. However in all these methods the solar exergy results to

be similar to the transferred exergy (93% to 95%). In the second class of solar exergy calculation methods, the mechanical work that can be produced using the portion of the solar emission intercepted by the collectors is calculated. In this case the collectors assumed to be in contact only with the sun. The energy transfer is limited by the temperature of the collector. Several models can be found in the literature, but in general the solar exergy results to be approximately the 85% of the solar thermal input.

Considering the control volume to include the heliostat field and that no useful work is generated in the receiver, the exergy destruction rate of the solar system can be calculated as:

$$\dot{\Psi}_{D,\text{solar}} = \dot{x}_2 - \dot{x}_3 + \dot{Q}_{sol} \cdot \vartheta_{sol} \tag{2.37}$$

where $\dot{Q}_{sol}$ is the thermal power collected by the heliostat field and it is calculated as :

$$\dot{Q}_{sol} = \frac{\dot{Q}_{rec}}{\eta_{field} \cdot \eta_{rec}} \tag{2.38}$$

The Carnot coefficients for the sun have been determined according to the equation proposed by Spanner (Mitsos, 2012):

$$\vartheta_{sol} = 1 - \frac{4}{3} \cdot \frac{T_{sun}}{T_0} \tag{2.39}$$

where T_{sun} is the surface temperature of the sun and it is assumed to be 5800 K.

2.3.2 Joule-Brayton Cycle Exergy Analysis

Assuming steady state condition, the exergy destruction rates for compressor and power turbine are calculated as:

$$\dot{\Psi}_{D,AC} = \dot{x}_1 - \dot{x}_2 + \dot{W}_{AC} \tag{2.40}$$

$$\dot{\Psi}_{D,GT} = \dot{x}_4 - \dot{x}_5 - \dot{W}_{GT} \tag{2.41}$$

Both the air compressor and the gas turbine mechanical work have to be considered positive.

The burner in an industrial gas turbine is equivalent to an insulated reactive thermodynamic system. Thus, the exergy balance in the combustion chamber can be written as:

$$\dot{\Psi}_{D,\text{burner}} = \dot{x}_3 - \dot{x}_4 + \dot{\Psi}^{CH}_{fuel} \tag{2.42}$$

The term $\dot{\Psi}^{CH}_{fuel}$ is defined as the fuel chemical exergy rate and it can be calculated using Equation (2.43):

$$\dot{\Psi}^{CH}_{fuel} = \dot{m}_{fuel} \cdot \psi^{CH}_{fuel} \tag{2.43}$$

where the ψ^{CH}_{fuel} is the specific chemical exergy of the fuel and it is defined as (Lozza, 2007):

$$\psi^{CH}_{fuel} = \lambda \cdot (h_{0,ox} - T_0 \cdot s_{0,ox}) + (h_{0,\,fuel} - T_0 \cdot s_{0,\,fuel}) + (1+\lambda) \cdot (h_{0,\,fg} - T_0 \cdot s_{0,\,fg}) \tag{2.44}$$

where λ is the ratio between the oxidizer and the fuel mass flow rate. The specific chemical exergy represents the useful work which could be extracted from the combustion when the flue gases are expanded to the dead point with a reversible process. The energy equivalent concept for the specific chemical exergy is the Lower Heating Value which is defined as the heat that is released by the flue gases when they are cooled to the reference temperature. It is noteworthy to highlight that the partial pressure of the component in the flue gases affect the value of ψ^{CH}_{fuel} because it consider the theoretical useful work that could be produced by the expansion of each element in the combustion product. In practice, the reversible work that can be actually extracted by the fuel has to be computed neglecting the mixing entropy. The corrected entropy to be used in Equation (2.43) can be expressed as:

$$s^{*} = s - \Delta s_{mix} = s - \frac{R}{MM_{\,fg}} \cdot \sum_i x_i \cdot \ln(\frac{1}{x_i}) \tag{2.45}$$

Considering exergy balances for real systems, the difference between the specific fuel chemical exergy and the combustion reversible work is neglected (for typical fuel the error is less than 1%). Furthermore the value of ψ^{CH}_{fuel} is usually close to the Lower Heating Value and for this reason the energy and exergy efficiency for combustors are similar. The value for the specific chemical exergy is taken for the literature (Galliani, 2006).

2.3.3 Heat Recovery Steam Generator And Rankine Cycle Exergy Analysis

The Heat Recovery Steam Generator can be simplified as a counter flow heat exchanger where the two flows involved are the exhaust gases and the water/steam. The exergy destruction rate can be determined using Equation (2.29). The mechanical work produced in the heat exchanger is zero. The thermal energy exchange with the surrounding is null, since the Heat Recovery Steam Generator is assumed to be isolated. The source of the irreversibility is given by the difference in the physical exergy of the two streams:

$$\dot{\Psi}_{D,\mathrm{HRSG}} = \dot{x}_5 - \dot{x}_6 + \dot{x}_{15} - \dot{x}_{21} + \dot{x}_{18} - \dot{x}_{17} \tag{2.46}$$

The last term refers to the exergy destruction related to the regenerator pump.

The exergy destruction rate in the steam turbine is calculated as follow:

$$\dot{\Psi}_{D,\mathrm{ST}} = \dot{x}_{21} - \dot{x}_{22} - \dot{W}_{ST} \tag{2.47}$$

where the generated mechanical work is considered to be positive. The exergy lost due to the irreversibility in the pumping system of the bottoming cycle can be computed as:

$$\dot{\Psi}_{D,\mathrm{pumps}} = \dot{x}_{14} - \dot{x}_{15} + \dot{W}_{pump.cond} + \dot{x}_{18} - \dot{x}_{17} + \dot{W}_{pump,reg} \tag{2.48}$$

where the useful work of the pumps should be assumed positive.

The condenser is modeled as a counter flow shell and tube heat exchanger, similarly to the HRSG. Referring to Figure 2.1, the exergy destruction rate is calculated as:

$$\dot{\Psi}_{D,\mathrm{cond}} = \dot{x}_{22} - \dot{x}_{14} + \dot{x}_{w1} - \dot{x}_{w2} \tag{2.49}$$

2.4 ECONOMIC ANALYSIS

In order to demonstrate the economic feasibility of the solar hybrid combined cycle, the total investment cost, the net present value (NPV) and the internal rate of return (IRR) of the investment must be determined. The total investment cost represents the capital costs associated with the purchase and installation of each component: refer to the cost analysis in Section 2.4.1. Net present value is used for capital budgeting and it measures the excess or shortfall of

cash flows, in present value terms, above the cost of funds. The NPV is used in decision making process to evaluate the profitability of an investment. The Internal rate of return can be defined as the discount rate at which the present value of all future cash flow is equal to the initial investment or in other words the rate at which an investment breaks even. IRR calculations are commonly used to evaluate the desirability of investments or projects. The higher the IRR of a project, the more desirable it is to undertake the project. Refer to Section 2.4.1 for the assumptions made to perform the financial assessment of the investment related to this power plant.

In order to compare the electricity production cost of different power generation systems, the levelized electricity cost (or levelised cost of electricity) is a useful parameter. The LEC is the generation cost of the electricity from a specific source necessary to break even over the lifetime of the power plant. It is particularly useful to compare the costs of generation from different sources.

2.4.1 Cost Analysis

To determine the total investment cost it is necessary to evaluate the capital cost of each component of the plant. This is calculated using cost functions available in the literature. The cost functions relate the thermodynamic effects of a system to the expenses associated with the purchase and the installation. The following paragraphs present the cost functions that have been used to estimate the investment for the SHCC plant. The costs are expressed in dollars.

2.4.1.1 Receiver and heliostat field

The cost of the receiver has been evaluated considering the data available from the Solgate Project (European Commission, 2005). In this report, the costs per unit of area for the low, medium and high temperature module have been estimated from the manufacturer (see Table 2.4). Since the receiver cluster has been model as a single unit, the average cost of the module is considered. The specific cost of the heliostat mirrors is assumed to be 132 €/m^2. The capital cost for the heliostat field has been estimated considering the reflective area. The expenses related to the receiver cluster and the collectors are converted in dollar using the current exchange rate.

Table 2-4 Pressurized volumetric receiver cost (European Commission, 2005)

LT module	15938	€/m^2
MT module	32813	€/m^2
HT module	37500	€/m^2

The cost of the tower has been computed according to the equation developed by Augsburger (Spelling, 2009):

$$z_{tower} = \begin{Bmatrix} 1.0903 \cdot \exp(0.0088 \cdot t) & t < 120 \\ 0.7823 \cdot \exp(0.0113 \cdot t) & t \geq 120 \end{Bmatrix} \cdot 10^6 \quad (2.50)$$

where the height of the tower is related to the peak power absorbed by the receiver:

$$t = 49.89 + 0.9825 * Q_{peak} - 0.011 * Q_{peak}^2 \quad (2.51)$$

where Q_{peak} must be expressed in MW. The installation expenses of the control instrumentation for the solar system are estimated in about $530000. The cost for the purchase of the land is not accounted in this work.

2.4.1.2 Joule-Brayton cycle components

The cost functions of the Joule-Brayton cycle are taken from Arsalis (2007). The cost of the air compressor can be determined as:

$$z_{AC} = \frac{39.5 \cdot \dot{m}_{air}}{0.9 - \eta_{AC}} \cdot \left(\frac{P_2}{P_1} \right) \cdot \ln \left(\frac{P_2}{P_1} \right) \quad (2.52)$$

The capital cost of the combustion chamber depends on the combustion air and the outlet temperature which is assumed to be equal to the turbine inlet temperature:

$$z_{cc} = \left(\frac{46.08 \cdot \dot{m}_{air}}{0.995 - \frac{P_4}{P_3}} \right) \cdot [1 + \exp(0.018 \cdot TIT - 26.4)] \quad (2.53)$$

The gas turbine cost is related to the mechanical work that can be extracted:

$$z_{GT} = \dot{W}_{GT} \cdot [1318.5 - 98.328 \cdot \ln(\dot{W}_{GT})] \quad (2.54)$$

The cost due to the adaptation of the gas turbine to the solar system accounts for $520000 (European Commission, 2005).

2.4.1.3 Rankine cycle components

The investment for the bottoming cycle considers the capital and installation cost for the heat recovery steam generator, the steam turbine, the condenser and the circulating pumps.

The cost of the waste heat boiler results from the summation of the expenses due to the heat exchanger, the steam/water piping section and the gas ducts:

$$z_{HTX\,(HRSG)} = 3650 \cdot \sum_i f_{P_i} \cdot f_{T_i,steam} \cdot f_{T_i,gas} \cdot \kappa^{0.8} \quad (2.55)$$

$$z_{piping} = 11820 \cdot \sum_j f_{P_i} \cdot \dot{m}_{j,steam} \quad (2.56)$$

$$z_{gas} = 658 \cdot (\dot{m}_{gas})^{1.2} \quad (2.57)$$

where the temperature and pressure coefficients for each section of the waste boiler can be calculated as follow (Arsalis, 2007):

$$f_{P_i} = 0.0971 * \left(\frac{P_i}{30}\right) + 0.9029 \quad (2.58)$$

$$f_{T_i,steam} = 1 + \exp\left(\frac{(T_{steam,i} - 830)}{500}\right) \quad (2.59)$$

$$f_{T_j,gas} = 1 + \exp\left(\frac{(T_{gas,j} - 990)}{500}\right) \quad (2.60)$$

$$\kappa = \frac{\dot{Q}_i}{\Delta T_{ML,i}} \quad (2.61)$$

where $\dot{Q}_i$ is thermal power exchanged between the steam and the flue gases in each section.

The steam turbine cost depends on the mechanical power generated:

$$z_{ST} = 3644.3 \cdot (\dot{W}_{steam})^{0.7} - 61.3 \cdot (\dot{W}_{steam})^{0.95} \quad (2.62)$$

The investment cost for a pump is estimated based on the power consumption and on the isentropic efficiency:

$$z_{pump} = 705.48 \cdot \dot{W}_{pump}^{0.71} \cdot \left(1 + \frac{0.2}{1 - \eta_{pump}}\right) \quad (2.63)$$

The condenser cost is influenced by the refrigerant mass flow rate and by the exchanger area:

$$z_{cond} = 248 \cdot A_{cond} + 659 \cdot \dot{m}_{cool} \quad (2.64)$$

where the term A_{cond} can be calculated assuming an average overall heat transfer coefficient of 1150 W/m^2.

The total investment cost account for the insurance expense. The insurance cost depends strongly on the components and the insured event: the insurance rate has been assumed to be the 1.5% of the total capital cost (European Commission, 2005).

2.4.2 Financial Analysis

The following assumptions have been considered to determine the net present value and the internal rate of return for the investment (Spelling, 2009):

- the interest rate on loan is set to 8% (typical for this kind of investment);
- no taxation;
- no inflation rate;
- no depreciation

The cost of the fuel is assumed to be 0.004 $/MJ, while the electricity is considered to be sold at 0.09 $/kWh. The actual electrical power is affected by the parasitic consumption of the power block (assumed to be 2.5% of the nominal power) and by the limitation due to interruption in the service (unexpected failure or scheduled down time for revision and overhaul). The outages factor is 2.5 % of the nominal power (European Commission, 2005).

The net present value is computed as the difference between the total investment cost and the summation of the discounted cash flows:

$$NPV = z_{tot} - \sum_{n} \frac{CF}{(1+\mathrm{m})^{n}} \tag{2.65}$$

The internal rate of return is calculated as the interest rate which allows the net present value to be zero. This parameter has been computed using the Excel function.

2.4.3 Levelized Electricity Cost

The Levelised electricity cost is defined as the lowest sale price per unit of generated power such that the initial investment is recovered. The LEC is computed according to the following equation (Spelling, 2009):

$$LEC = \frac{a + c_{O\&M} \cdot \int_{year} \dot{E}_{net} dt}{\int_{year} \dot{E}_{net} dt} \tag{2.66}$$

where $c_{O\&M}$ the operational and maintenance cost per unit of power and it can be assumed 0.03 $/kWh (Spelling, 2009). The produced energy is computed as the average actual electric power multiplied by the plant working hours per year. The power station is supposed to work all the year in order to exploit the potential of the hybrid system. The term a represents the annuity cost for the investment and it is computed as:

$$a = \frac{z_{tot}}{1-(1-\mathrm{m})^{-n}} \tag{2.67}$$

3 SOLAR HYBRID COMBINED CYCLE PERFORMANCES

3.1 PLANT LOCATION AND BOUNDARY CONDITIONS

The so called "Sun Belt region" represents the highest potential area for concentrating solar power technologies. India, the Middle East, Australia, South Africa/Namibia, South-America (Andean plateau, north-eastern Brazil), northern Mexico and even the south-west of the USA lay in the Sun belt zone and are well suited for the implementation of solar plants (IRENA, 2013). Another promising zone for the market introduction of CSP technology might be the Mediterranean area because of the elevated radiation level and the abundant electricity demand due to the proximity to Europe. Previous publication analyzed the possible implementation of solar-hybrid gas turbine power plants in Europe concluding that North Africa and South Europe have the greatest potential for the CSP market (European Commission, 2005). For these reasons the plant under consideration is assumed to be installed in Seville, Spain. The estimated yearly direct normal solar irradiation is about 2290 kWh/m^2. The available sunny hours are assumed to be 2510. Thus, the design direct normal irradiation considered for the heliostat field is 800 W/m^2. The average ambient temperature and the ambient pressure are assumed to be 25 °C and 1.013bar. Note that a more accurate design method should consider the hourly variation of the ambient conditions.

3.2 PLANT SIMULATION METHODOLOGY

The system is modelled using Matlab. The code is based on the energy balance in each component presented in Chapter 2. The results are exported and then analyzed using Excel. The performances of the system are calculated for each hour of the year, considering the typical meteorological year for southern Spain from the 1st Jan to 31st December (Turner, 2014). The plant is always supposed to work in hybrid mode: the combustion chamber supplies the thermal power necessary to the air pre-heated by the solar energy to reach the target turbine inlet temperature.

Several assumptions have been made to simulate the plant. The air mass flow rate at the inlet section of the compressor is constant. The isentropic efficiencies of the components in the power block are considered to be consistent with time. The turbine inlet temperature is fixed. This means that the power block is assumed to maintain the full-load design characteristic for each time step. More detailed analysis should assess the off-design behavior of the

system. The optical efficiency of the heliostat field and the thermal efficiency of the receiver calculated for the design condition are not varied for solar radiations different from the design one. This approximation has been done to increase the calculation speed, but more accurate simulation will be carried out considering the change in the heliostat and receiver efficiency.

The receiver is designed considering that the fluid can reach a specific maximum allowed temperature (see Chapter 2). However, the thermal power collected overcomes the limit value when the solar radiation is higher than the design DNI. Since the receiver cannot absorb all the radiation without damages, the excess power is dissipated by defocusing part of the mirrors.

3.3 CYCLE PERFORMANCES

3.3.1 Nominal And Solar Hybrid Yearly Average Performances

Table 3.1 reports the calculated annual average value for the most important parameters used to describe the system. The nominal conditions refer to the plant running without any solar input.

Table 3-1: Nominal and yearly average performances for the SHCC plant

	Solar -hybrid	Nominal plant
Q_{sun} [MW]	14.85	0
P_{rec} [MW]	7.74	0
$P_{el,gas}$ [MW]	10.90	11.14
$P_{el,steam}$ [MW]	6.25	6.41
$P_{el,CC}$ [MW]	17.15	17.54
$\eta_{I°,gas}$	0.27	0.32
$\eta_{I°,steam}$	0.33	0.33
$\eta_{I\,CC}$	0.43	0.50
$\eta_{II°}$	0.43	0.49
m fuel [g/s]	0.53	0.70

The average collected solar power in one year is defined as Q_{sun} while the variable P_{rec} refers to the thermal power transmitted to the air by the receiver. The total electricity produced in the SHCC plant is the sum of the power generated in the gas turbine system and in the Rankine cycle power block. The energy efficiency of the combined cycle is defined according to the first principle of thermodynamics:

$$\eta_{I^\circ} = \frac{\dot{E}_{el,\text{tot}}}{\dot{m}_{fuel} \cdot LHV + \dot{Q}_{sol}} \tag{3.1}$$

The exergy efficiency can be determined according to Equation (2.35). The yearly average fuel consumption has been calculated considering the hourly methane mass flow rate.

Note that the system seems to achieve the highest performance in nominal conditions rather than in hybrid mode. The total power supplied to the grid is higher and both the yearly average energy and exergy efficiency are lower than the ones in nominal conditions. A monthly analysis has been carried out to investigate the behavior of the plant (see section 3.3.3).

3.3.2 Solar Related Performances

In order to evaluate the characteristics of the solar integration system previously modelled and analyzed, three main parameters have to been selected: the solar share, the net incremental solar efficiency and the incremental CO_2 avoidance (Mitsos, 2012).

The solar share is defined as the ratio between the solar input in the system and the total thermal power needed for the cycle. It can be determined as:

$$X_{sol} = \frac{\dot{Q}_{sol}}{\dot{Q}_{sol} + \dot{Q}_{fuel}} \tag{3.2}$$

The solar share is usually based on the solar input such the case of Equation (6.1), but it can be also defined considering the power output. For hybrid systems, this variable could have an upper limit significantly less than one because the power plant is generally supposed to work even when the sun radiation is not available, so the value of $\dot{Q}_{fuel}$ increases.

The net incremental solar efficiency can be defined as:

$$\eta_{net\_incr\_sol} = \frac{\dot{E}_{el} - \eta_{ref} \cdot \dot{m}_{fuel} \cdot LHV}{\dot{Q}_{solar}} \tag{3.3}$$

where η_{ref} is the efficiency of the reference plant. In general, the reference plant is represented by the highest efficiency system having the same scheme of the hybrid plant except for the solar integration. The fuel type and fuel consumption must be the same for both the analyzed and reference system, but the operating conditions can change (Mitsos, 2012). However, when the hybrid system has to be estimated relatively to a traditional power plant it is recommended to use the highest efficiency system as reference plant. This means that for a solar-hybrid combined cycle, the reference plant should be a standard gas turbine combined cycle power plant instead of the same system with no solar contribution. Using a traditional plant for the comparison allows an evaluation of the performance of a hybrid system in a more general sense rather than just for the specific case. In this study the efficiency of the reference plant is assumed to be 60%. It is noteworthy to highlight that the rated power of high efficiency combined cycle power stations is higher than the electrical power output of the analyzed hybrid schemes. For this reason, a comparison with a reference plant with the same characteristics of the hybrid systems is also considered.

The incremental CO_2 avoidance is another parameter used to analyses the performance of a hybrid system. This variable can be computed according to Equation (6.3):

$$\Delta CO_2 = \left(\frac{\dot{E}_{el}}{\eta_{ref}} - \dot{Q}_{fuel} \right) \cdot f_{CO_2} \tag{3.4}$$

The factor f_{CO_2} indicates the amount of carbon dioxide emissions per fuel heating rate. This parameter has been calculated for different fuels and it is assumed equal to 0.055 kg/MJ for methane (Mitsos, 2012). The incremental CO_2 avoidance can be lower than zero for poor solar integration systems. The results are reported in tonnes. Table 3.2 reports the yearly average value for the solar related variables.

Table 3-2 Solar related yearly average performances for the SHCC plant

X	0.36
$\eta_{net\_incr\_sun}$	0.02
$\eta_{net\_incr\_sun}'$	0.20
ΔCO_2 [tonCO_2]	874.10
$\Delta CO'_2$ [tonCO_2]	10111.54

3.3.3 Monthly Average Performances

In order to better understand the performances of the system, the hourly results have been grouped for each month.

Figure 3.1 represents the electrical power produced in different months. The hybrid mode operation can guarantee almost constant electrical output. As a matter of fact the combustion chamber is always operative. However, since the plant is supposed to be connected to the grid, it is interesting to analyze the hourly variation in the supply output. As can be appreciated in Figure 3.2, the electrical power output of the system is fluctuating in time and it decreases during sunny hours. The variable behavior of the output power is not surprising since it has been reported in previous studies about solar-hybrid gas turbines. Barigozzi et al. (2012) demonstrated that the installation of a pressurized volumetric receiver to pre-heat the air in a gas turbine causes additional pressure drops and reduces the compressor pressure ratio and the gas turbine inflow. These were the sources of the reduction in the power output. In the current study the compressor inlet mass flow rate is assumed to be constant. However the flue gases mass flow rate is reduced during sunny hours because less fuel is burn to reach the fixed turbine inlet temperature.

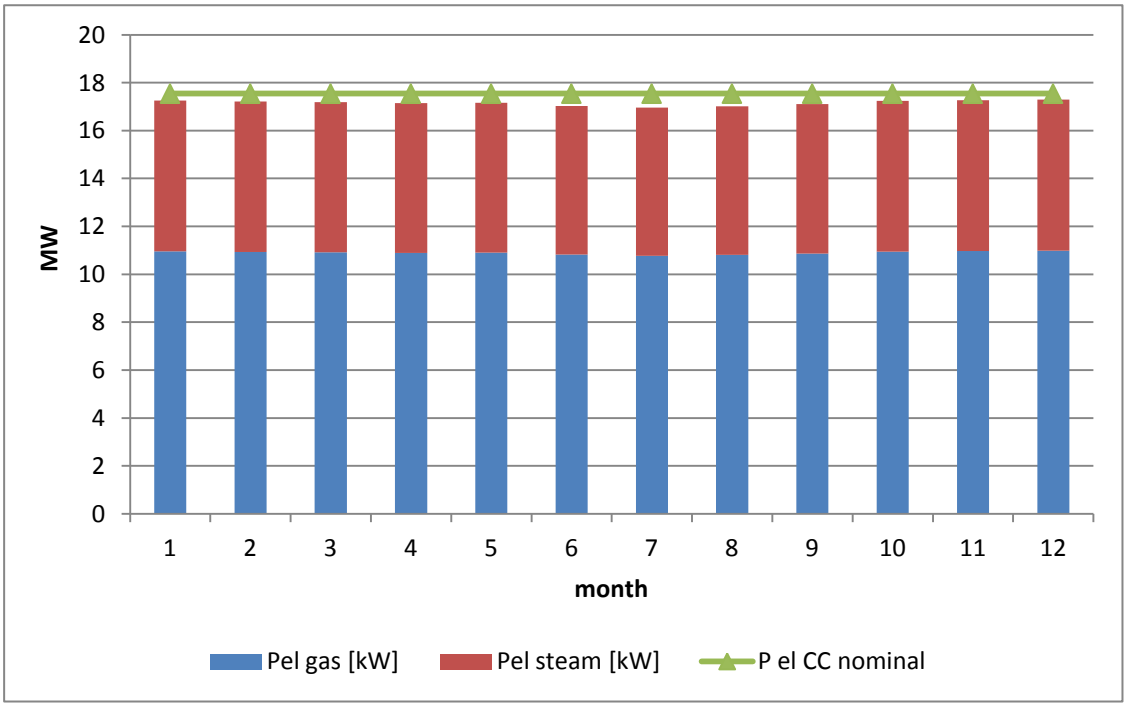

Figure 3-1 Electrical power output SHCC plant

Figure 3.1:

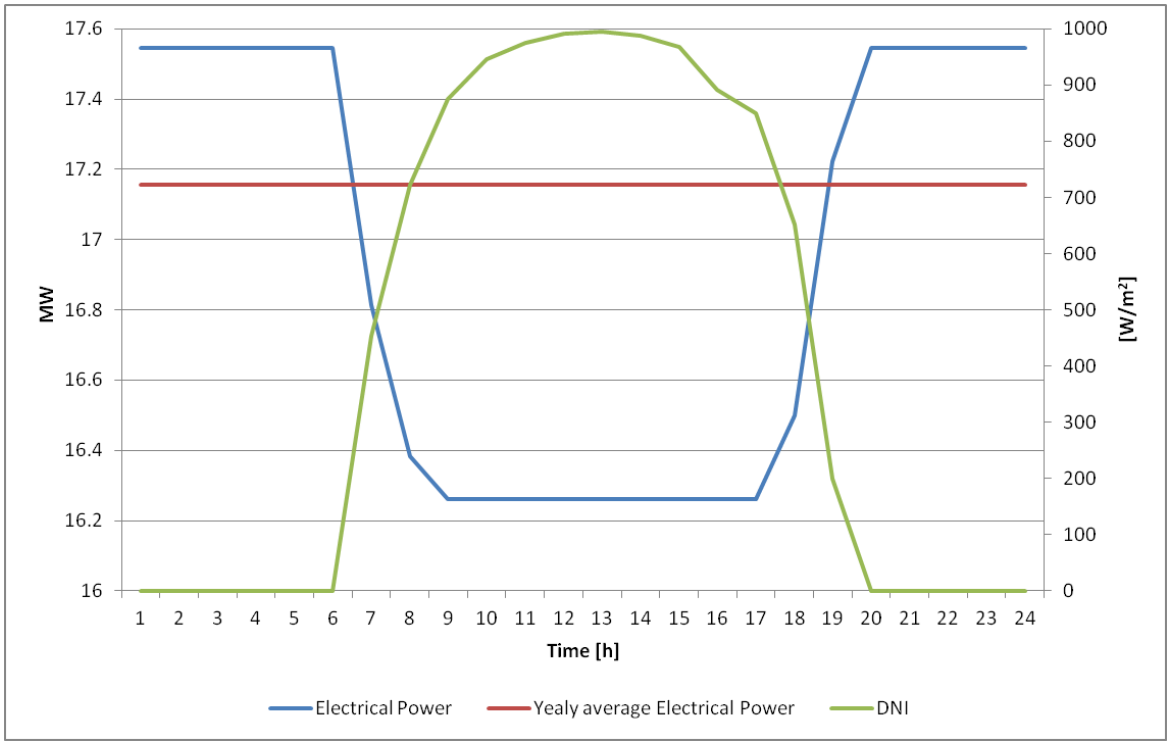

Figure 3-2 solar hybrid combined cycle electric power output, 14th April

Figure 3.3 shows the mass flow rate of the flue gases during a day (the 14th of April is considered to be significant to show the trend).Furthermore the characteristics of the gas mixture change when hot air is burned. Assuming ideal combustion, the water and CO_2 mass fractions decrease and the mixture is more similar to the standard air composition (Figure 3.4). For this reason the enthalpy at the outlet section of the combustion chamber decreases (Figure 3.5). On the other hand, the polytrophic index increases (Figure 3.6), leading to a lower enthalpy at the outlet section of the turbine. As a result, the enthalpy drop across the turbine decreases. The effect of a lower flue gas mass flow rate and the reduced enthalpy difference is a smaller mechanical work at the gas turbine.

Since the enthalpy at the outlet section of the turbine is reduced, also the temperature of the flue gases at the inlet section of the waste heat boiler decreases. The energy that could be recovered by cooling the gas stream is smaller and the generated steam flow rate diminishes. Thus the mechanical work that can be extracted by the stream turbine decreases.

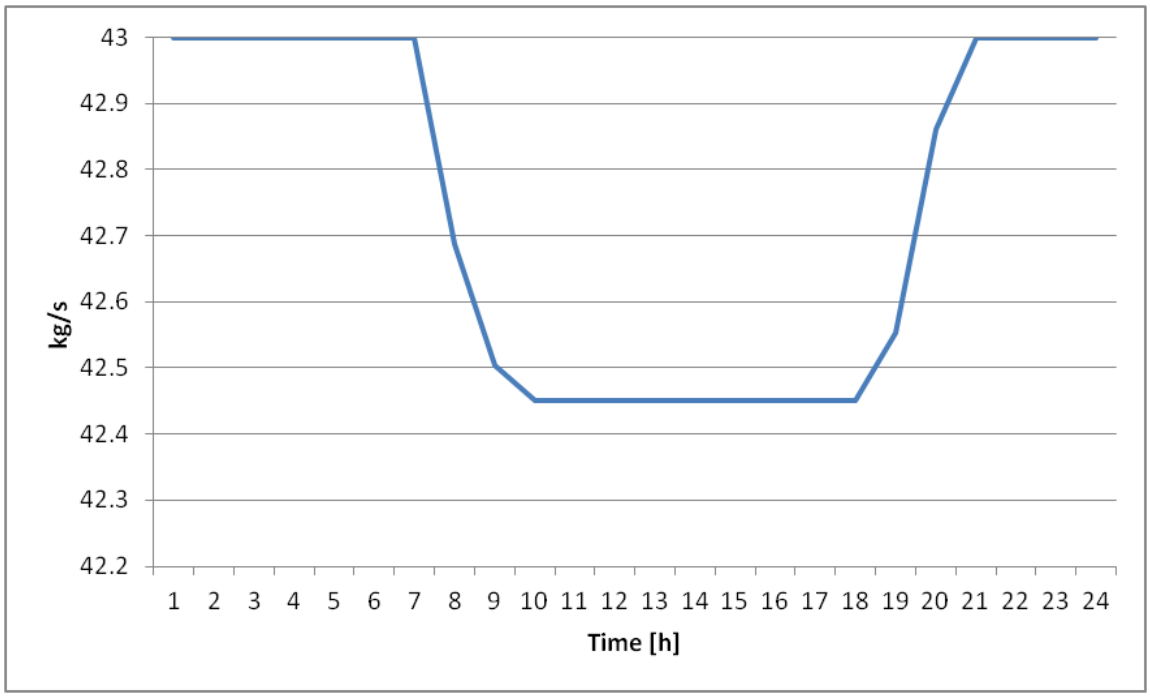

Figure 3-3 Flue gases mass flow rate, 14th April

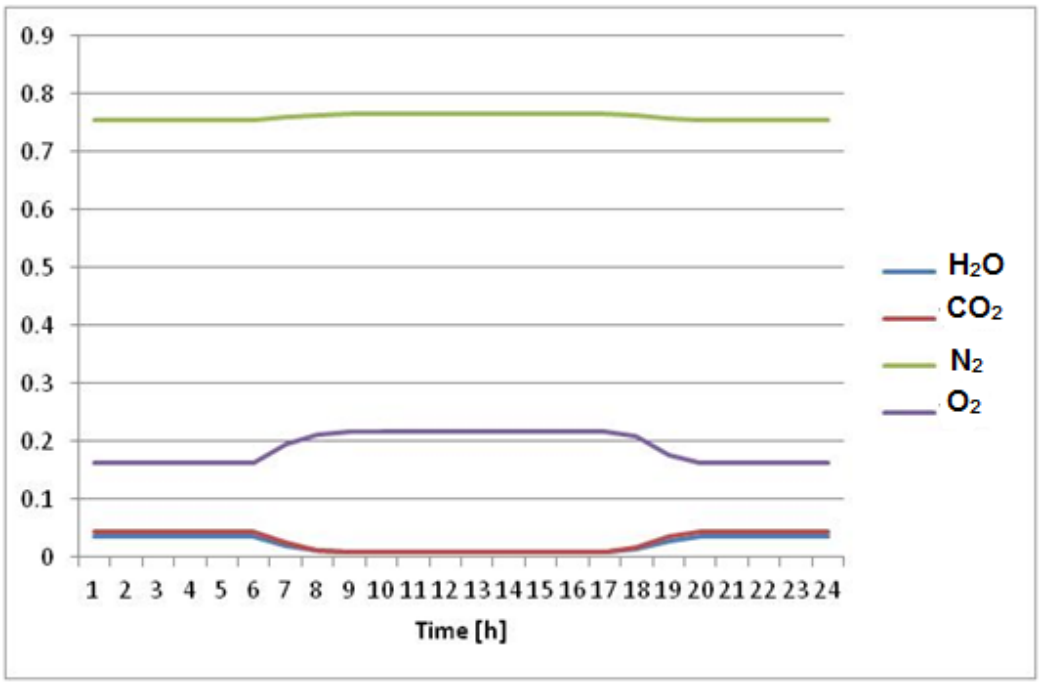

Figure 3-4 Components Mass fractions in flue gases, 14th April

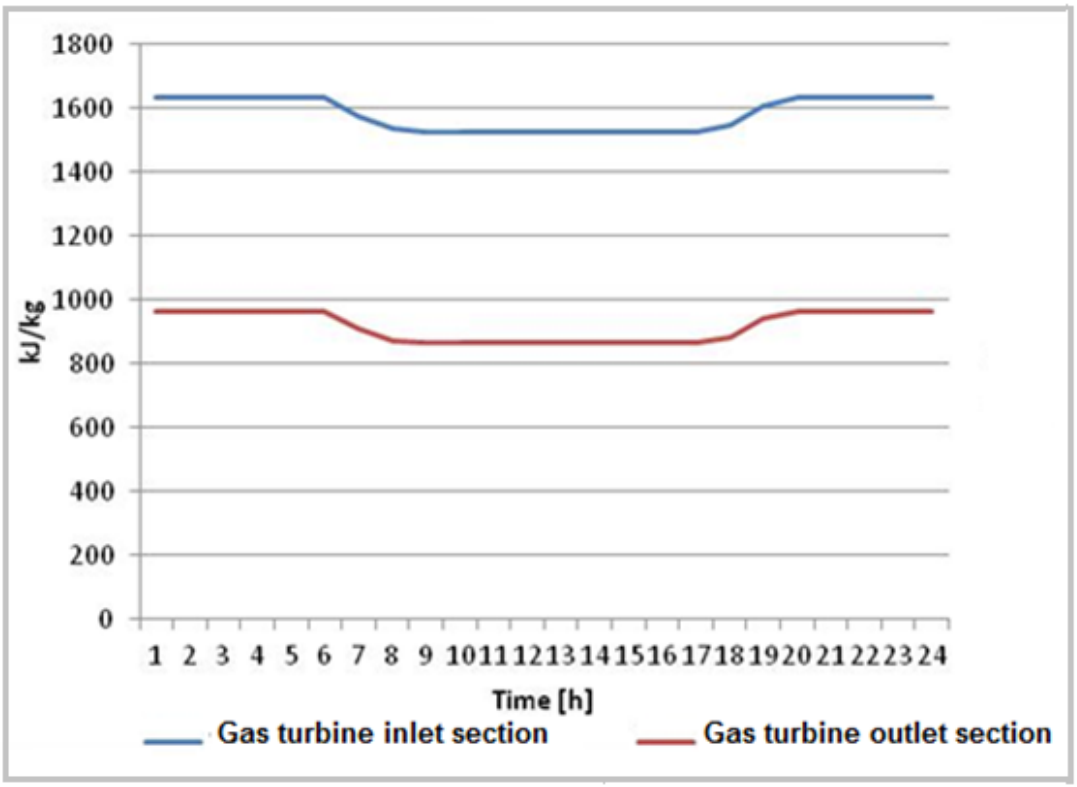

Figure 3-5 Enthalpies of the flue gases at the inlet and outlet section of the turbine, 14th April

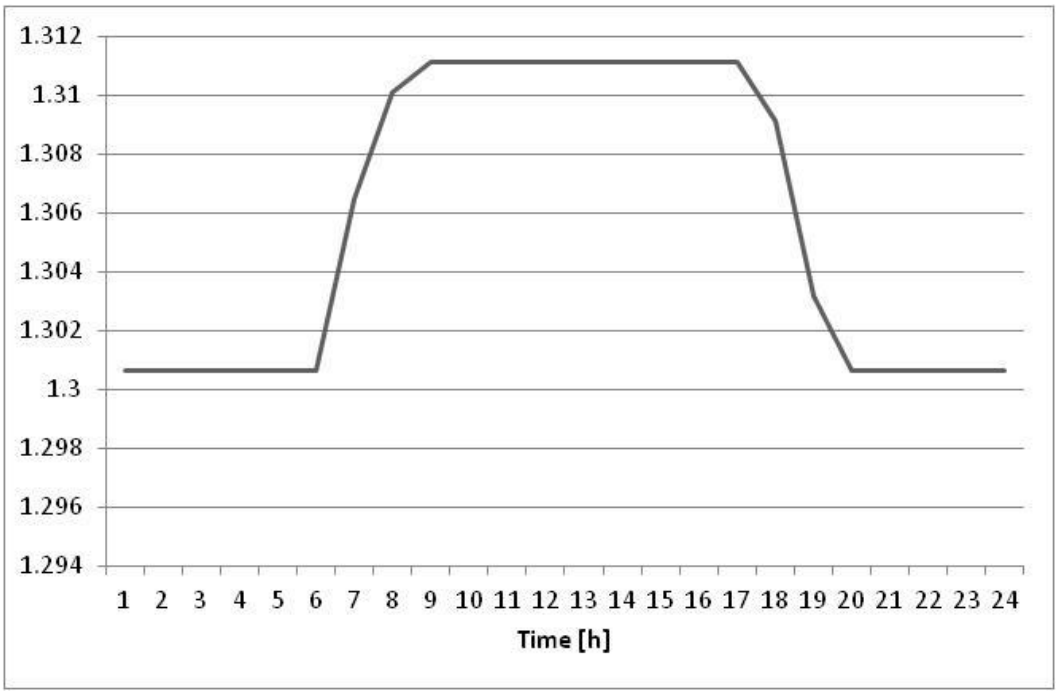

Figure 3-6 Polytrophic index for the flue gases, 14th April

As can be expected, the trend of the energy efficiency of the SHCC system is similar the one of the output power: the plant efficiency decreases in summer when the solar radiation is higher (See Figure 3.7). Furthermore, Figure 3.7 shows that the inlet thermal power slightly reduces in summer. This is due to the design of the model of the combustion chamber: the limiting parameter that should be kept constant is the turbine inlet temperature and for this reason the thermal input varies

The monthly variation of exergy efficiency is reported in Figure 3.8. As expected, the trend is similar to the one of the energy efficiency. The minimum value of the exergy efficiency is reached when the solar power input in the system increase. Higher the power collected at the receiver, higher the exergy destruction rate in the solar system. Indeed, the exergy destruction in the considering the heliostat field and the volumetric receiver represents the 37% of the total amount. The combustion chamber accounts for the highest share because of the hybrid operation mode (the burner works continuously).

The solar contribution mitigate the fuel consumption. As can be seen from Figure 3.9, the methane which is burned in summer is lower than the yearly average fuel consumption. On the other hand, when the solar radiation decreases the monthly average fuel consumption increases

The monthly average solar share reaches the peak in July, when the power generate is at the minimum. In the summer the plant produces a lower amount of electricity but the thermal input supplied by the sun is higher (See Figure 3.10).

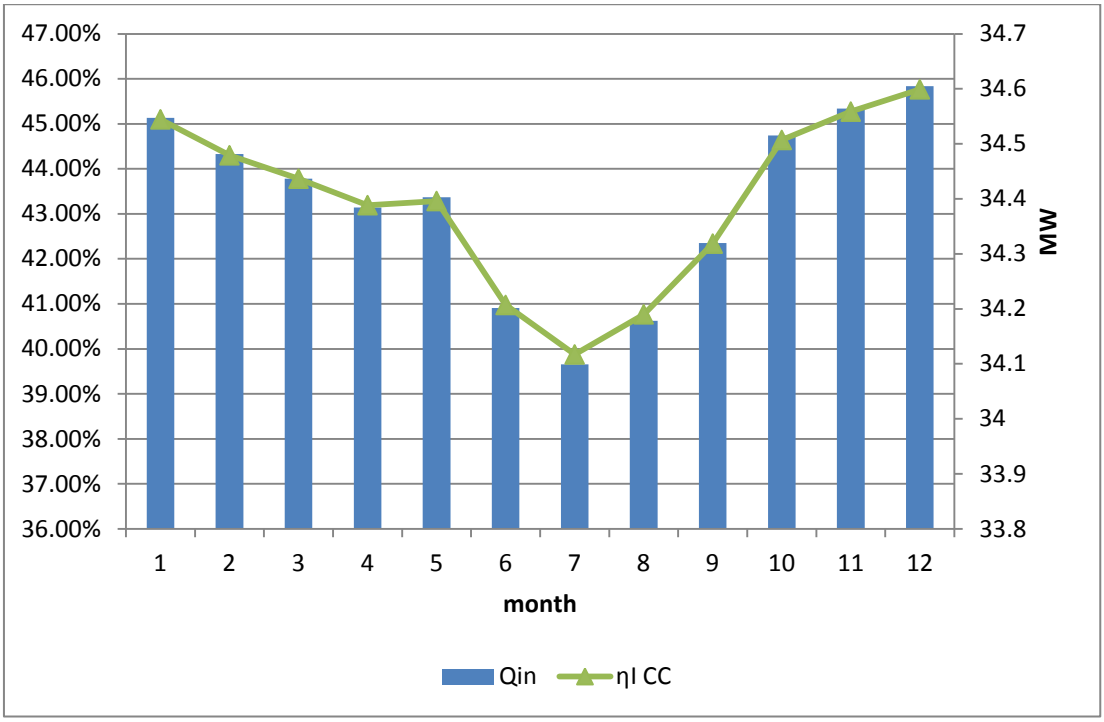

Figure 3-7: SHCC Energy Efficiency

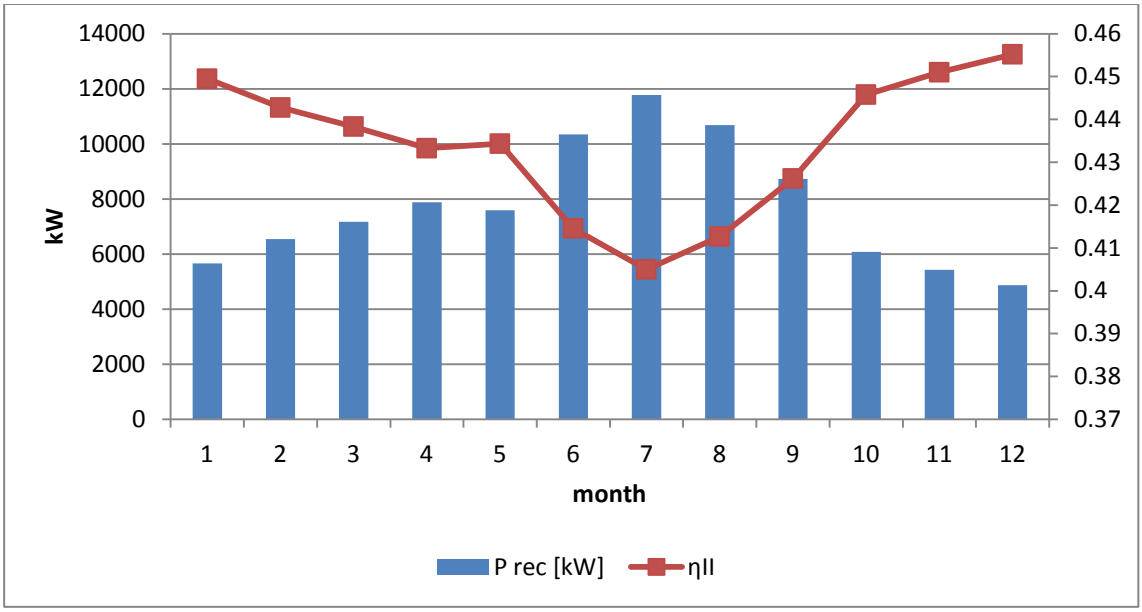

Figure 3-8: SHCC Exergy Efficiency

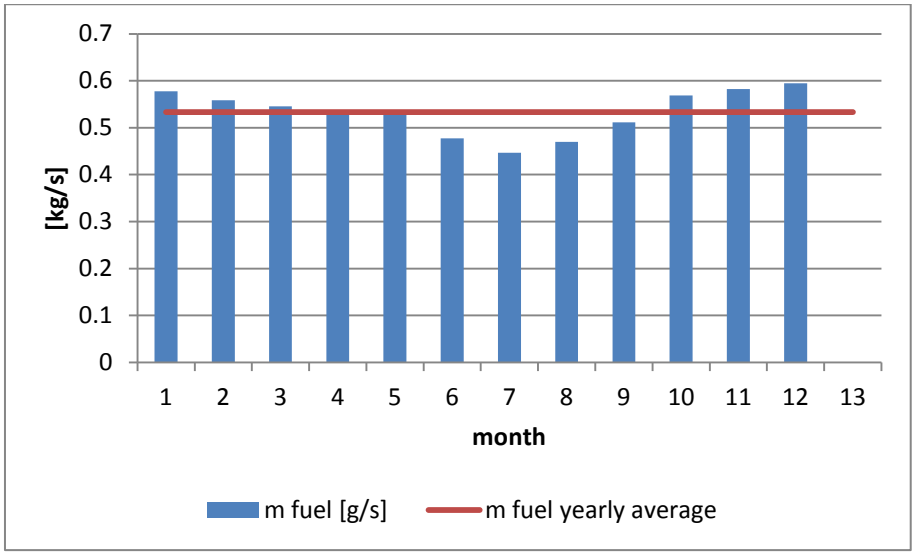

Figure 3-9: Fuel consumption

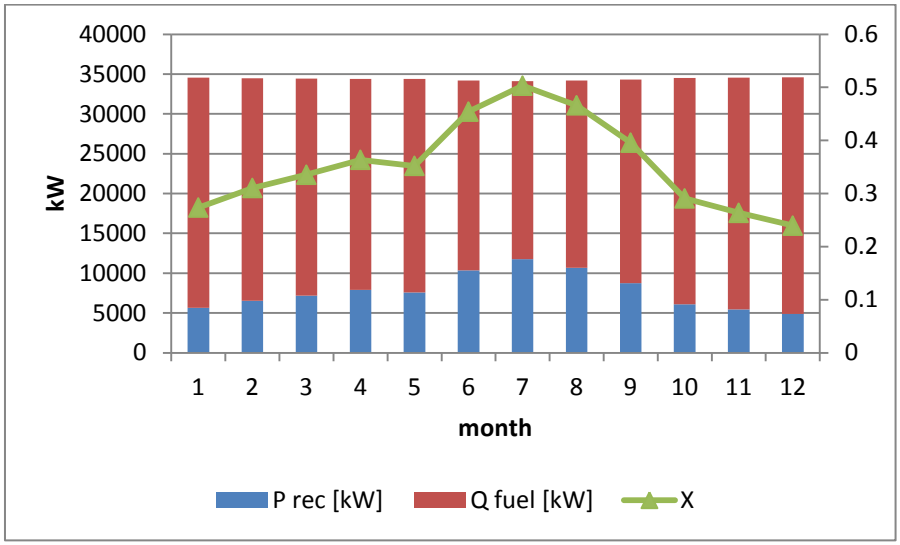

Figure 3-10: solar share

The net incremental solar efficiency has been studied considering two different reference plant. The parameter $\eta_{net\_incr\_sol}$ is determined assuming an high performance state of the art combined cycle power system with a nominal energy efficiency of 60%. The parameter $\eta'_{net\_incr\_sol}$ refers to the net incremental solar efficiency calculated assuming the nominal efficiency as the reference efficiency. In other words, the reference plant is considered to be a combined cycle power plant similar to the SHCC system but without solar input. It is noteworthy to highlight that the $\eta'_{net\_incr\_sol}$ assumes a negative value in December. When the net incremental solar efficiency is lower than zero, it

means that the reference plant would have produce more power under the same condition and this indicate a bad design for the hybrid system.
Furthermore, this variable increase when the solar input increases: higher solar share could improve the hybrid system performances (see Figure 3.11).

The trend of the carbon dioxide avoidance is shown in Figure 3.12. The most important conclusion that we can derive from the analysis of this variable is that the reference combined cycle would have used less fuel to produce the same amount of power and thus the $\Delta CO'_2$ is negative.

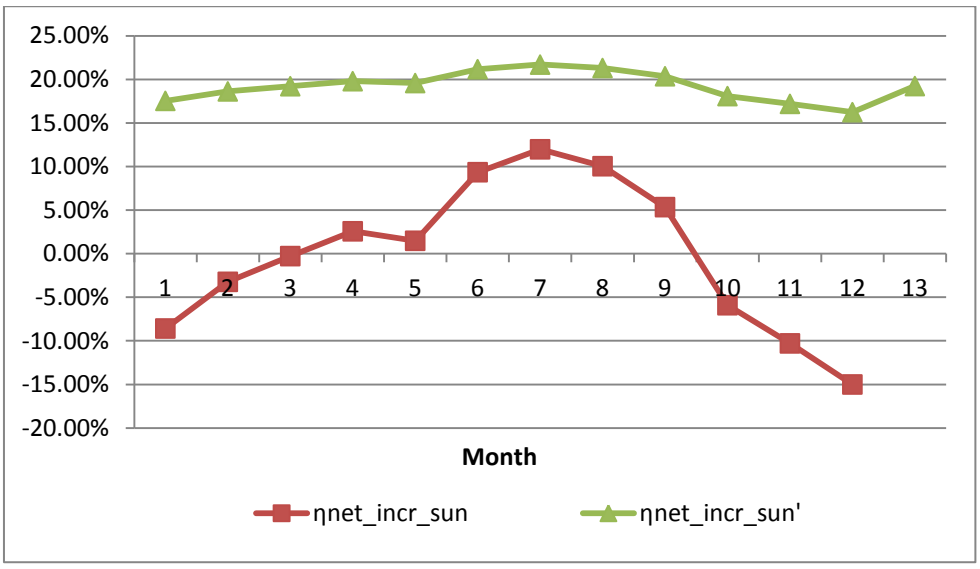

Figure 3-11: Net incremental solar efficiency.

Figure 3-12 Co_2 avoidance

3.3.4 Economic Analysis Evaluation

Total investment cost for the solar hybrid combined cycle is estimated in $29.8 million. The total cost of the solar system (the heliostat field, the tower and the receiver) represents the 54% of the total investment (see Figure 3.9). The gas turbine modifications capital cost refers to the expense needed for the integration of the traditional layout of the gas turbine with the solar tower.

From the financial point of view, the investment seems to be profitable. The net present value is $52.08 million while the internal rate of return is 31.55%.

The levelized electricity cost for the solar hybrid combined cycle is estimated in 0.0544 $/kWh.

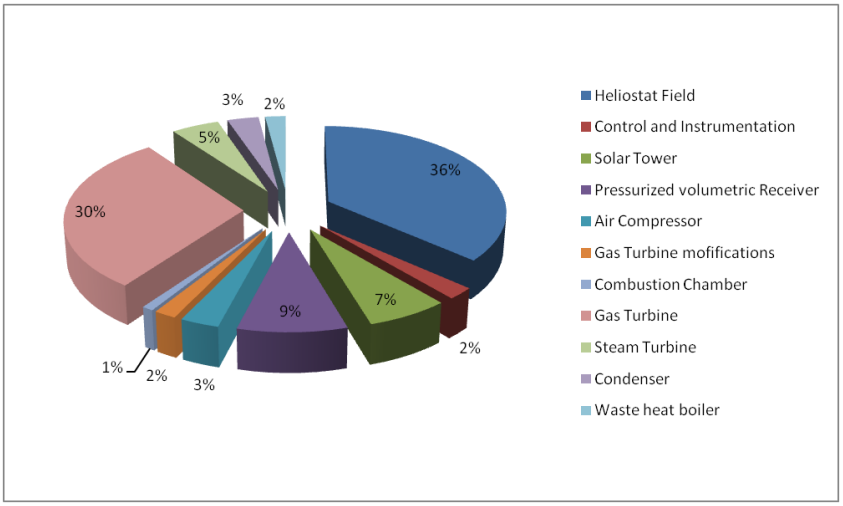

Figure 3-13 Component capital costs for the solar hybrid combined cycle

4 MODELLING THE INTEGRATED SOLAR COMBINED CYCLE SYSTEM

4.1 MODEL DESCRIPTION

The layout of the integrated solar combined cycle plant considered in this study is represented in Figure 4.1. The system is composed by a gas turbine, a heat recovery steam generator and the Rankine cycle power block which consists of a steam turbine, a condenser with evaporative tower and the feed-water pumps. A parabolic through collector field is connected to the bottoming cycle through a heat exchanger (the solar evaporator).

Ambient air is compressed and it is burned with fuel in the combustion chamber. The flue gases are expanded in the power turbine. The residual thermal power in the exhausts is recovered in the waste heat boiler. In the HRSG the feed-water is pre-heated to reach the saturated condition and then the steam is generated in a solar evaporator and in the evaporation section of the waste heat boiler. The solar evaporator is connected to a parabolic trough collector field. The thermal oil passing in the solar system absorbs the solar radiation and exchanged it with the water/steam. This heat is used to generate steam in the solar evaporator. Specific details about the solar system are explained in Section 4.1.1. The model is similar to the one developed for the system considered previously. Modifications occur only in the heat recovery steam generator and for this reason the thermodynamic analysis is limited to this part (Section 4.2).

4.1.1 Parabolic Trough Collectors

Parabolic trough system is one of the more popular options for use in a hybrid combined cycle because the technology is relatively mature and the costs are decreasing. Parabolic troughs can be used to increases the flow of steam into the steam turbine in order to produce more power without consuming extra fuel. Furthermore, parabolic troughs are installed in all the existing solar-hybrid power plants (Mitsos et al, 2012). For these reasons, PTCs have been selected as concentrating solar power technology for the current study.

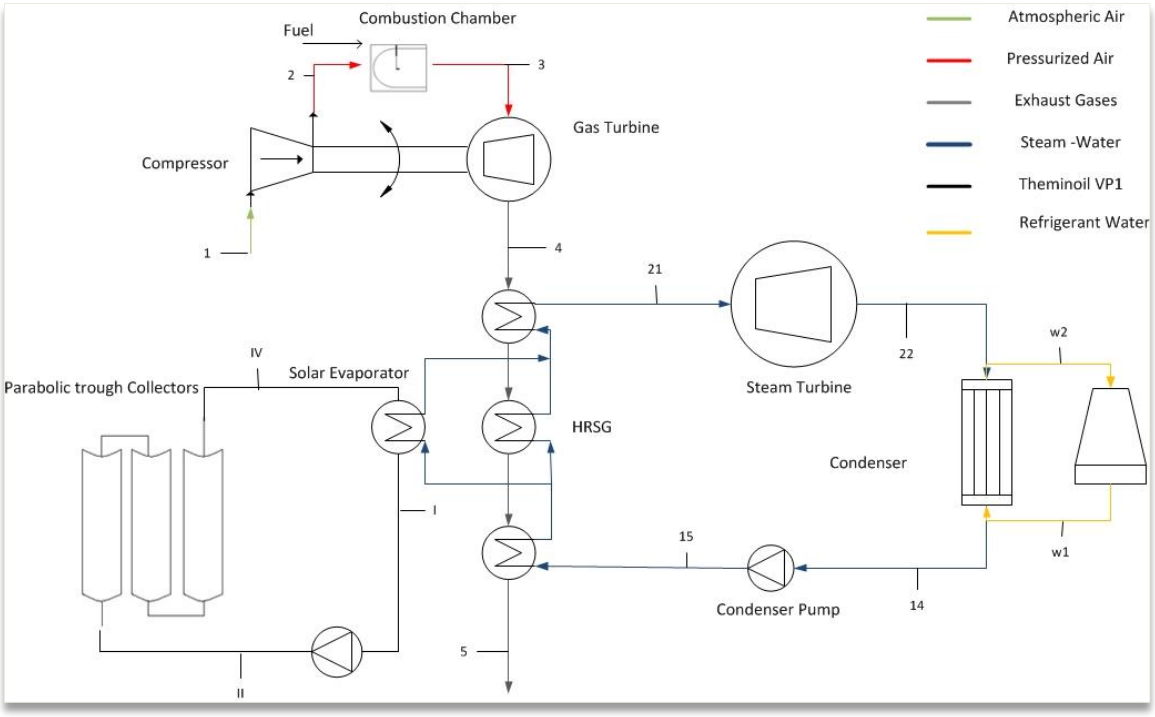

Figure 4-1 Integrated solar combined cycle diagram

Different way to integrate the solar energy into the Rankine cycle of a combined cycle power plant has been studied in the literature. Previous papers have considered the following utilization of the solar radiation (Odeh et al, 2003):

- Feed-water pre-heating: a parabolic trough system is used to preheat a fraction of the feed water in a solar boiler. This arrangement has been studied also for plants in Egypt and Iran (Horn, 2004; Baghernejad, 2010).
- Feed-water boiling: solar collector field is connected in parallel with the boiler of the steam cycle.
- Feed-water pre-heating and boiling: a combination of the boiling and preheating arrangement in that the collector field is connected in parallel with both the boiler and the feed-water heaters in the steam cycle

The best arrangement in terms of fuel savings and CO_2 avoidance resulted to be the boiling configuration. In the current study, the solar evaporator is connected in parallel with the HRSG.

A parabolic trough collector is composed by the following elements:

- Supporting structure;
- Mirrors;

- Receiver;
- Piping system.

The supporting structure is design to be robust enough to account for wind loads and to guarantee minimal deviation of the reflective surface from normal insulation incidence angle. One of the most recent supporting structure is the so called EuroTrough system (Figure 4.2(a) and (b)). This project has been developed since 1998 by a European consortium and it was funded by the European Union. The innovative reticular design allows this structure to be more resistant to torsion stress using less material. In this way, the module length can be increased to 150 m. The collector has the main characteristics of low weight and cost and the employment of evacuated quartz envelop for the absorber tube further reduces the thermal losses. The concentration ratio is about 80 suns and the highest temperature achieved during testing campaign using thermal oil as working fluid was 395°C (Badr, 2013 ; Lupfert et al., 2001)

Figure 4-2 Euro-Trough system: a) Supporting structure sketch, b) Test facility (Lupfert et al, 2001).

The mirrors used for parabolic trough collectors are multi-layer elements with a total thickness of 4 millimeter in order to ensure low specific weight per unit of

area. The silver layer, protected by a glass stratum is used to increase the reflectivity. This arrangement allows obtaining a 96.5% reflectivity. The optical efficiency is also affected by the geometrical characteristic of the mirrors. Thanks to the modern manufacturing technology, high precision mirrors have been developed (Passoni et al., 2010).

The receiver of a parabolic trough collector is basically a glass tube, usually evacuated, where the working fluid is heated. The design of the absorber element is crucial for the efficient heat transfer to the working fluid. Heat losses due to radiation from receiver tubes play an important role in collector performance. The systems thermal efficiency is also affected by the losses related to the temperature gradient between the receiver and the ambient air (Barlev, 2010).

Modern absorbers are optimized to reduced heat loss to the environment. Different strategies have been adopted to increase the performances of the heat collector element (Burkholder, 2009):

- Evacuate the absorber tube to prevent heat conduction/convection;
- Coat the absorber tube with a selective surface with high solar absorption and low thermal emittance to reduce radiative heat loss;
- Increase the length of the receiver to decrease the effect of heat conduction at the extremities;
- Reduce the ratio between the absorber area and the collecting aperture area to diminishing the reflection losses.

The German company Schott developed the receiver PTR70 (Fig. 4.3). The optical and thermal efficiency of this absorber are higher because a particular material with high absorbtance and low reflectance is used for the surface coating. The thermal losses are limited to 250W/m, when the average value of 350W/m. The glass transmittance is optimized for the wave-length specific of the solar radiation and is opaque to the infra-red radiation typical for the working temperature of this element. The receiver PTR70 has a longer life-span because the innovative design of the glass to metal valve.

Parabolic trough collectors are usually mounted on a single-axis sun-tracking system in order to keep the sun rays parallel to the reflective surface and focused on the receiver throughout the day. It has been demonstrated that the east-west orientation of the system provides a better performances (Barlev, 2010).

Figure 4-3 Schott receiver (Passoni et al., 2010)

Mineral oil or synthetic thermal oil can be used as heat transfer fluids. The latter is most often used for steam generation (Mitsos et al.,2012). In the current study, Therminol VP-1 is selected, because it represents one of the most conventional synthetic oil for solar applications (Giostri et al., 2012). Therminol VP-1 is a eutectic mixture of 73.5% diphenyl oxide and 26.5 % diphenyl and it is thermally stable and suitable for operation at bulk temperature up to 370-400°C. This thermal oil is suitable for most heating process or waste heat recover applications (Solutia, 2014).

4.2 PARABOLIC TROUGH COLLECTOR INTEGRATION IN THE HEAT RECOVERY STEAM GENERATOR

4.2.1 Energy Analysis

The assumptions made for the energy analysis of the solar hybrid combined cycle hold for the system under consideration. For the thermodynamic analysis of the main components of the power block refer to Chapter 2.

The integration system of the parabolic trough collectors in the waste heat boiler is shown in Figure 4.4. The solar power input in the ISCC system is exploited to evaporate part of the feed-water. The feed-water is pre-heated and the vapor is superheated using the heat recovered from the exhaust gases.

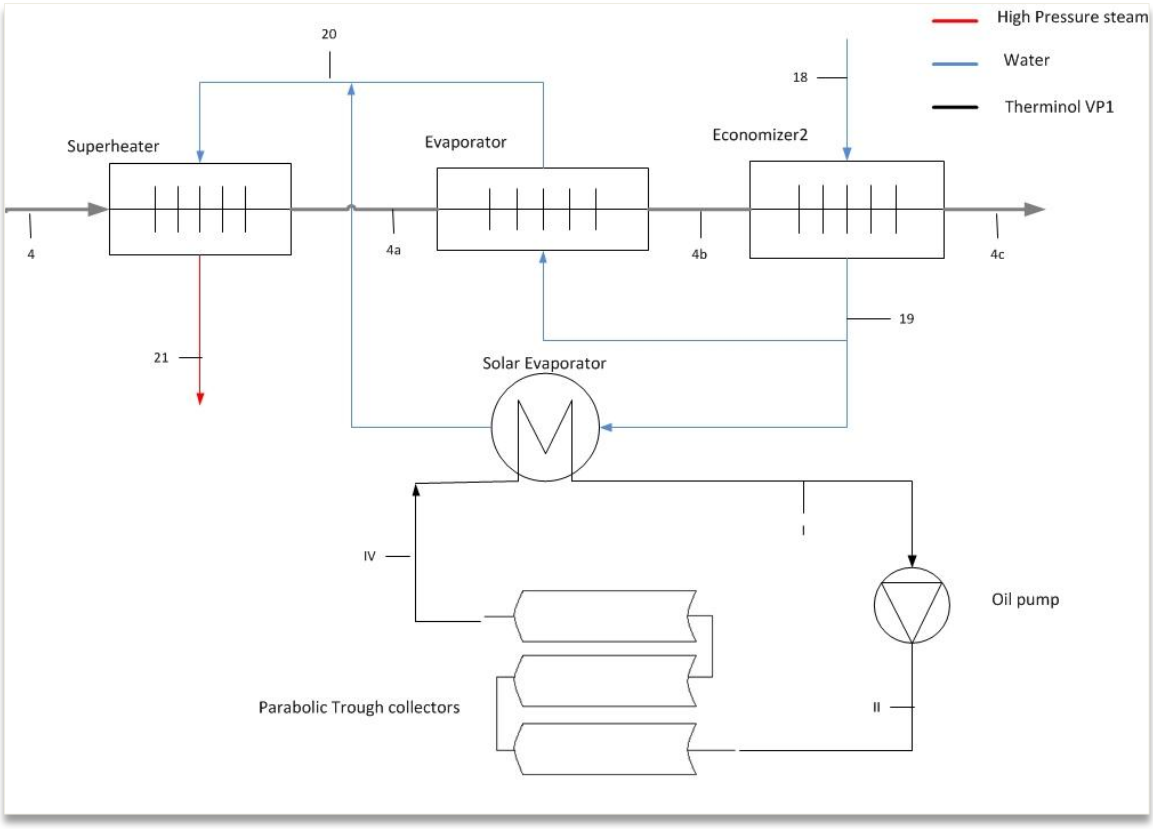

Figure 4-4 Solar system integration for the ISCC plant

Assuming the plant to work in steady condition for each hour of the day, the energy balance between the economizer and the super-heater section can be written as following linear system:

$$\dot{m}_{steam}^{sun} \cdot (h_{20} - h_{19}) = DNI \cdot A_{field} \cdot \eta_{field} \cdot eff_{HTX} \tag{4.1}$$

$$\dot{m}_{steam}^{HRSG} \cdot (h_{20} - h_{19}) = \dot{m}_{fg} \cdot (h_{4a} - h_{4b}) \tag{4.2}$$

$$\dot{m}_{steam}^{tot} \cdot (h_{21} - h_{20}) = \dot{m}_{fg} \cdot (h_{4} - h_{4a}) \tag{4.3}$$

Equation (4.1) represents the heat exchange in the solar evaporator. The solar power that is actually transmitted to the water is calculated considering the efficiency of the solar field and the effectiveness of the heat exchanger.

The efficiency of the parabolic trough collectors is defined by the optical efficiency of the mirrors and the thermal efficiency of the absorber. The overall efficiency of the selected solar system can be computed with the equation used by Franchini et al. (2013):

$$\eta_{PTC} = K \cdot \left(A + B \cdot \Delta T\right) + C \cdot \frac{\Delta T}{DNI} + D \cdot \frac{\Delta T^2}{DNI} \tag{4.4}$$

The term K represents the incident angle modifier and it accounts for the effect of the non-perpendicularity of solar radiation incident angle. This parameter is defined as:

$$K = \cos(\gamma) - 0.0003512 \cdot (\gamma) - 0.00003137 \cdot (\gamma)^2 \tag{4.5}$$

For the purpose of this study the incident angle modifier is assumed to be constant and equal to one for any incident angle. The tracking system modifies the position of the trough in order to have perpendicular solar radiation any time.

The term ΔT is the temperature difference between the heat transfer fluid and the ambient temperature:

$$\Delta T = \frac{T_{HTF}^{in} + T_{HTF}^{out}}{2} - T_{amb} \tag{4.6}$$

The value of A represents the optical efficiency and the absorptivity of the receiver selective coating. B, C and D describe the heat losses of the heat collector element. The value of the constants are reported in Table 4.1 and they have been interpolated to fit the efficiency curve of the PTR40 Schott absorber (Franchini et al., 2013).

Table 4-1 Value of the constants used to compute the overall efficiency of the parabolic trough collectors. (Franchini et al., 2013)

A	77.8
B	-0.022
C	0.5
D	-0.033

The effectiveness of the evaporator is computes as (Lozza, 2007):

$$eff_{HTX} = \frac{\Delta T_{C_{\min}}}{\Delta T_{\max}} \tag{4.7}$$

Since the water is evaporating, the fluid with the lowest thermal capacity is the thermal oil. The maximum temperature drop is achieved when the heat transfer fluid is ideally cooled to the evaporation temperature. The inlet temperature of the thermal oil is fixed to 390 °C, while the temperature at the outlet section of the evaporator is 290°C.

The enthalpies of the water/steam are computed using the software Refprop. The evaporation temperature and pressure are computed following the same procedure used for the SHCC system (see Chapter 2).

The work required to the pump to circulate depends on the pressurization level of the liquid thermal oil can be computed as:

$$\dot{W}_{pump.oil} = \dot{m}_{HTF} \cdot \frac{\Delta P}{\rho_{HTF}} \tag{4.8}$$

The density of the fluid is calculated at the inlet section of the pump using the empirical correlation available in Therminol data-sheet (Solutia, 2014).

The required mass flow rate of Therminol is determined considering the energy balance at the solar evaporator:

$$\dot{m}_{HTF} = \dot{m}_{steam}^{sol} \cdot \frac{(h_{20} - h_{19})}{(h_{IV} - h_{I})} \tag{4.9}$$

The value for the thermal oil enthalpy can be found in the Therminol data-sheet (Solutia, 2014).

4.2.1 Solar Field Design

In the current study only the value of collector area is computed to define the solar field. However, more design parameters such as the number of collectors and the number of loops should be included in a correct design procedure.

The solar field is designed in order to provide, in nominal conditions, the same amount of thermal power as the HRSG evaporator of the reference combined cycle. This means that the steam flow rate is doubled when the plant runs in design condition.

Since the temperature of the exhaust gas at the outlet section of the evaporator is fixed, the heat released by the gas stream depends only on the gas turbine outlet temperature. Considering the plant working without any solar input (when the solar radiation is null), the thermal power released by the exhaust in the evaporator of the reference combined cycle can be calculated as:

$$\dot{Q}_{evap\_HRSG} = \dot{m}_{fg} \cdot (h_{4a} - h_{4b}) \cdot (1 - \xi) = \dot{m}_{steam} \cdot (h_{20} - h_{19}) \quad (4.10)$$

In design conditions, the solar evaporator provides the same amount of thermal power. The thermal oil mass flow rate to be pumped in the PTC system is computed using energy balance for the heat exchanger:

$$\dot{m}_{steam} \cdot (h_{20} - h_{19}) = \dot{m}_{HTF} \cdot (h_{IV} - h_{I}) \cdot eff_{HTX} \quad (4.11)$$

The solar field area is calculated considering the energy balance in the parabolic trough collectors:

$$A_{field} \cdot \frac{DNI}{1000} \cdot \eta_{PTC} = \dot{m}_{HTF} \cdot (h_{IV} - h_{II}) \quad (4.12)$$

The design DNI is assumed to be 800W/m.

4.2.1 Exergy Analysis

The exergy balance for the solar field and the modified heat recovery steam generator are described in this section. The exergy analysis for the remaining components is performed according to the equations presented in Section 2.4 and they are not reported.

The exergy destruction rate in the parabolic trough collector is calculated as:

$$\dot{\Psi}_{D,PTC} = \dot{x}_{II} - \dot{x}_{IV} + \dot{Q}_{sol} \cdot \vartheta_{sol} \quad (4.13)$$

The term $\dot{Q}_{sol}$ represents the solar radiation that is absorbed by the collectors. The Carnot coefficient is computed using Equation (2.39).

The solar evaporator exergetic balance can be written as:

$$\dot{\Psi}_{D,evap\_sun} = \dot{x}_{IV} - \dot{x}_{I} + \dot{x}^{*}_{19} - \dot{x}^{*}_{20} \quad (4.14)$$

The physical exergy $\dot{x}_{19}^{*}$ and $\dot{x}_{20}^{*}$ are computed considering the steam mass flow rate produced in the solar evaporator.

The exergy destruction in the oil pump is determined as:

$$\dot{\Psi}_{D,pump.oil} = \dot{x}_{I} - \dot{x}_{II} + \dot{W}_{pump.oil} \tag{4.15}$$

The exergy balance for the super-heater, evaporator and economizer sections of the waste boiler are respectively:

$$\dot{\Psi}_{D,SH} = \dot{x}_{20} - \dot{x}_{21} + \dot{x}_{4} - \dot{x}_{4a} \tag{4.16}$$

$$\dot{\Psi}_{D,\text{evap\_HRSG}} = \dot{x}_{19}^{**} - \dot{x}_{20}^{**} + \dot{x}_{4a} - \dot{x}_{4b} \tag{4.17}$$

$$\dot{\Psi}_{D,\text{eco\_HRSG}} = \dot{x}_{15} - \dot{x}_{19} + \dot{x}_{18} - \dot{x}_{17} + \dot{x}_{4b} - \dot{x}_{5} \tag{4.18}$$

Note that $\dot{x}_{19}^{*}$ and $\dot{x}_{20}^{*}$ are computed considering the steam in the HRSG evaporation section. Summarizing all the contributions, the total exergy destruction for the considered system can be calculated as:

$$\dot{\Psi}_{D,\text{HRSG}} = \dot{x}_{4} - \dot{x}_{5} + \dot{x}_{15} - \dot{x}_{21} + \dot{x}_{18} - \dot{x}_{17} + \dot{Q}_{sol} \cdot \vartheta_{sol} + \dot{W}_{pump.oil} \tag{4.19}$$

4.2.2 Economic Analysis

The capital costs for the proposed integration of the parabolic trough collector with a Rankine cycle of are discussed in this section.

The direct costs of a parabolic collector system can be summarized into the following categories (S&L, 2003):

- Heat collection element (HCE) ;
- Mirror;
- Support Structure;
- Drive;
- Piping system;
- Civil Work;

In this study, the costs of supporting structure, the collector mirrors and the absorber defines the total expenses related to a parabolic trough system since they represent the most significant cost driver. The supporting structure and the collector expenses are considered as the cost of the solar field. The cost of the solar field is computed assuming a specific cost per unit of area equal to 270 $/m^2$. The cost related to the heat collection elements (the absorber and the cost of the heat transfer fluid) is estimated considering the specific cost of 80 $/ m^2. The specific cost for the solar field and the HCE are taken from the library of the software System Advisor Model implemented by NREL.

The cost for the solar evaporator is estimated to be the same as for the evaporator section of the Waste Heat boiler. The cost of the pump for the thermal oil is computed using Equation (2.63) assuming the same isentropic efficiency considered for the feed-water pump.

The total investment cost for the plant is computed using the cost functions explained in Chapter 2. The NPV and the IRR are calculated assuming the parameters from the previous case.

5 INTEGRATED SOLAR COMBINED CYCLE PERFORMANCES

5.1 PLANT LOCATION AND BOUNDARY CONDITIONS

The integrated solar combined cycle power plant is assumed to be located in the same region of the SHCC system. The yearly direct normal radiation and the external ambient conditions are the same for the two different arrangements.

5.2 PLANT SIMULATION METHODOLOGY

The plant model is implemented in Matlab and the analysis of the results has been carried out using Excel. The solar radiation is taken for the southern Spain typical meteorological year for 1st January to 31st December. The code is based on the energy and exergy balances discussed in previous chapter (see Chapter 4).

The system is supposed to run always in hybrid mode for 24 hours per day. The thermal energy to the gas turbine power block is entirely supplied by the fuel combustion. The fuel is assumed to be pure methane. The solar energy is exploited, when available, in the solar evaporator of the Rankine cycle power block.

The same assumptions made for the simulation of the solar hybrid combined cycle plant holds for the considered system: the compressor inlet mass flow rate and the TIT remain constant. The isentropic efficiencies of the pumps and turbines do not vary with time.

The overall efficiency of the parabolic trough collector depends on the solar radiation intensity and it becomes higher as the value of the DNI increases. The temperatures of the thermal oil at inlet and outlet section of the parabolic trough system are fixed parameters. Since the evaporation temperature of the steam is constant, the effectiveness of the solar evaporator is supposed to be constant, even if the mass flow rate of the Therminol VP-1 changes hourly. Refers to Equation (4.7) for the definition of the solar evaporator effectiveness.

5.3 CYCLE PERFORMANCES

5.3.1 Nominal and Solar hybrid Yearly Performances

The yearly average value of most significant parameters used to describe the system are reported in Table 3.1. The nominal conditions refer to the plant running without any solar input.

Table 5-1 Yearly average solar-hybrid and nominal performances of the ISCC system

	Solar - Hybrid	Nominal plant
Q_{sun} [MW]	3.43	-
Q_{PTC} [MW]	0.89	-
$P_{el,gas}$ [MW]	11.14	11.14
$P_{el,steam}$ [MW]	7.92	6.45
$P_{el,CC}$ [MW]	19.05	17.59
η_{PTC}	0.26	-
$\eta_{I,gas}$	0.32	0.32
$\eta_{I,steam}$	0.29	0.33
$\eta_{I,CC}$	0.45	0.50
$\eta_{II,CC}$	0.45	0.49
m_{fuel} [kg/s]	0.7	0.7

The variable Q_{sun} refers to the annual average solar power that is intercepted by the collectors. The thermal power the is actually absorbed by the thermal oil is computed as Q_{PTC}. The parameter η_{PTC} represents the annual average efficiency of the solar field and it has been calculated considering the whole year (8670 hours). The energy efficiency of the gas turbine in the solar hybrid system is equal to the one in the nominal plant because this parameter is not affected by the solar integration. Indeed, the fuel mass flow rate is unchanged. Finally, the energy efficiency and the exergy efficiency of the solar- hybrid plant

are lower than the one in the nominal condition. The following sections investigate the main reason behind these results.

5.3.2 Solar Related Yearly Average Performances

Table 3.2 reports the computed value for the main parameters related to the evaluation of the integrated solar system. The definitions for these variables have been presented in Chapter 3.

Table 5-2 Solar related yearly average performances for the ISCC system

X	0.09
$\eta_{net,incr\_sun}$	-0.84
$\eta_{net,incr,sun}$ '	0.15
ΔCO_2 [TonsCO_2]	-8286.17
$\Delta CO'_2$ [TonsCO_2]	1816.92

The solar share that could be achieved integrating the parabolic trough collector system with the heat recovery steam generator of the nominal combined cycle is less than 10% of the actual thermal input. Furthermore the annual net incremental solar efficiency related to an high efficiency reference plant result to be negative. When the value of this parameter is lower than zero the solar integration system design is not appropriate. The carbon dioxide avoidance is negative, meaning that a natural gas fired combined cycle power plant with 60% efficiency would have been produced less emissions that the ISCC system.

5.3.3 Monthly Average Performances

The monthly average electrical power production of the integrated solar combined cycle is reported in Figure 5.1. The minimum value of the power is 17.59MW produced during the winter. In the hot season, the peak power increased 23.34MW. During the year the monthly average electricity generated is higher than the power of plant in nominal conditions.

The system power curve demonstrates that the integration of the solar energy in the Rankine cycle power block of a combined cycle is able to boost the power output during sunny hours. The increase in the produced electric energy is due to the additional steam that is generated in the solar evaporator. Figure 5.2 shows the trend in time of the total steam mass flow rate. For the sake of simplicity, the hourly trend is reported for a single day only. When the solar radiation is more intense, the heat transferred to the water in the solar evaporator increase and more saturated vapor can be created. However the steam that is produced with the heat recovered by the flue gases in the HRSG evaporator decreases. This effect is related to the design of the system.

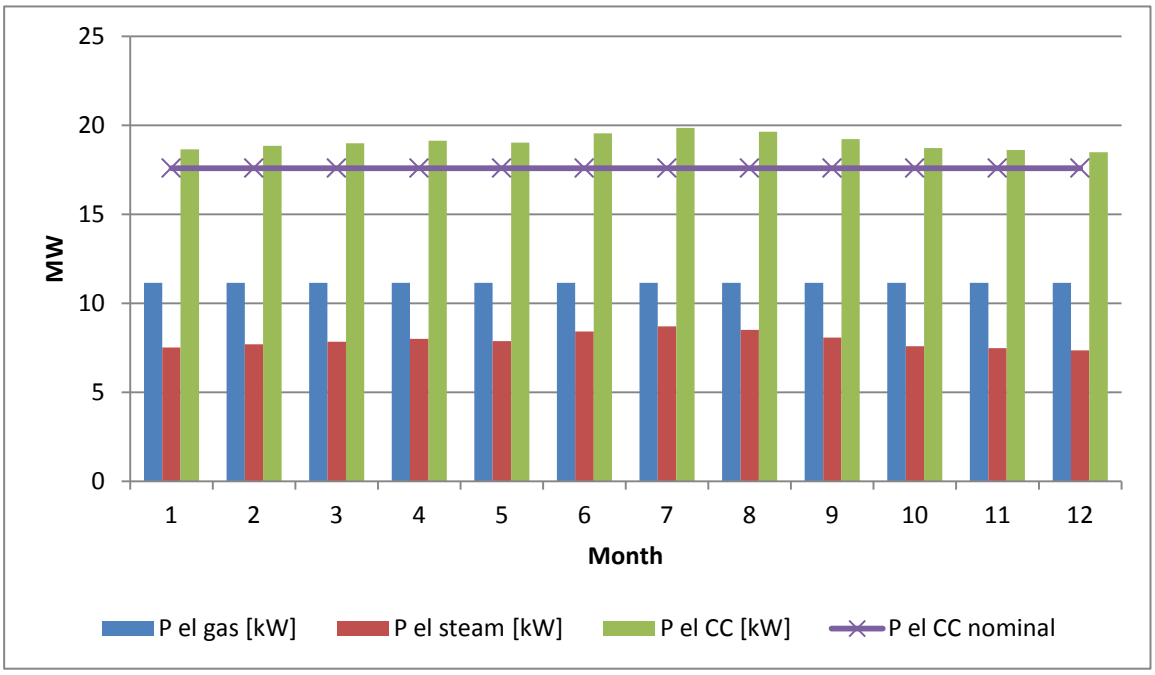

Figure 5-1: Integrated solar combined cycle monthly power output

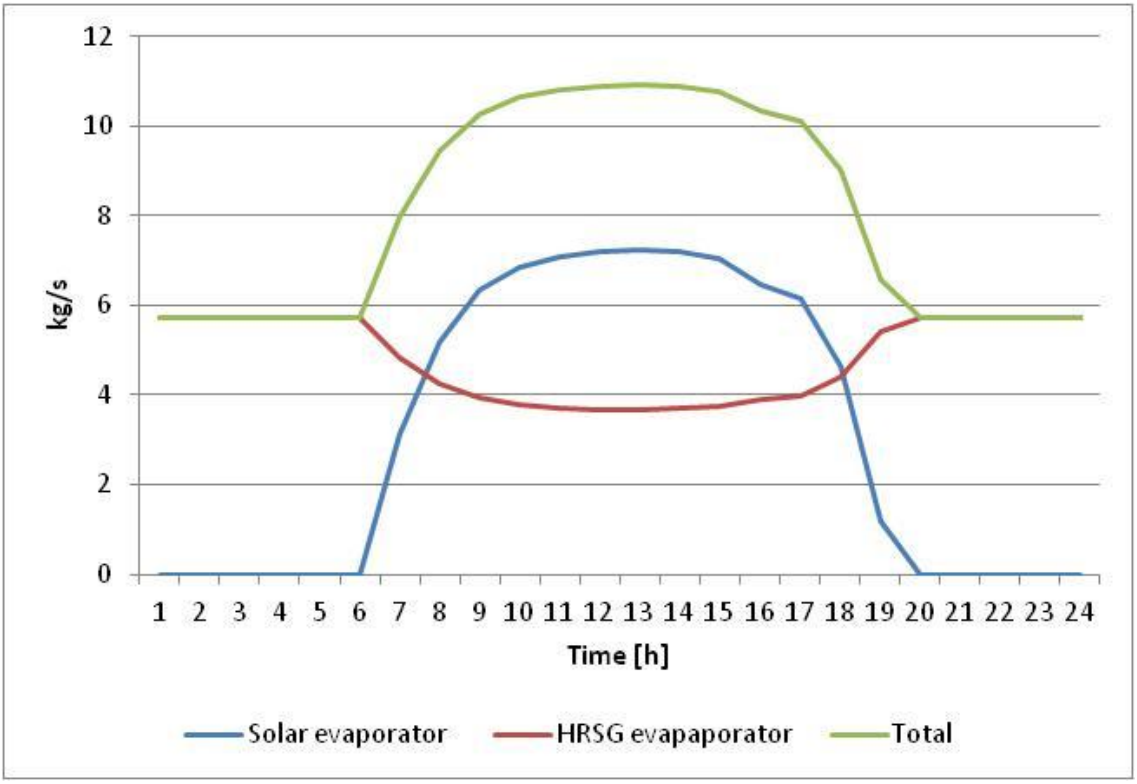

Figure 5-2 Steam mass flow rate in the Rankine cycle power block for the ISCC system for the 14th of April

The thermal power to the super-heater and the economizer is supply by the cooling of exhaust gases. During sunny hours the steam flow rate increases and the hot exhausts have to provide more heat in the super-heating heat exchanger. For this reason, the temperature of the gas steam at the inlet section of the evaporator is lower and the steam flow rate decreases. Figure 5.3 represents the temperature calculated at different hours at the inlet section of the super-heater (T21 and T4), at the inlet section of the evaporator (T20 and T4a) and at the outlet section of the evaporator (T19 and T4b) respectively.

The definition of the energy efficiency for a solar-hybrid combined cycle has been given in Chapter 3. The ISCC power plant monthly average efficiency trend is shown in Figure 5.4. The highest efficiency value is 50.29% while the minimum is at 33.74%. The yearly average energy efficiency is 45.20%. Note that in this case the energy efficiency drops even if the power output is higher. During solar hour the contribution of the sun is null, so only the thermal energy provided by the combustion is considered as input. When the solar radiation is available, the increase in power output is due to an additional thermal input, thus the efficiency reduces.

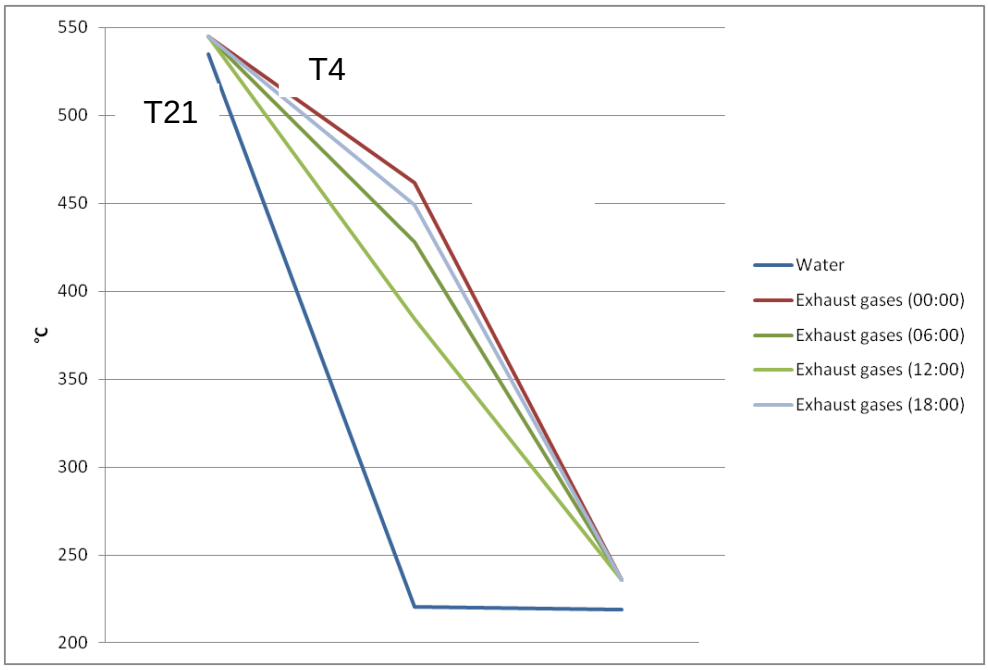

Figure 5-3 Temper . 'o T20 e HRSG for the 14th of .9 ferent hours

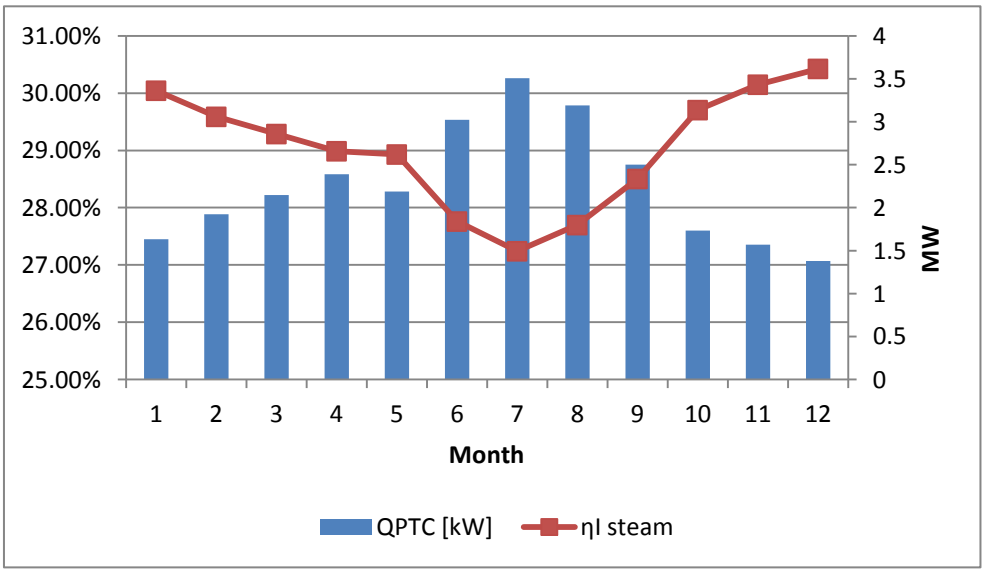

Figure 5-4: Monthly average energy efficiency

The monthly average value of the exergy efficiency is represented in Figure 5.5. The nominal efficiency value is 49.22 % while the yearly average efficiency is 43.40 %. The trend is similar to the one of energy efficiency. The minimum value of the exergy efficiency is reached with the highest solar power and when the exergy destruction rate is high higher. The hourly exergy destruction rates for each component have been calculated using the equation listed in Chapters

2 and 4. Since the solar system is integrated with the waste heat boiler, the exergy destruction in the parabolic trough collector and in the solar evaporator are summarized to the losses of the Heat Recovery Steam Generator. The exergy destruction rate indicated as pumps accounts for all the pumping system including the thermal oil circulation pump. The losses in the solar system and in the waste boiler represent the 28% of the total exergy destruction. The highest share is due to the combustion chamber since it is supposed to run continuously at the same rate for all the year.

Figure 5.6 report the trend of the solar field efficiency. As explained in Chapter 4, the efficiency of the parabolic trough collector depends on the solar irradiance and on the difference between the fluid and the ambient temperature. Since the latter is assumed to be constant, the solar field result to be more efficient during the summer.

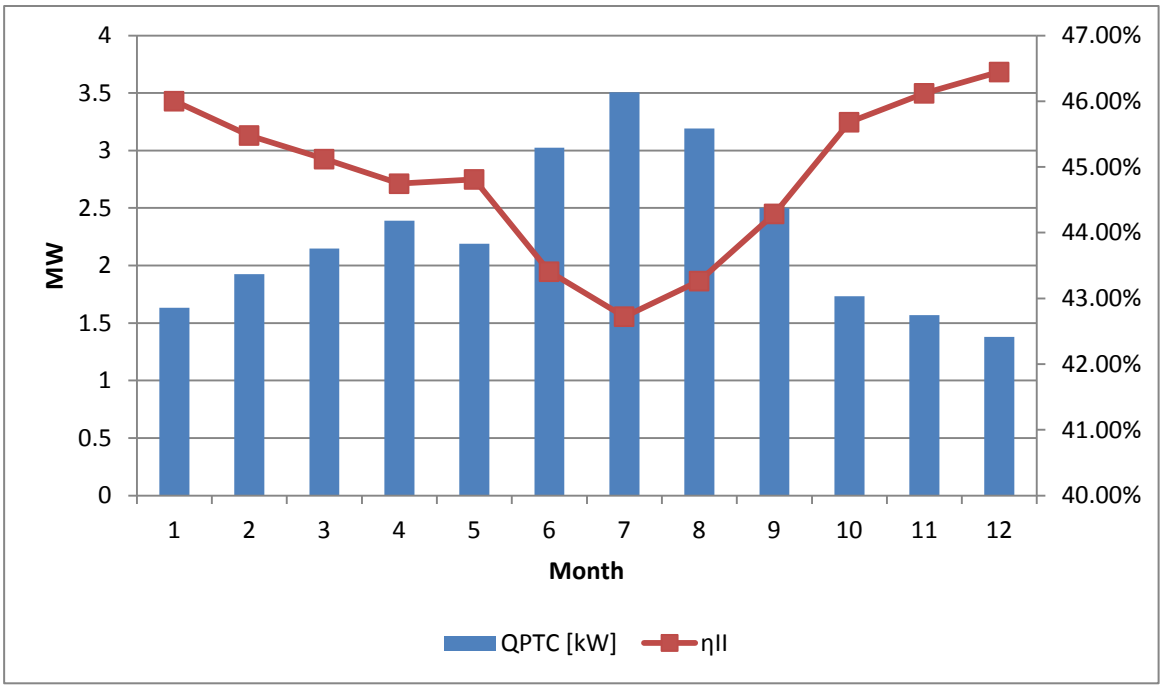

Figure 5-5: Monthly average exergy efficiency

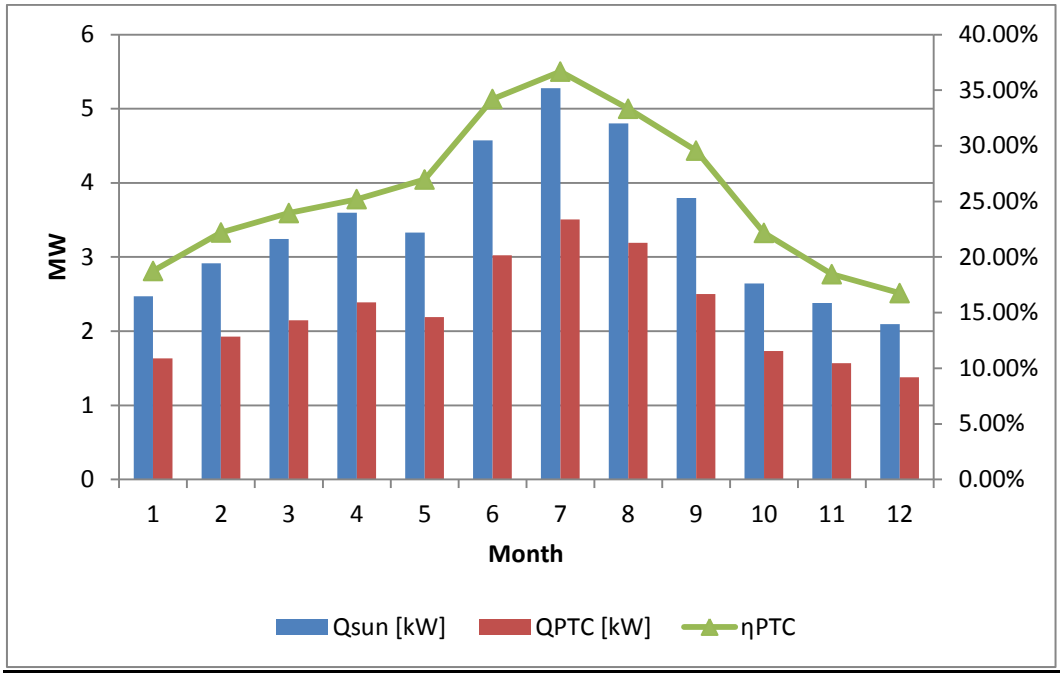

Figure 5-6: Parabolic trough collectors efficiency

The monthly average of the solar share is shown in Figure 5.7. The highest value is reached in July, when the solar field is more efficient and an higher amount of solar radiation is transmitted to the fluid.

The net incremental solar efficiency is affected by the limited solar share of the ISCC system. In particular, this design is much less efficient compared to a natural gas fired high efficient power plant. However, the integrated solar combined cycle under consideration shows an higher net incremental solar efficiency than the same plant in nominal conditions.

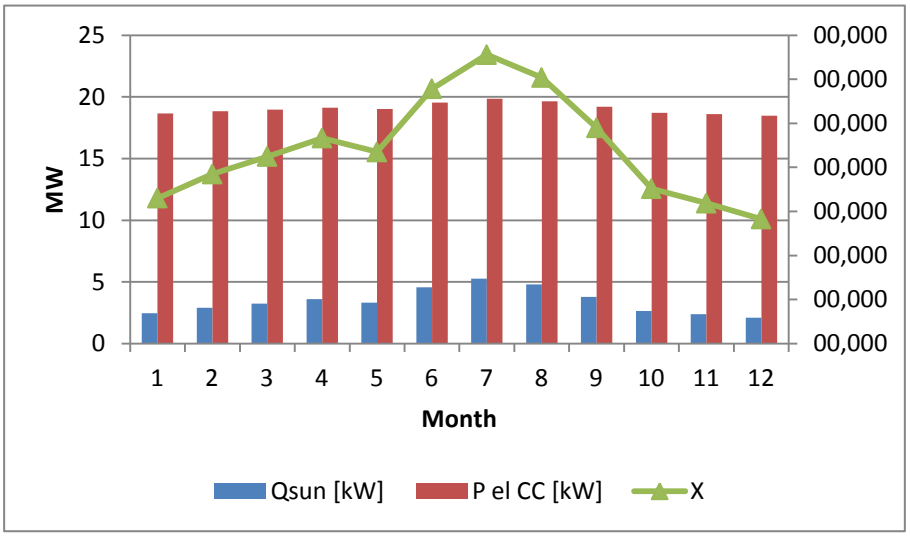

Figure 5-7: Monthly average solar share

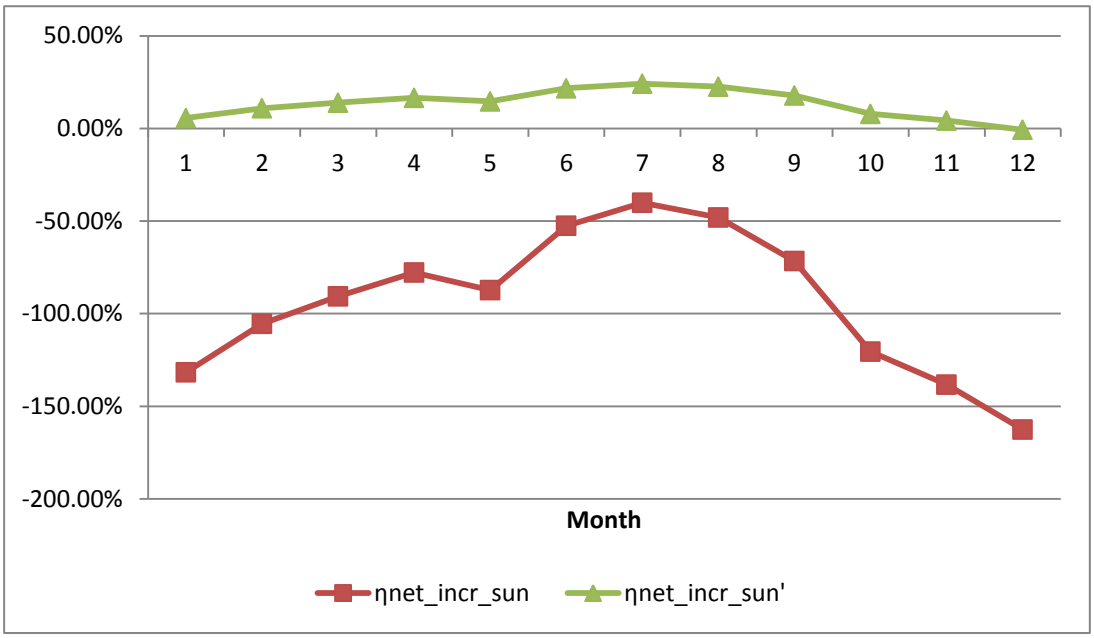

Figure 5-8: Monthly average incremental solar efficiency

The CO_2 avoidance is computed in tons of greenhouse emission saved. Only considering as a reference system the combined cycle in nominal condition, the ISCC plants is able to show be a lower impact on the environment (refer to the green line in the diagram). The integration strategy considered in this section have higher emission than a state-of-the-art combined cycle power system exploiting natural gas: the CO_2 avoidance results to be negative (red line in the diagram).

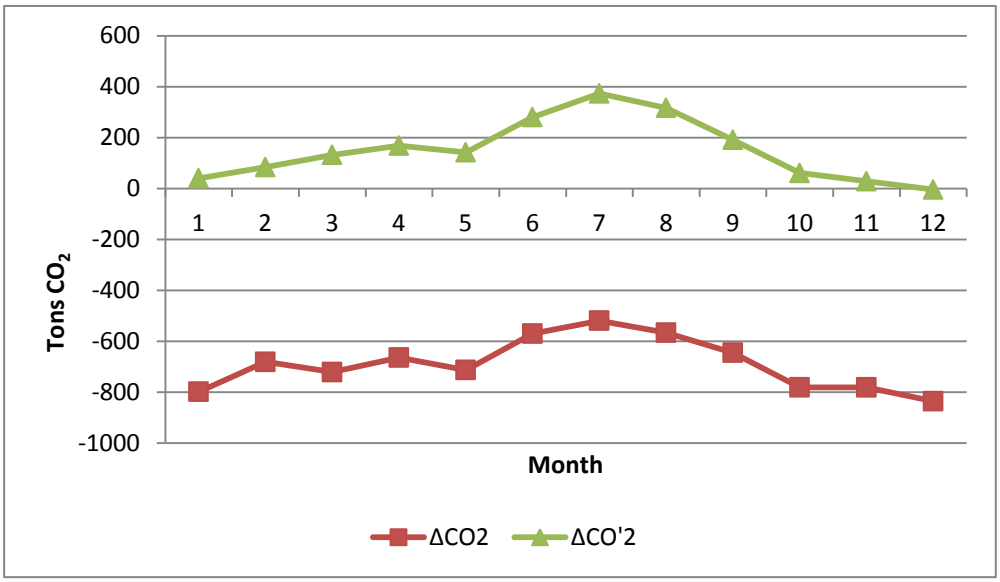

Figure 5-9: Monthly average CO_2 avoidance

5.3.4 Economic Analysis Evaluation

The integrated solar combined cycle requires an investment of $26.4 million. The capital cost for the parabolic trough collector considering the cost for the solar field and for the absorber represents the 45% of the total investment. (see Figure 5.6).

The results of the financial analysis of the investment have been evaluated: the net present value is $64.43 million, while the internal rate of return is 37.39%. The Integrated Solar Combined Cycle power plant can be considered to be a profitable investments. The minimum selling price of the electricity is calculated to be 0.0483 $/kWh.

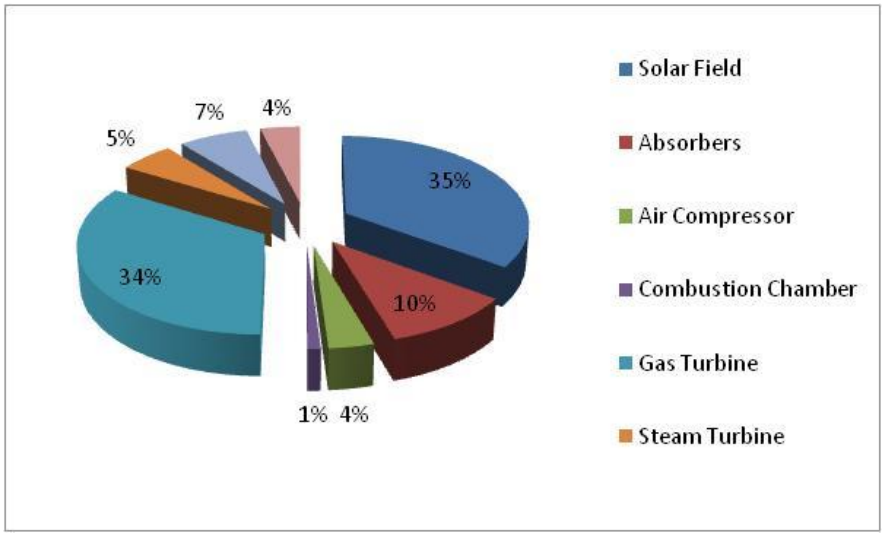

Figure 5-10 Components capital cost for the integrated solar combined cycle

6 PERFORMANCES COMPARISON

Different evaluation metrics have been used in previous literature to characterize and evaluate solar hybrid cycles (Mitsos, 2012). Most metrics can be either defined instantaneously or for a period of time (a year) taking into account the fluctuation of the solar input. These metrics can be grouped into first law efficiencies and solar-related (Section 6.1), second law efficiencies (Section 6.2) and economic metrics (Section 6.3).

6.1 FIRST LAW EFFICIENCY METRIC COMPARISON

The trend of the monthly average output power is shown in Figure 6.1. The electricity generated by the SHCC system is always lower than the plant in working in nominal conditions and it decreases during the summer period for the reasons explained in Chapter 3. On the other hand, the boosting function of the parabolic trough collector is evident in the ISCC: the power generated is always higher than the nominal one and the peak is reached in July.

The fuel consumption in the gas turbine power block of the ISCC system is constant, while the thermal power provided by the combustion decreases in the SHCC plant when the sun is available. Refer to Figure 6.2 for the monthly average values of the fuel thermal input. The SHCC arrangement represents a fuel saving solar integration system, rather than a power boosting solution.

It is interesting to notice that the SHCC plant results to be the solar-hybrid system which is able to collected the higher amount of solar radiation (see Figure 6.3). This is due to the fact the solar field need to be sized larger to be able to concentrated enough radiation for heating the gas turbine working fluid. Note that the heliostat field and the receiver efficiency are assumed to be constant in the model, while the overall efficiency of the parabolic trough collector depend on the hourly irradiance.

Finally, Figure 6.4 reports the monthly average energy efficiency for the two solar-hybrid plants. The energy efficiency reduces during the summer period. Both hybrid solutions seems to have a lower efficiency respect to the plant running in nominal condition. However, the performance of the ISCC is higher because the electric power output increases.

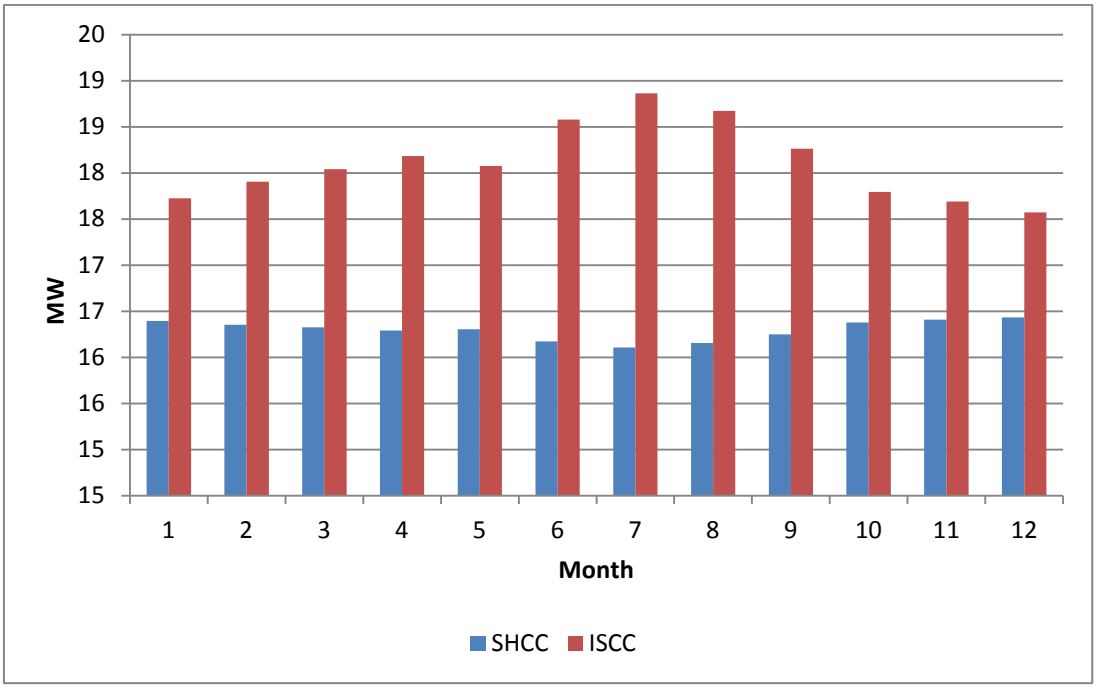

Figure 6-1: Monthly average electric output power

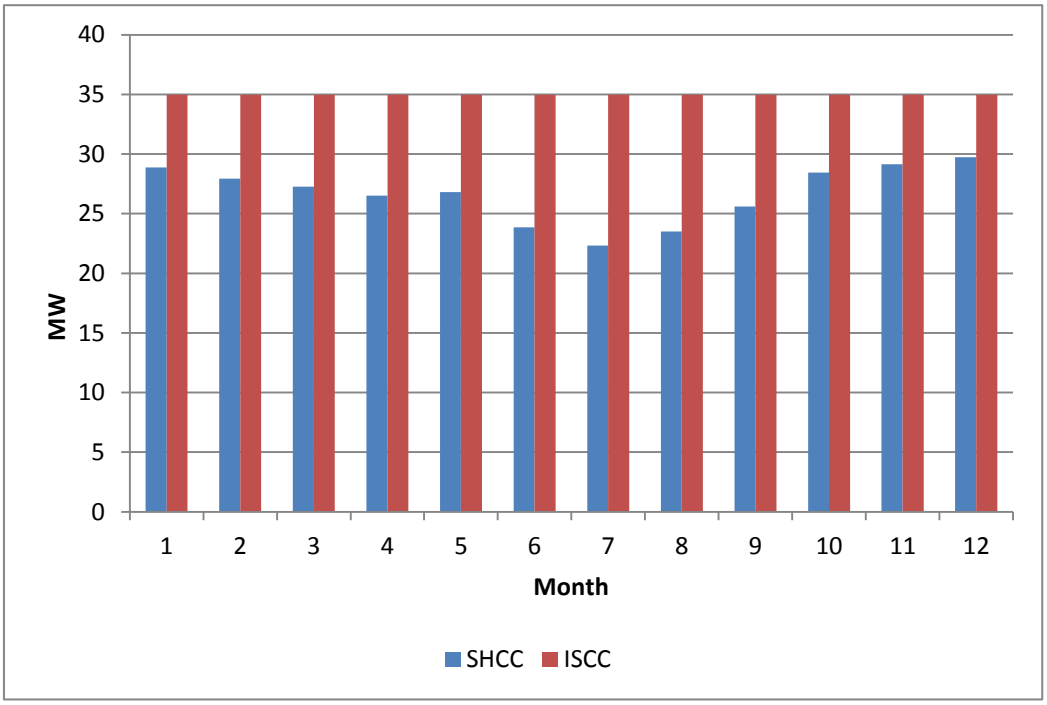

Figure 6-2: Monthly average fuel thermal input

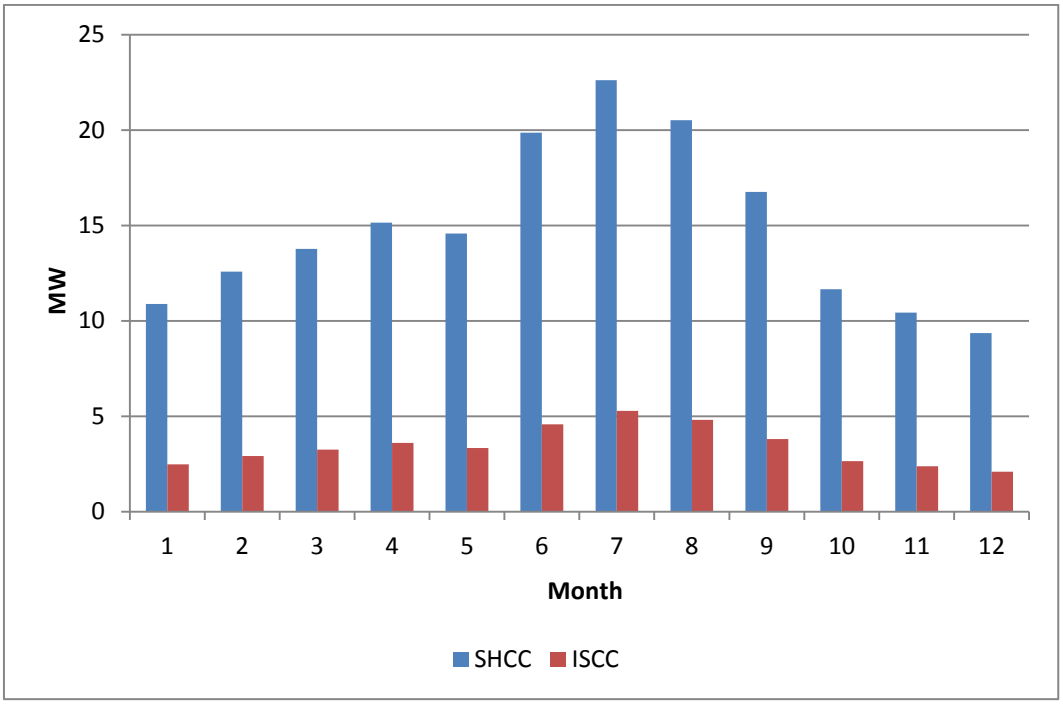

Figure 6-3: Monthly average solar input

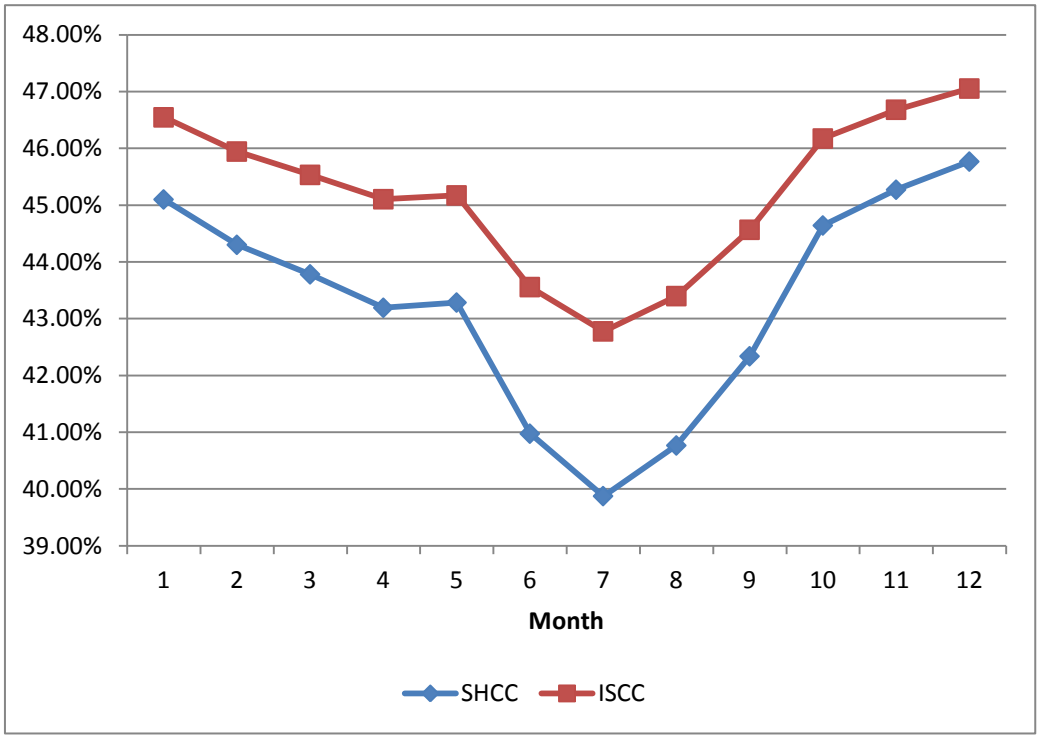

Figure 6-4: Monthly average energy efficiency

6.2 SOLAR RELATED METRICS COMPARISON

The annual average values for the solar share, the net incremental solar efficiency and the incremental CO_2 avoidance are reported in Table 6.1.

The solar share that is possible to achieve in the SHCC plant is higher than the one for a integrated solar combined cycle. In the ISCC model, the solar input in the bottoming Rankine cycle power block is limited due to the design of the system. The solar energy is introduced in the evaporator section only, while the exhaust gases from the gas turbine provide the thermal power to superheat the steam and to pre-heat the total feed-water mass flow rate. The thermal power that can be recovered from the exhaust gases is limited since the temperature at the outlet section of gas turbine is constant. For these reasons, the solar system has to be sized considering the energy balance between the evaporator and the super-heater section in the HRSG (Equations (4.1) and (4.3)). Thus the solar field is reduced and the solar input is penalized. For a real plant, further considerations should be made. The steam turbine power block must be designed to be bigger to account for the increased steam flow rate. However, when the solar radiation is not available, the produced steam mass flow rate is lower and the system runs in off-design condition. Thus, the efficiency and the power output of the Rankine cycle power block reduces. In order to provide the same thermal input to this section of the plant, the exhaust gas temperature must increases. However, this event should be avoided because the efficiency of the gas turbine system decreases and the plant results to be unbalanced. Figure 6.5 represents the monthly average solar share for the two systems.

Table 6-1 Solar related evaluation metrics results

	SHCC	ISCC
X_{sol}	0.36	0.09
$\eta_{net\_incr\_sol}$	0.02	-0.83
$\eta'_{net\_incr\_sol}$	0.20	0.15
ΔCO_2	874.10	-828.62
ΔCO_2 '	10111.54	1814.97

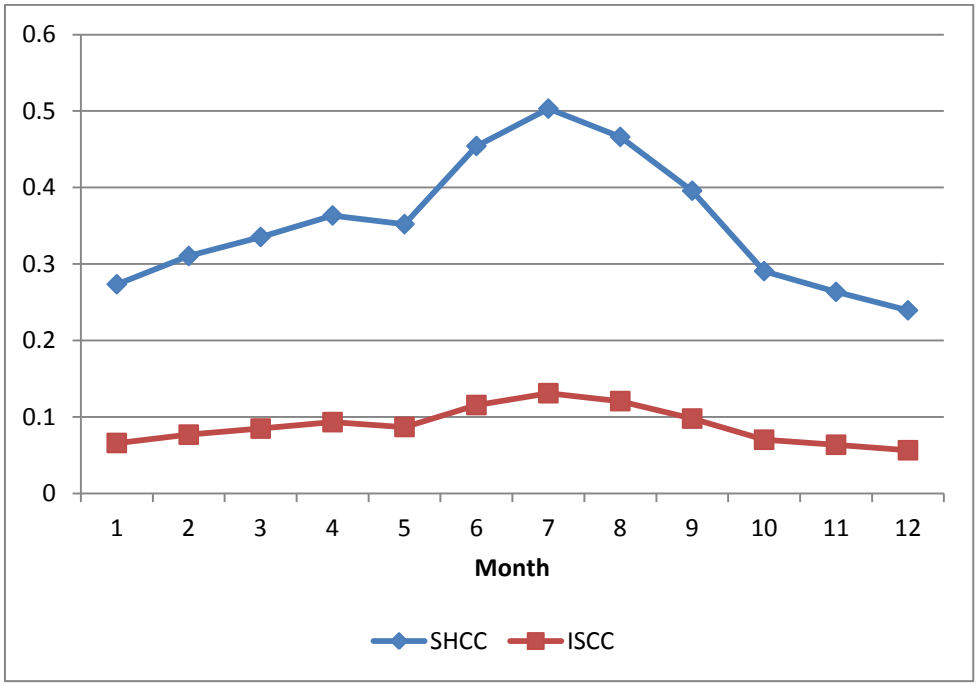

Figure 6-5: Monthly average solar share

The annual average net incremental solar efficiency of the ISCC plant calculated respect to a high efficiency combined cycle power plant is negative. This means that the reference plant would have produced more power assuming the same fuel consumption of the Integrated solar combined cycle. Note that the solar input in the steam cycle increases the power output of this section, but it does not affect the fuel consumption. The increase in the electrical power is not compensated by a reduction in the fuel consumption, leading to a negative value for the net incremental solar efficiency. Figure 6.6 report the monthly trend for this variable. The $\eta_{net\_incr\_sol}$ of the SHCC plant is always higher than respect to the ISCC system.

The parameter $\eta'_{net\_incr\_sol}$ refers to the net incremental solar efficiency calculated assuming the reference efficiency to be 50.29 %. This value is the electrical efficiency of the ISCC system when the DNI is zero. In other words, the reference plant is considered to be a combined cycle power plant similar to the ISCC system but without solar input. In this case the net incremental solar efficiency is positive, but the value is still lower than the one for the SHCC plant calculated considering the new reference plant.

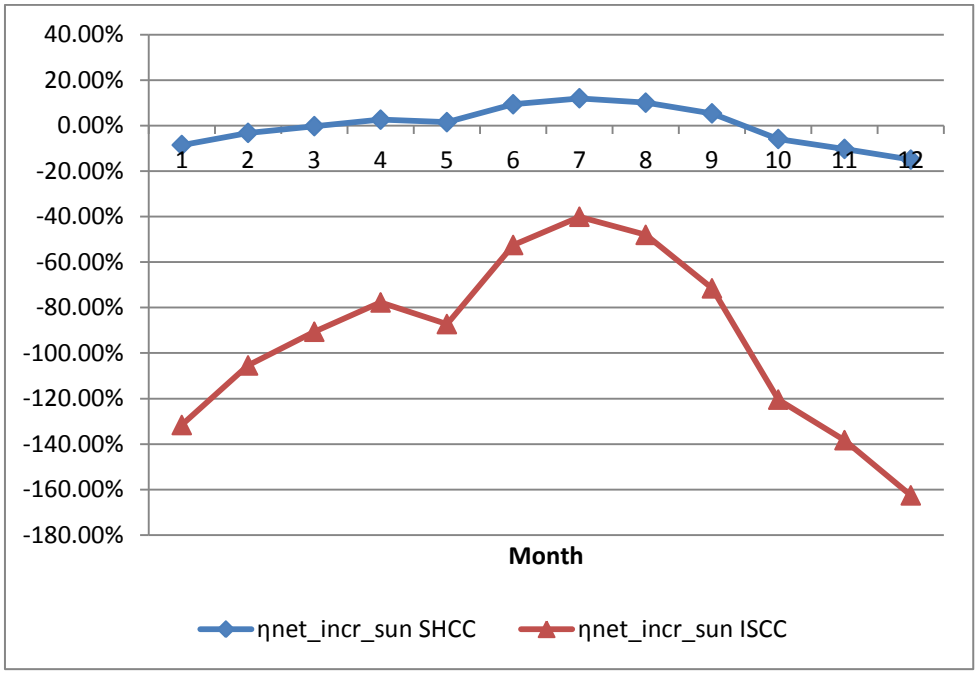

Figure 6-6: Net incremental solar efficiency, η_{ref}= 60%.

The monthly variation of the $\eta'_{net\_incr\_sol}$ is shown in Figure 6.7. Note that in summer the ISCC performs better than the SHCC because the power generated increases significantly respect to the system with the solar integration in the gas turbine. It is noteworthy to highlight that the parabolic trough solar field efficiency is higher during the summer and this contribute the increase the output power.

The incremental CO_2 avoidance results to be negative in the case of the ISCC system. This is due to the fact that the thermal power necessary to the reference plant to produce the same amount of electricity of the ISCC plant is lower than the input used in the hybrid system. As a result, for the same power output, an efficient conventional combined cycle power plant would have produced less greenhouse gas emission respect to the hybrid arrangement. On the other hand, the incremental CO_2 avoidance becomes positive when it is calculated considering the reference plant to be similar to the hybrid system (refer to the variable ΔCO_2'in Table 6.1). In any case, the carbon dioxide emissions saved due to the integration of the solar system is higher for the SHCC scheme. Figure 6.8 reports the monthly trend for the CO_2 avoidance respect to the high efficiency combined cycle power plant, while the variation of ΔCO_2' for every month is shown in Figure 6.9.

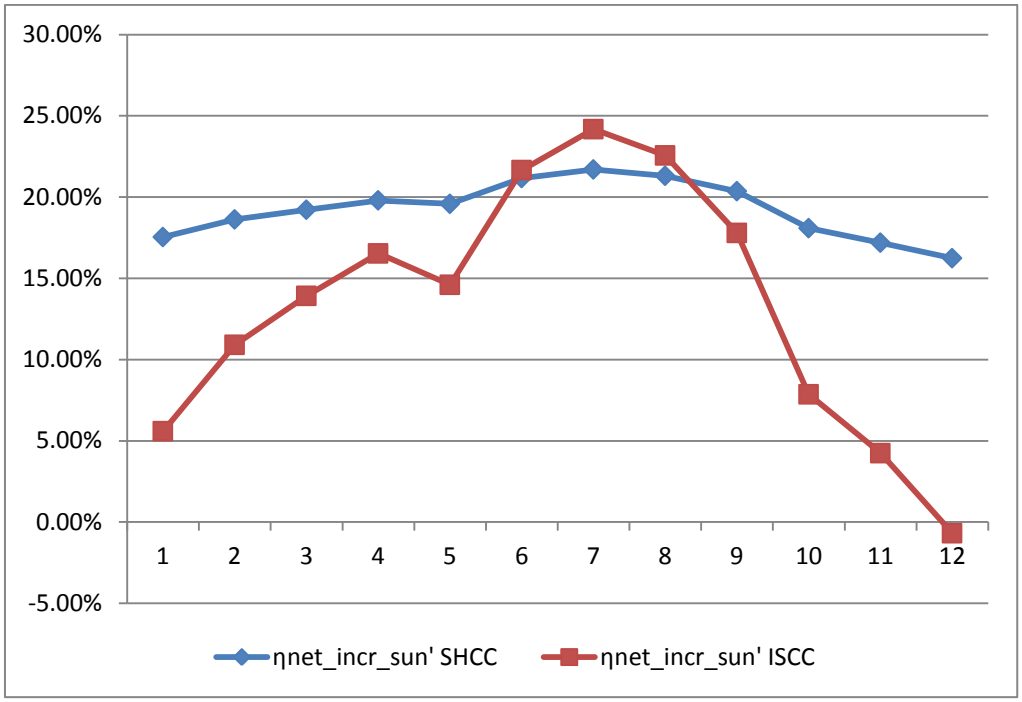

Figure 6-7: Net incremental solar efficiency, η_{ref}= 50.29%.

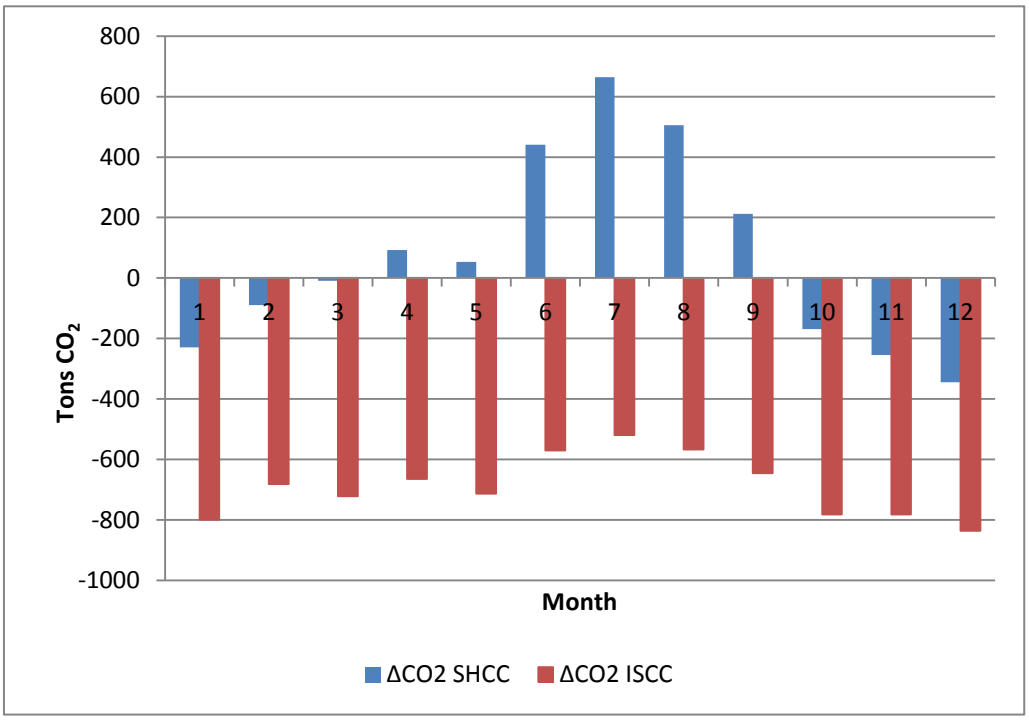

Figure 6-8: Monthly CO_2 avoidance, η_{ref}= 60%.

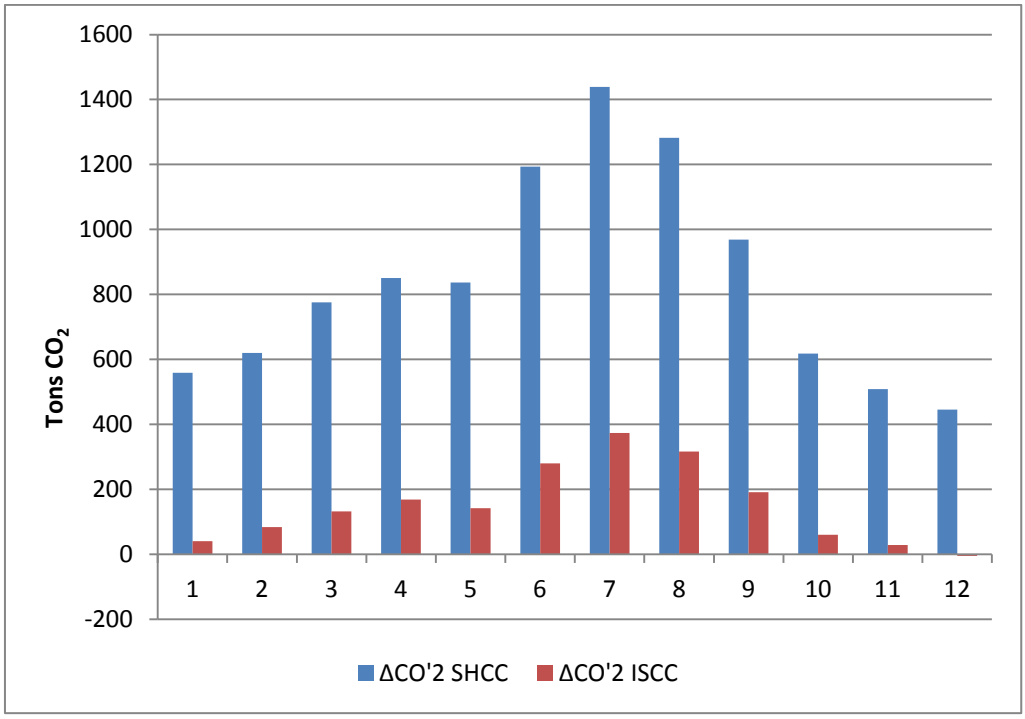

Figure 6-9: Monthly CO_2 avoidance, η_{ref}= 50.29%.

6.3 SECOND LAW EFFICIENCY COMPARISON

The average, the peak and the minimum values of the exergy efficiency for the two different solar integration system are reported in Table 6.2.

Note that the ISCC plant shows better exergetic performances than the solar hybrid combined cycle system. This result needs to be discussed. As a matter of fact, the introduction of heat in a system at high temperature reduces the amount of exergy destroyed. Thus the exergy efficiency of the SHCC system should be higher since the air in the pressurized volumetric receiver can be heated up to about 1000°C, while the temperature of thermal oil at the outlet section of the parabolic trough collector field is about 400°C. However, the exergy losses are proportional to the value of the thermal power injected in the system. Since the solar input in the SHCC scheme is much higher than the one in the ISCC system, the exergy destruction rate is also higher. Furthermore, the annual average power output is higher for the ISCC system. Thus, the exergy efficiency of the combined cycle power plant integrated with the solar tower is lower than the exergy efficiency of the ISCC system. The higher solar share seems to penalize the SHCC scheme from the exergetic point of view. Figure 6.10 represents the monthly average exergy efficiency for the two arrangements. The trend is similar but the exergy efficiency of the ISCC system results to be always higher respect to the SHCC plant.

Table 6-2 Annual average exergy efficiency

	SHCC	ISCC
$\eta_{II\_average}$	43.40 %	44.83 %
η_{II_max}	49.22 %	49.26 %
η_{II_min}	30.89 %	34.79%

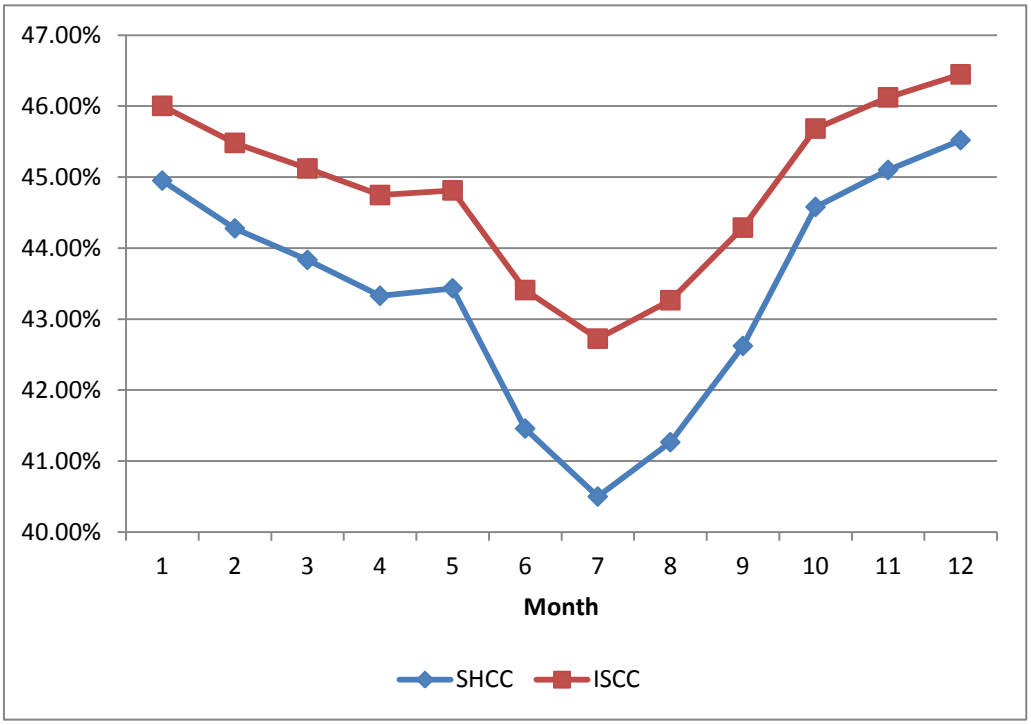

Figure 6-10: Monthly average exergy efficiency

At this point it is interesting to evaluate how the solar system integration affects the exergy efficiency of the combined cycle considering the actual solar input. For this reason, the specific variation of the exergy efficiency per unit of power has been defined as:

$$\Delta\eta_{II} = \frac{\eta_{II}^{min} - \eta_{II}^{max}}{\bar{\dot{Q}}_{sun}} \tag{6.4}$$

The average thermal power collected by the solar system is considered. The exergy efficiency decreases by 4.21% for every MW of solar thermal power injected in the ISCC system. On the other hand, the specific exergy efficiency

reduction in the SHCC plant is only 1.23%. This parameter has been introduced in the current study to quickly analyze the trend of the solar hybrid systems exergy efficiency and it is helpful to the comparison of the characteristic for different solar integration arrangements. However, a more precise exergy analysis of the solar system should be carried out in future studies.

6.4 ECONOMIC ANALYSIS COMPARISON

From the economic point of view, it is important to assess which solar integration system with combined cycle is more profitable. In the current study, only solar-hybrid power plants are compared without considering other traditional CSP technologies such as parabolic trough collector and central receiver solar tower.

The most common evaluation parameter of the economic performance for power generation systems is the levelized electricity cost which has been defined in Chapter 2. The LEC of the solar hybrid combined cycle system is estimated in 0.0544 $/kWh, while the minimum selling cost of the electricity generated with the ISCC plant is 0.048 $/kWh. The integrated solar combined cycle scheme appears to be the most economic system because the average produced power is higher and the investment cost is lower. Refer to Chapters 3 and 5 for the numerical values.

The levelized electricity cost can be related to the solar share when considering solar hybrid power plants in order to determine the cost associated with solar system. To this purpose, the solar LEC can be defined as (Mitsos, 2012):

$$LEC_{sol} = \frac{LEC - (1 - X_{sol}) \cdot LEC_{ref}}{X_{sol}} \tag{6.5}$$

The LEC_{ref} is defined as the levelized electricity cost of the reference plant. In this case the reference plant is assumed to be the combined cycle working in nominal condition. Indeed, the LEC_{ref} value has been calculated considering the electric power generated by the two analyzed schemes without any solar radiation. The capital cost for the reference plant has been computed using the cost functions described in Chapter 2. The LEC_{ref} is 0.04 $/kWh. The computed solar levelized electricity cost for the ISCC and SHCC system are 0.13 $/kWh and 0.08 $/kWh. The SHCC plant utilizing the solar tower has a lower solar levelized electricity cost since the solar share is so much higher. The limited solar share is really not sufficient to make an impact on the

marginal cost of electricity for the ISCC system. In brief, the LEC for the ISCC scheme results to be lower because the cost related to the solar system integration are smaller due to the reduced solar contribution. As a matter of fact, the solar LEC decreases considering the integration with the solar tower, when higher value of X_{sol} can be achieved.

Figure 6.11 summarize the results discussed before: the LEC for the SHCC system is higher but the relative cost of the solar electricity is lower (almost the half).

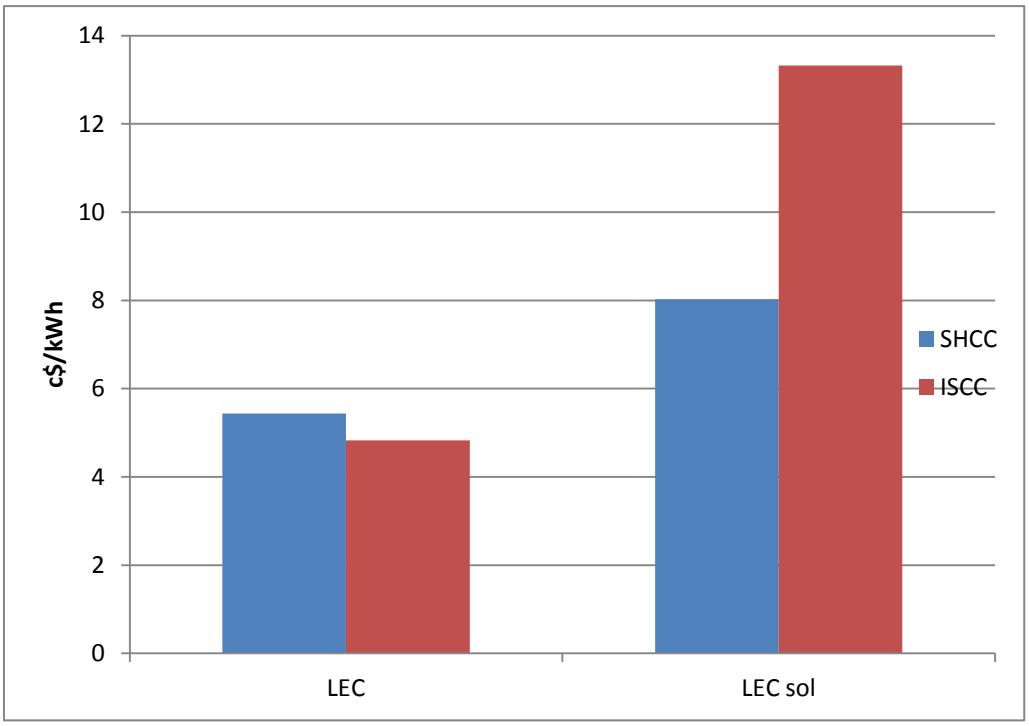

Figure 6-11: Levelized electricity cost and solar levelized electricity cost.

7 CONCLUSIONS

In this study, two different integration system for concentrating solar energy technologies with combined cycle have been analyzed and the advantages and disadvantages of each scheme have been discussed.

The solar hybrid combined cycle plant consists of a heliostat field, a solar tower equipped with a pressurized volumetric receiver, a gas turbine and a heat recovery steam generator which supplies thermal energy to a steam Rankine-cycle power block. The solar energy is used to pre-heat the combustion air in the gas turbine power block. In order to achieve higher temperatures, the pressurized volumetric receiver is installed. This technology has been previously studied in the literature, but no real plants have been built yet.

The integrated solar combined cycle is composed by a gas turbine power block, a heat recovery steam generator linked to a solar field and the Rankine cycle system which consists of a steam turbine, a condenser with evaporative tower and the feed-water pumps. Parabolic trough collectors provide thermal power to a solar evaporator which operates in parallel with the waste heat boiler. The produced steam is super-heated by the exhaust gases. The ISCC scheme represents the most common integration strategy adopted for solar hybrid combined cycle power plants nowadays.

The models of the systems have been implemented in Matlab. The gas turbine and the Rankine cycle power block are supposed to be the same for the two different integration systems. Both plants are supposed to be located in Seville, Spain. The yearly performances have been simulated using the hourly typical meteorological year for southern Spain. Both plants are supposed to operate 24 hours per day in hybrid mode.

The energy, exergy and economic analyses of the different schemes have been carried out. The yearly average produced net electrical power in the SHCC plant is 16 MW with a yearly average efficiency of 43.27 %. The ISCC system can generate an annual average net electricity equal to about 18 MW and the plant yearly average energy efficiency results to be 45.20%. The ISCC configuration increase the power output and the energy efficiency is higher respect to the SHCC system. The integrated solar combined cycle results to be a power boosting option.

From the exergetic point of view, the integrated solar combined cycle system shows better performances than the SHCC plant: the yearly average exergy efficiencies of the plant are 44.83% and 43.4% respectively. However, the variation of the second law efficiency per unit of solar power input is higher in

the case of ISCC scheme. This means that the specific exergy destruction of solar thermal power is higher in the system using the parabolic trough collectors.

Regarding the solar related metrics, the solar share of 35% can be achieved with the SHCC system, while the percentage of the total thermal power delivered by the parabolic trough system is limited to 9% in the ISCC arrangement. The net incremental solar efficiency for the SHCC plant is 20% and it is higher respect to the other system (15%) because the solar share is increased. The CO_2 avoidance is larger for the solar hybrid combined cycle. However, both the analyzed solar-hybrid system show limitation respect to conventional combined cycle power plant: this is mainly due to the high efficiency and the larger output power of these systems.

From the economic point of view, the levelized electricity cost is the most significant parameter to be evaluated. The minimum electricity selling price for the SHCC plant is 0.05 $/kWh and 0.04 $/kWh for the ISCC system. However, the solar LEC for the combined cycle system integrated with solar tower is 0.08 $/kWh and it is lower than the 0.13 $/kWh calculated for the ISCC scheme.

In conclusion, the yearly average exergy and energy efficiency of the integrated solar combined cycle scheme (ISCC) results to be higher than the solar hybrid combined cycle system. The levelized electricity cost for the overall ISCC plant is lower. However, the SHCC arrangement shows the higher solar share and the lowest solar LEC.

Since the solar related metrics performance of the SHCC are higher than the ISCC system, the former appears to be the most promising option for the integration of concentrating solar technologies with combined cycle power plant. The reason being the higher solar share achievable and consequently lower solar levelized electricity cost can be achieved. Furthermore, considering the solar system integration in the gas turbine, the annual CO_2 emission are reduced assuming continuous hybrid mode operation.

In future works a more precise exergy analysis of the solar systems should be performed in order to properly access the irreversibility related to the different technologies. Furthermore, the advantages and disadvantages of the integration with a thermal storage system within the proposed schemes should be analysed.

REFERENCES

Allani, Y., Favrat, D., Von Spakovsky, M. R. (1997). CO2 mitigation through the use of hybrid solar-combined cycles. *Energy Conversion and Management,* Vol. 38, Supplement **,** pp. S661-S667.

Aringhoff, R., Brakmann, G., Geyer, M., Teske, S. (2005). Concentrated solar thermal power –Now!. Report of Greenpeace International, the European Solar Thermal Industry Association (ESTIA) and the IEA SolarPACES programme. September. Available from European Solar Thermal Electricity Association (ESTELA), www.estela.eu .

Arsalis, A. (2007). Thermo-economic Modeling and Parametric Study of Hybrid Solid Oxide Fuel Cell-Gas Turbine-Steam Turbine Power Plants Ranging from 1.5 MWe to 10 MWe. Master Thesis, Virginia Polytechnic Institute and State University. Blacksburg, Virginia (USA).

Augsburger, G., Favrat, D. (2013). Modelling of the receiver transient flux due to cloud passage on a solar tower thermal power plant. *Solar Energy,* Vol. 87, pp**.** 42-52.

Ávilà-Marìn, A. L.(2011). Volumetric receivers in Solar Thermal Power Plants with Central Receiver System technology: A review. *Solar Energy,* Vol. 85**,** No. 5, pp**.** 891-910.

Badr, O. (2013). Solar Power Generation : Solar Thermal Systems. Cranfield University, UK (unpublished material).

Baghernejad, A., Yaghoubi, M. (2010). Energy Analysis of an Integrated Solar Combined Cycle System. *Renewable Energy*, Vol 35, No. 10, pp. 2157-2164.

Barigozzi, G., Bonetti, G., Franchini, G., Perdichizzi, A. , Ravelli, S. (2012). Thermal performance prediction of a solar hybrid gas turbine. *Solar Energy,* Vol. 86**,** No. 8, pp. 2116-2127.

Barlev, D., Vidu, R. , Stroeve, P. (2011). Innovation in concentrated solar power. *Solar Energy Materials and Solar Cells,* Vol. 95**,** No. 10, pp. 2703-2725.

Buck, R., Brauning, T., Denk, T., Pfander, M., Schwarzbozl, P., Tellez, F. (2002). Solar-hybrid Gas Turbine-based Power Tower System (REFROS). ASME Journal of Solar Energy Engineering, Vol. 124, pp. 1-9.

Burkholder, F., Kutscher, C. (2009). Technical Report. *Heat Loss Testing of Schott's 2008 PTR70 Parabolich Trough Receiver*. Report number NREL/TP-550-45633, NREL, Golden, Colorado (USA).

Collado, F. (2008). Quick evaluation of the annual heliostat field effiency. *Solar Energy*, Vol. 82, No. 4, pp. 379-384

Dersch, J., Geyer, M., Herrmann, U., Jones, S. A., Kelly, B., Kistner, R., Ortmanns, W., Pitz-Paal, R., Price, H. (2004). Trough integration into power plants—a study on the performance and economy of integrated solar combined cycle systems. *Energy,* Vol. 29**,** No 5-6, pp**.** 947-959.

DLR, (2009). *Jülich solar tower power plant – research facility officially handed over to the operator* Available at: www.dlr.de [Accessed: 05/05/2014].

Dunham, M. T., Iverson, B. D., (2014). High efficiency thermodynamics power cycle for concentrated solar power. *Renewable and Sustainable Energy Reviews,* Vol. 30**,** pp. 758-770.

European Commission (2005). Project Report. *Solgate: Solar hybrid gas turbine electric power system*. Report number ENK5-CT-2000-00333, European Commission, Brussels, Belgium.

Franchini, G., Perdichizzi, A.,Ravelli S., Barigozzi, G. (2013). A comparative study between parabolic trough and solar tower technologies in Solar Rankine Cycle and Integrated Solar Combined Cycle plant. *Solar Energy*, Vol. 98, pp. 302-314.

Galliani, A., Pedrocchi, E. (2006). Analisi Exergetica, Polipress, Hoepli, Milan. [Exergy Analysis]

Giostri, A., Binotti, M., Astolfi, M., Silva, P. , Macchi, E., Minzolini, G. (2012). Comparison of different solar power plant based on parabolic trough technology. *Solar Energy*, Vol. 86, No. 5, pp. 1208-1221

Greenpeace International, ESTELA, (2009). Concentrating solar power outlook 2009. Available at: http://www.greenpeace.org/international/en/publications/reports/concentrating-solar-power-2009/. [Accessed: 13/08/2014].

Heide, S., Beukenberg, U. O. M., Gerike, B., Freimark M., Langnickel, U., Pitz-Paal, R., Buck, R., Giugliano, S. (2010). Design and operational aspects of gas and steam turbines for the novel solar hybrid combined cycle SHCC. *Proceeding of the ASME Turbo Expo 2010: Power for Land Sea and Air*, June 2010, Glasgow, UK.

Heller, P., Pfander, M., Denk, T., Tellez, F., Valverde, A., Fernandez, J., Ring, A. (2006). Test and evaluation of a solar powered gas turbine system. Solar Energy, Vol. 80, No. 10 , pp. 1225-1230.

Ho, C. K. ,Iverson, B. D. (2014). Review of high-temperature central receiver designs for concentrating solar power. *Renewable and Sustainable Energy Reviews,* Vol. 29**,** pp. 835-846.

Horn, M., Fuhring, H., Rheinlander, J. (2004). Economic analysis of integrated solar combined cycle power plant. A sample case: The economic feasibility of an ISCCS power plant in Egypt. *Energy*, Vol. 29, No. 5-6, pp. 935-945.

IEA, (2011). Executive summary: Solar Perspective, 2011, Paris, France.

IEA, (2010). Technology Road Map: Concentrated Solar Power, 2010, Paris, France.

IEA, (2012). Renewable energy: Medium-term market report , 2012, Paris, France.

IRENA, (2013). Concentrating Solar Power: Technology Brief, 2013. Available at: www.irena.org

Jamel, M. S., Rahman, A. A., Shamsuddin, A. H. (2013). Advanced in the integration of solar thermal energy with conventional and non-conventional power plants. *Renewable and Sustainable Energy Reviews,* Vol. 20, pp. 71-81.

Kribus, A., Zaibel, R., Carey, D., Segal, A. ,Karni, J. (1998). A solar-driven combined cycle power plant. *Solar Energy,* Vol. 62**,** No 2, pp. 121-129.

Li,Y., Yang, Y. (2014). Thermodynamic analysis of a novel integrated solar combined cycle. *Applied Energy,* Vol. 122, pp. 133-142.

Lozza, G. (2007). Turbine a gas e cicli combinati, Second Edition, Società Editrice Esculapio, Bologna.[Gas turbine and combined cycle].

Lupfert, E., Geyer, M., Schiel, W., Esteban, A., Osuna, R., Zarza, E., Nava, P. (2001). EuroTrough design issues and prototype testing at PSA. Paper presented at the Solar Forum 2001 “Solar Energy: The Power to Choose”, 21-25 April. Washington DC.

Mitsos, A., Eter, A. A., Mokheimer, E. M. A., Habib A. M., Al-Qutub, A., Sheu, E. J. (2012). A Review of Hybrid Solar-Fossil Fuel Power Generation System and Performance Metrics, *ASME Journal of Solar Energy Engineering*, Vol. 134, pp. 1-17.

Mokri, A., Aal ALI, M., Emziane, M. (2013). Solar energy in the United Arab Emirates: A review. *Renewable and Sustainable Energy Reviews,* Vol. 28, pp. 340-375.

NREL, (2013). *Concentrating solar power projects*. NREL, Colorado, USA. . Available at: www.nrel.gov [Accessed: 05/05/2014].

Oda, S.,D., Hashem, H. (1988). A Case Study for Three Combined Cycles of a Solar-Conventional Power Generation Unit. *Solar Wind Technology*, Vol. 5, pp. 263-270.

Odeh, S., D., Behnia, M., Morrison, G. (2003). Performance Evaluation of a Solar Thermal Electric Generation System. *Energy Conversion and Management*, Vol. 44, pp. 2425-2443.

Passoni, M., Radice, M. (2010). Analisi tecnico-economica di sistemi di accumulo termico per impianti solari termodinamici a concentrazione parabolico-lineare. Bachelor Degree Thesis, Politecnico di Milano, Milano, Italia. [Technical and economic analysis of thermal storage system for parabolic trough collectors]

Peng, S., Wang, Z., Hong, H., Xu, D., Jin, H. (2014). Exergy evaluation of a typical 330 MW solar-hybrid coal-fired power plant in China. *Energy Conversion and Management*, Vol. 85, pp. 848-855.

Perry, R. H., Green, D. W. (2008). Perry's Chemical Engineers' Handbook, Eighth Edition, McGrawn-Hill, New York.

Schwarzbozl, P., Buck, R., Sugarmen, C., Ring, A., Crespo, M. J., Altwegg, P. , Enrile, J. (2006). Solar gas turbine systems: Design, cost and perspectives. *Solar Energy,* Vol. 80, No. 10, pp. 1231-1240.

Sargent and Lundy Cosulting Group (2003). Assessment of Parabolic Trough and Power Tower Solar Technology Cost and Performance Forecasts, available at: http://www.solarpaces.org/Library/docs/SargentLundyReport.pdf

Segal, A., Epstein, M. (1999). Comparative performances of the 'Top tower' and 'Tower Reflector' central solar receiver. *Solar Energy*, Vol. 65, No. 4, pp. 207-226.

Shirazi, A., Aminyavari, M., Najafi, B., Rinaldi, F., RazaghiI, M. (2012). Thermal-economic-environmental analysis and multi-objective optimization of an internal-reforming solid oxide fuel cell-gas turbine hybrid system. *International Journal of Hydrogen Energy*, Vol. 37, No. 24, pp. 19111-19124

Silva, P., Manzolini, G., (2013). Solar energy conversion with thermal cycle, Napoleon Enteria & Aliakbar Akbarzadeh*, Solar EnergySciences and Engineering Applications,* CRC Press/Balkema.

SOLUTIA (2014). Therminol VP-1: Vapour phase and liquid phase heat transfer fluid. Available at: http://www.solutia.com. [Accessed: 06/06/2014].

Spelling, J. (2009). *Thermoeconomic optimization of solar tower thermal power plant.* Master Thesis, Ecole Polytechnique Federale de Lausanne, Lausanne.

Spelling, J., Favrat, D., Martin, A. ,Augsburger, G. (2012). Thermo-economic optimization of a combined-cycle solar tower power plant. *Energy,* Vol. 41**,** No.1, pp. 113-120.

Turner, P. (2014). Performance measurement and evaluation of CSP plants. Cranfield University, UK (unpublished material) .

Tyagi, S. K., Wang, S., Singhal, M.K., Kaushik, S. C., Park, S. R. (2007). Exergy analysis and parametric study of concentrating type collectors. *International Journal of Thermal Science*, Vol. 46, No. 12 , pp. 1304-1310.

Williams, T. A., Bohn, M. S., Price, H. W. (1995). Solar Thermal Electric Hybridization Issues. Proceeding of ASME/JSME/JSES International Solar Energy Conference, March 1995,Maui,(HI, USA).

Xu, C., Zhifeng, W., LiI, X., Sun, F. (2011). Energy and exergy analysis of solar power tower plant. *Applied Thermal Engineering*, Vol. 31, No. 17-18, pp. 3904-3913.

Zhang, H. L., Baeyens, J., Degrève, J. ,Cacères, G. (2013). Concentrated solar power plants: Review and design methodology. *Renewable and Sustainable Energy Reviews,* Vol. 22**,** pp**.** 466-481.

APPENDICES

Appendix A Validation of the solar field model

A.1 Matlab code

```
clear all, close all, clc
%% MATLAB CODE FOR VALIDATION OF THE SOLAR FIELD MODEL
%Input Parameters from Solgate Project (European Commission, 2005)
%DNI = Location direct solar radiation [W/m2];
%beta = design solar share;
%etha_sec = thermal efficiency secondary concentrator [-];
%apha = receiver equivalent absorbitivity [-];
%epsilon = receiver equivalent emissivity [-];
%Fview = absorber view factor [-];
%f = convection losses fraction [-];
%H = convective coefficeint [W/m2K];
%It should be computed according to the geometrical feature of the
receiver
%Trec = receiver outlet temperature [°C];
%Tamb = ambiente temperature [°C];
%h = Tower heigth (optical aim) [m];
%m = d/h ratio d : distance of the first heliostat row from tower
%rho_field = Afield/Aland :
%rho_field is the ratio between the reflective area and the land area
%occupied by the heliostats

DNI = 880/1000 ; %[kW/m2]
mair_in =  42.3 ;          %kg/s
etha_GT = 0.325;
Pel = 10660 ; %[kW]
beta_nominal = 0.88;
P_rec_nominal = 35750; %[kW]
A_field_nominal = 62733; %[m2]
A_rec_nominal = 82.32; %[m2]
h_in_rec = 714 ; %kJ/kg
T_rec = 1000 ; %[°C]
P3 = 14.8 ; %[bar]
h_out_rec = refpropm('H','T',T_rec+273,'P',P3*100,'air.mix')/1000;
%[kJ/kg]
h_out_CC = refpropm('H','T',1100+273,'P',P3*100,'air.mix')/1000;
%[kJ/kg]
etha_sec = 0.902 ;
alpha = 0.96;
epsilon = 0.85 ;
Fview = 0.5 ;
f = 0 ;
H = 0 ; %[W/km2]
Trec = 960 ; %[°C]
Tamb = 25 ; %[°C]
rho_field = 0.22;
h = 130 ; %[m]
m = 0.5 ;
d = m*h ;
P_rec = [100 90] ;
```

```
F = 100  ; %[kW/m2]
tol = 0.001 ; %[1 W]
it= 0;
Pcycle = mair_in*(h_out_rec - h_in_rec);

    while abs(P_rec(1) - P_rec(2)) > tol
        etha_rec = etha_sec*ETHAREC(F, alpha, epsilon, Fview, f, H,
T_rec,Tamb);

        P_rec_calc = Pcycle/(etha_rec); %[kW]

        P_rec(1) = P_rec(2) ;

        P_rec(2) = P_rec_calc ;

        etha_field = ETHAFIELD(P_rec_calc);

        A_field = P_rec_calc / (DNI*etha_field) ; %[m2]

        L = sqrt(A_field*2/(rho_field))+ d ; %[m]

        D_rec = 0.0129*L + 0.0214 ; %[m]

        A_rec = pi*(D_rec^2)/4 ; %[m2]

        F = P_rec_calc / A_rec ; %[kW/m2]

        it= it+1;

    end

Pcycle
beta_design = Pcycle*etha_GT / Pel
F
P_rec_calc
A_field
A_rec
etha_rec
etha_field

err = Pcycle - DNI*A_field*etha_field*etha_rec
e_rel_P_rec = (P_rec_calc - P_rec_nominal) / P_rec_nominal
e_rel_A_field = (A_field - A_field_nominal) / A_field_nominal
e_rel_A_rec = (A_rec - A_rec_nominal) / A_rec_nominal
e_rel_beta = (beta_design - beta_nominal) / beta_design
```

A.2 Validation Results

Table A.1 Matlab code numerical results

Power intercepeted by the receiver	37435	kW
Power transmitted to the fluid	27566	kW
Incident flux on the receiver area	440.84	kW/m^2
Area of the heliostat field	60136	m^2
Receiver area	84.92	m^2
Design solar share	84	%
Optical efficiency of the field	73.64	%
Thermal efficiency of the receiver	70.74	%

Table A.2 Validation code relative errors

Power transmitted to the fluid	4.71	%
Area of the heliostat field	-4.14	%
Receiver area	3.15	%
Design solar share	-4.71	%